

STRAIN DISTRIBUTION FORMABILITY
IN SHALLOW PARTS

C

by
E. WADDINGTON, B.E.

A Thesis.

Submitted to the Faculty of Graduate Studies
in Partial Fulfilment of the Requirements
for the Degree
Master of Engineering

McMaster University

March, 1980

STRAIN DISTRIBUTION FORMABILITY
IN SHALLOW PARTS

TO MY PARENTS

MASTER OF ENGINEERING (1980) ~
(Mechanical Engineering)

McMASTER UNIVERSITY
HAMILTON, ONTARIO

TITLE: STRAIN DISTRIBUTION FORMABILITY IN SHALLOW PARTS

AUTHOR: ERNEST WADDINGTON
 B.E. (Mech.Eng.),
 Monash University, Melbourne, Australia

SUPERVISOR: Dr. J. L. Duncan

NUMBER OF PAGES: xiii,143

ABSTRACT

In shallow parts it is important to obtain strain over the face of the part if a satisfactory part is to be produced. The strain distributing formability of materials is an important parameter influencing the amount of face strain in shallow parts. Strain distributing formability is not well defined or measured.

The increased use in automobile components of high strength to weight materials such as dual phase steels requires greater precision in ranking materials for formability if these steels are to replace the conventional low strength steels.

In this work an analytical modelling technique simulating a shallow part was developed. The technique was then used to examine how various parameters (geometric, material, and friction) affect the face strain in a shallow part.

An experimental rig was designed and constructed which simulated a simple shallow part. The strains in the part were measured and used to verify the accuracy of the analytical modelling as well as give some indication of the friction conditions in a pressing operation. The experimental bottom strains are a possible means for ranking material formability in shallow parts. This ranking method and other methods based on tensile test data are discussed.

ACKNOWLEDGEMENTS

I wish to thank my supervisor, Dr. J. L. Duncan for his support while this work was being done.

Also, many thanks are extended to Dr. J. D. Embury (Dept. of Metallurgy and Materials Science), Dr. R. Sowerby, Dr. R. M. Hobbs, A. E. Cornford (Dofasco), and my fellow students whose discussions and comments helped me with this work.

I would also like to thank the Dofasco, Inland Steel, Republic Steel, and Armco Steel companies for supplying of materials and information.

My thanks also to my fiancée, Miss Nancy Hassan for her typing of the manuscript, Pat Dillon and Betty Petro of the Word Processing Centre for their help.

Finally, I wish to thank the National Science and Engineering Research Council for their financial support.

TABLE OF CONTENTS

		PAGE
LIST OF FIGURES		viii
LIST OF TABLES		xiii
CHAPTER I	INTRODUCTION	
1.1	Background	1
1.2	Formability	5
1.3	Scope	6
CHAPTER II	DUAL PHASE STEEL	
2.1	Introduction	8
2.2	Mechanical Properties of Dual Phase Steel	11
2.3	Mechanisms Operating in Dual Phase Steel	12
2.4	Production of Dual Phase Steel	14
CHAPTER III	MATERIALS	
3.1	Materials	15
3.2	Describing Formability	20
3.3	Formability in Shallow Parts	22
CHAPTER IV	PRELIMINARY WORK	
4.1	Tensile Tests	34
4.2	Hydraulic Bulge Test	37
4.3	Work Hardening and Strain Distributing Ability	39
4.4	Ranking Materials	39
CHAPTER V	ANALYTICAL MODEL	
5.1	Simulative Modelling	65
5.2	Analytical Modelling	67
5.3	End Point Criteria	71
5.4	Results of Analytical Modelling	73
5.5	Influence of Geometry	74
5.6	Influence of Friction and Materials	77

TABLE OF CONTENTS (continued)

		PAGE
CHAPTER VI	SHALLOW PAN TESTS	
6.1	Experimental Rig	89
6.2	Experimental Procedure	91
6.3	Experimental Results	93
6.4	Strain Conditions in Test Pieces	94
6.5	Friction	96
6.6	Effect of Lubrication	99
6.7	Effect of Strain Index on the Bottom Strain-	100
6.8	Shallow Pan Formability	101
CHAPTER VII	GENERAL DISCUSSION	131
CHAPTER VIII	CONCLUSIONS	
8.1	Conclusions	135
8.2	Suggestions for Further Work	136
APPENDIX A	REFINEMENTS TO ANALYTICAL MODEL	137
REFERENCES		140

LIST OF FIGURES

FIGURE	CAPTION	PAGE
1a & 1b	Optical Micrographs of the dual phase steel, 1a; X120 and 1b; X900	24
2	Scanning Electron Micrographs of the D.P. steel	25
3a & 3b	Optical Micrographs of the HSLA 80 steel, 3a; X120 and 3b; X900	26
4	Scanning Electron Micrograph of HSLA 80 steel	27
5a & 5b	Optical Micrographs of the HSLA 50 steel, 5a; X120 and 5b; X900	28
6	Scanning Electron Micrograph of the HSLA 50 steel.	28
7a & 7b	Optical Micrographs of the I.F. steel, 7a; X120 and 7b; X900	29
8	Scanning Electron Micrograph of the I.F. steel	29
9	Typical load-extension curves	33
10	True Stress - strain curves from tensile tests	45
11	"m", strain rate sensitivity versus strain	46
12	True Stress-Strain curve for the 6010-T4 material	47
13	True Stress-Strain curve for the 7146 material	48
14	True Stress-Strain curve for the IF material	49

LIST OF FIGURES (continued)

FIGURE	CAPTION	PAGE
15	True Stress-Strain curve for the DP2 material	50
16	True Stress-Strain curve for the DP3 material	51
17	True Stress-Strain curve for the DP4 material	52
18	True Stress-Strain curve for the DP5 material	53
19	Stress-Strain curves from the bulge test for the DP1, IF and HSLA 80 steels	54
20	Stress-Strain curve from the bulge test for the DP2 steel	55
21	Stress-Strain curve from the bulge test for the DP3 steel	56
22	Normalized Slope, $1/\sigma \cdot d\sigma/d\epsilon$ curves for DP1, DP2, and DP3 steels	57
23	Instantaneous n , n^* curve for DP1 steel	58
24	Instantaneous n , n^* curve for DP2 steel	59
25	Instantaneous n , n^* curve for DP3 steel	60
26	Normalized Slope, $1/\sigma \cdot d\sigma/d\epsilon$ curves for DP1, IF, and HSLA 80 steels	61
27	Bar Chart of Material Ranking from Tensile Parameters	62
28(a)	Schematic of a shallow pan part	63
28(b)	Typical strain distribution in shallow pan	63
29(a)	Idealized part before pressing	64
29(b)	Idealized geometry of shallow pan at a depth H	64

LIST OF FIGURES (continued)

FIGURE	CAPTION	PAGE
29(c)	Idealized strain distribution	64
30	Detail of tractions around punch corner	80
31	Results of one theoretical simulation of a shallow pan	81
32(a)	Depth as a function of punch half width, a	82
32(b)	Bottom strain as a function of punch half width, a	82
33	Depth against friction μ showing the effect of pre-strain ϵ_0	83
34	Comparison of the computed strains for the basic and refined models	84
35	Theoretical depth, H and bottom strain ϵ_{1b} as a function of friction for several n values	85
36	Theoretical depth, H and bottom strain ϵ_{1b} as a function of n value for several values of friction	86
37	Schematic of experimental rig showing dimensions	87
38	Extensometer layout for the experimental rig	88
39	Experimental strain and load results for the 6010-T4 material	105
40	Experimental strain and load results for the 7146 material	106
41	Experimental strain and load results for the IF material	107
42	Experimental strain and load results for the DP2 material	108

LIST OF FIGURES (continued)

FIGURE	CAPTION	PAGE
43	Experimental strain and load results for the DP3 material, oil only lubrication	109
44	Experimental strain and load results for the DP3 material, oil and polyethylene lubrication	110
45	Experimental strain and load results for the DP4 material	111
46	Experimental strain and load results for the DP5 material	112
47	Exaggeration of strain non-uniformity in test pieces	113
48	Side wall angle θ versus depth	114
49	Friction coefficient μ calculated from experimental strains for 6010-T4 material	115
50	Friction coefficient μ calculated from experimental strains for 7146 material	116
51	Friction coefficient μ calculated from experimental strains for IF material	117
52	Friction coefficient μ calculated from experimental strains for DP2 material	118
53	Friction coefficient μ calculated from experimental strains for DP3 material, both types of lubrication	119
54	Friction coefficient μ calculated from experimental strains for DP4 material	120
55	Friction coefficient μ calculated from experimental strains for DP5 material	121
56	Comparison 6010-T4 friction coefficient μ with work of Ref. [24]	122
57	Comparison of experimental strains with those computed from the refined model for the 6010-T4 material	123

LIST OF FIGURES (continued)

FIGURE	CAPTION
58	Comparison of experimental strains with those computed from the refined model for the DP3 material, oil only lubrication
59	Effect of changing the friction coefficient μ on the theoretical strains
60	Effect of changing the friction coefficient μ on the experimental strains
61	Effect of changing the n value on the experimental strains
62	Experimental bottom strain ϵ_{1b} versus friction for several n values
63	Experimental bottom strain ϵ_{1b} versus n value for several values of friction
64	Bar chart of material ranking from n value and the maximum experimental bottom strain.
65	Refined Model Geometry

LIST OF TABLES

TABLE	CAPTION	PAGE
I	Chemical composition of the steels	30
II	Grain size (μm) of the steels (determined by the linear intercept method)	31
III	Tensile properties for all materials	32
IV	Strain condition in shallow pan test pieces	95

CHAPTER I
INTRODUCTION

1.1 BACKGROUND

High strength steels are now being used in more automotive components than ever before. One of the reasons for the increased use of high strength steels in automobiles is the influence of the shortage of oil. The United States (a major user of oil) has been one of the countries most affected by oil shortages. In the year 1978, the world consumption of oil amounted to a total of fifty two million (52,000,000) barrels of oil per day.[1] Of this amount 20,771,000 barrels of oil per day (39.9%) was consumed by the United States. Seven million six hundred thousand (7,600,000) barrels of this was used as fuel in automobiles.[2]

The United States government has embarked on a program to reduce the country's consumption of oil. While this program has looked at many uses of oil, a large amount of the program's effort is centered on reducing the consumption of oil as fuel in automobiles. Because automobiles are responsible for a large proportion of the United States' oil consumption this is an area where significant gains could be

made in reducing the amount of oil consumed.

There are many methods by which the fuel consumption of automobiles could be reduced, such as lowering maximum speed limits, limiting the engine capacities in automobiles, improving engine efficiency, using cars less, reducing the size of vehicles, or reducing the weight of automobiles. All of these methods are under investigation at present and some are now being introduced into the latest automobile designs.

There are several methods where by the weight of a vehicle may be reduced. These include: reducing the size of the vehicle (making a smaller car); redesigning the vehicle structure and its shape; or by replacing the low strength-to-weight ratio material in the vehicle with materials having higher strength-to-weight ratios. High strength steels are used for weight reduction.

The United States government has now passed legislation requiring certain fuel economy standards from the automobile manufacturers for all future cars [3]. To meet this legislation the United States automobile manufacturers have been forced to implement all of the above methods for reducing vehicle weight. While producing a smaller car is the easiest method to reduce weight, it is not possible to reduce the size of cars by the amount required since the American automobile buyer prefers large vehicles. For this

reason the use of high strength-to-weight ratio materials is an acceptable alternative although there maybe a cost penalties involved with the use of these materials.

High strength-to-weight ratio materials reduce the weight of a vehicle component because it is possible to use a thinner gauge of material without reducing the strength of the component. At present there are many components of a vehicle which are made with mild steel, which has a low strength-to-weight ratio. These components are now being replaced by high strength-to-weight materials such as aluminium alloys, fibre composites, plastics and high strength steels. All of these high strength-to-weight ratio materials tend to suffer from either poor mechanical formability properties, or high costs, or both, when compared with the more conventional mild steel. It is these two factors which are limiting the wide spread introduction of high strength-to-weight ratio materials.

There are five major types of high strength steels used in automotive sheet stamping;

Renitrogenized steel

Rephosphorized steel

Recovery-Annealed steel

HSLA (high strength low alloy) steel

Dual phase steel

All of these types of steels have been under study as

possible materials for reducing the weight of vehicles, but it is dual phase steels which are of interest in this work. Dual phase steel has been one of the latest high strength-to-weight ratio materials to be developed in recent years. While this steel belongs in the category of high strength steels, it has better mechanical properties than other conventional high strength steels of similar strength levels and thus appears to be a likely candidate as a material for light weight automobile parts.[4] But the material for a vehicle component cannot be selected on just the strength level; there are several requirements which must be met. These could be listed as follows;

Formability

Strength

Toughness (fracture)

Fatigue Resistance

Corrosion Resistance

Weldability

Surface finish

Paintability

Stability of properties with time

Cost

The relative importance of each of these requirements is dependent on the current political, social, and economic conditions. At present the shortage of oil has led to

strength (for weight reduction) being an important requirement for a material. Whatever material is selected for a vehicle component it is usually a compromise on all of the above property requirements since it is not possible to meet all of these perfectly. Before selecting a material it is necessary that the material properties be known and understood.

1.2 FORMABILITY

A large part of research in sheet metal forming is determining how materials behave in press operations and what mechanical properties describe this behaviour. With the increasing use of high strength-to-weight ratio materials like HSLA and dual phase steels there is a greater need to understand the mechanical properties of materials much better than is presently known if the performance of these materials in pressing operations is to be predicted.

How a material behaves in a pressing operation is determined by the material's formability. Describing material formability has proven to be a very difficult task since there are many factors which can influence material formability. Formability is the ability of a material to form a given part. It is often confused or interchanged with ductility which is a material's ability to undergo strain without failure. Ductility and formability are

closely related but differ in one respect. Formability is a function of the strain distribution in a part as well as the amount of straining the material can undergo. The strain distribution in a part is a function of the geometry, the friction conditions, and the material properties. How these parameters interact and how they affect the strain distribution in a part is an area of great interest and potential, but one where little quantitative work has been done. Chapter three gives more on describing formability.

1.3 SCOPE

One possible application of dual phase steels is in shallow pan type parts. The aim of this study has been to obtain a more quantitative means of determining the formability of the dual phase steels as compared with other high strength steels, with special regard to the strain distributing abilities of these materials in shallow parts. Dual phase steels were used since dual phase steel is potentially the steel which may have considerable application in the automotive field. First a hot rolled dual phase steel is compared with two HSLA (high strength low alloy) steels with different strength levels (and formabilities) and a low strength highly formable steel known as an Interstitial Free (IF) steel.

Because of the many factors which influence

formability it is difficult to express material formability in a direct quantitative manner. The mechanical behaviour of the above materials is expressed in this work by a number of conventional parameters but none of these on its own gives a satisfactory indication of strain distributing behaviour. In an attempt to improve on this aspect of formability an analytical modelling technique is developed which incorporates many of the material properties which are thought to influence formability in stretch forming processes, as well as geometric and friction parameters.

To check on the accuracy and usefulness of this modelling, an experimental rig was built and experimental results obtained to compare with the theoretical results of the model. The materials used in these experiments consisted of four dual phase steels; the Interstitial Free steel ; and two aluminium alloys. Some of the assumptions made in the model and the limitations of the model are discussed. A better understanding of the geometric, friction and material properties, and how these properties interrelate to determine material formability is possible with the analytical modelling technique presented.

A brief description of the important features of a dual phase steel is given in the next chapter.

CHAPTER II

DUAL PHASE STEEL

2.1 INTRODUCTION

The term "dual phase steel" describes a family of high strength steels which have a microstructure characterized by two phases. The two phases are usually a matrix of ferrite and a second phase of martensite. Some dual phase steels have more than two phases; the other phases constituting only a small volume fraction when compared with the ferrite and martensite phases. The "martensite" phase may not, in fact, be pure martensite but a mixture of martensite and austenite. The second phase is sometimes referred to as martensite/austenite. In some dual phase steels there may also be small amounts of other phases such as pearlite and lower bainite. The total amount of non-ferrite phases varies between 8-20%. It depends on the way in which the steel is produced, the chemical composition and the heat treatment process received.

While the term "dual phase" implies only the two phases, ferrite and martensite, the steels which also contain small percentages of austenite, pearlite and lower bainite are also accepted as dual phase steels since these

steels tend to have the same type of properties as pure ferrite-martensite dual phase steel. More discussion of these other phases will be presented later.

The ferrite phase which makes up the matrix of a dual phase steel usually has the following properties. The ferrite has a fine grained equiaxed structure, with a grain size of around 5 μm . The ferrite has a very low interstitial atom content (for this reason the ferrite is sometimes referred to as a "clean" ferrite). Some precipitates and solid solution atoms may be present in the ferrite. The amount of carbon in the ferrite is usually very small, in the order of 0.02% so as to keep the interstitial carbon to a minimum. The amount of interstitial atom content, solid solution atoms, and precipitates will depend on the chemical composition and the heat treatment process by which the dual phase steel is made. The strength of the ferrite in dual phase steels is thought to be similar to that of an interstitial free steel. The actual strength level will again depend on the interstitial atom content, solid solution content and the amount of precipitate.

The phases that occur in this second phase are functions of the chemical composition, heat treatment and type of process by which the dual phase steel is produced. The secondary phases can be found in separate grains or as

grains which contain more than one phase as is the case of martensite-austenite grains. To get typical, dual phase mechanical properties it is usually necessary to have a significant amount of martensite, bainite, or austenite and very little pearlite present in the microstructure.

The grains of the second phase are usually slightly smaller than those of the ferrite and tend to occur at the triple points of the ferrite grains since this is where the grains of austenite are nucleated during the production of the dual phase steel. The grains of second phases are isolated from each other (topologically separated) and thus can be described as "islands" of martensite in a ferrite matrix. The grain boundary between the ferrite and martensite grains is usually very clean and free from impurities, and in general the amount of impurities in dual phase steels is very low. The low level of impurities is thought to be very important in determining the fracture behaviour of the dual phase steel.

The carbon content of the second phase martensite varies depending on the chemical composition and the heat treatment process received. The hardness and the strength of the martensite is related to the carbon content of the martensite.[5]

2.2 MECHANICAL PROPERTIES OF DUAL PHASE STEELS

High ultimate tensile strength (U.T.S.) is one of the mechanical properties of a dual phase steel, this can vary from as low as 90 ksi to as high as 150 ksi. The strength level of the Dual Phase steels is a function of the percentage martensite and the carbon content of the martensite [6]. Another feature of dual phase steels is the low yield stress; a dual phase steel of 90 ksi U.T.S. has a yield stress around 50 ksi. Other types of high strength steel with an equivalent ultimate tensile strengths tend to have a yield stress of about 70 ksi. Following from the above properties, the ratio of ultimate tensile strengths to yield stress (ultimate tensile strengths/yield stress ratio) for dual phase steels is also very high, ranging between 1.4 to 2.0. The importance of this particular property is discussed later.

The dual phase steels also have continuously yielding stress strain curves. High Strength Low Alloy steels tend to show luddering in the first few percent of strain. Luddering in a material limits the number of possible automotive applications, as it leads to "stretcher-strain" marks in the formed part. The most distinctive feature of the dual phase steel's stress strain curve is the very large increase in flow stress that occurs in the first few percent of strain giving very high initial work hardening rates.

The work hardening rate of dual phase steels throughout the tensile strain range is very high as indicated by the n values which are produced. The range of n values for dual phase steels varies between 0.18 and 0.22. Typical uniform elongation strains of 20% in tensile tests for 90 ksi ultimate tensile strength dual phase steels have been obtained, while total elongations of 30% or more have been recorded. [7]

2.3 MECHANISMS OPERATING IN DUAL PHASE STEELS

Dual phase steel is produced by the transformation of a ferrite-austenite microstructure to martensite-ferrite. Either the steel must be cooled rapidly to avoid the formation of pearlite (and bainite) or there must be alloying elements added which increase the hardenability of the steel enough so that pearlite or bainite are not formed at the slower cooling rate. When the transformation of the austenite phase to martensite occurs there is an increase in the volume. Since the martensite phase is constrained by the ferrite matrix around it, this increase in volume leads to the generation of residual stresses in the ferrite and the martensite. While the stresses in the martensite are still in the elastic region the ferrite matrix yields plastically. Using transmission electron microscopy it is possible to see the plastic regions in the ferrite which

surround the martensite because of the high density of dislocations which occur. [8] The ferrite grains tend to have relatively low dislocation density except in the areas in close proximity to the martensite-ferrite interfaces. These residual stresses in the martensite have been put forward as an explanation for lowering the effective yield stress of dual phase steels and producing the initial high work hardening rate [10]. The continuous yielding behaviour of dual phase steels has also been explained in terms of dislocations produced in the ferrite as a result of plastic deformation.

Another explanation put forward for the high work hardening rate is the effect of untransformed austenite changing to martensite under the applied strain. While this effect does occur [8] it is not the only mechanism since dual phase steel without any austenite still have a low yield point elongation and high initial work hardening. It has been suggested [9] that the high n values and work hardening throughout the tensile strain range can be explained in terms of the Composite theory put forward by Mileiko [11]. It has also been shown that considerable deformation also occurs in the martensite; this would not be expected from a high carbon untempered martensite phase. It is believed that the low impurity content (cleanliness) of the dual phase steel is responsible for a high interface

strength between the ferrite-martensite grain boundary and thus the two phases act as a composite material. The large amount of strain observed at fracture in the dual phase steels is also thought to be a function of the cleanliness of the steel.

These are the very basic concepts of dual phase steels. There are many phenomena related to the dual phase steels which are not fully understood. Further information on the mechanisms and properties of dual phase steels can be found in Refs. [12] to [18].

2.4 PRODUCTION OF DUAL PHASES STEELS

There are four basic ways of producing a dual phase steel. These are the Direct From The Mill (DFTM), Continuous Annealing Line (CAL), Continuous Annealing Process Line (CAPL), and the Batch Annealed (BA) techniques. The chemical composition of a dual phase steel is directly related to the method used for producing a dual phase steel. At present the Batch Annealed process is still in the experimental stage. A large amount of information on the production of dual phase steels is also found in Refs. [12] to [18].

CHAPTER III

MATERIALS

3.1 MATERIALS

Before beginning the study of the strain distributing ability of dual phase steels a preliminary study was undertaken in which a hot rolled dual phase steel (henceforth called DP1) was compared with three other steels; an interstitial free steel (IF) which is a low strength highly formable steel; an HSLA 80 steel which is a steel of similar ultimate tensile strength to the dual phase steel; and an HSLA 50 steel which is a steel of intermediate strength but with similar formability to the dual phase steel. The materials are described in detail below:-

(i) The Dual Phase Steel (DP1)

The dual phase steel DP1 is a "direct from the mill" type. The steel contains substantial additions of Mn, Si, Cr, and Mo, primarily to increase the hardenability and suppress the formation of pearlite. The chemical composition is given in Table I. The optical micrographs in Figure (1) indicate a fine, uniform microstructure with freedom from "micro


structural banding", while the micrograph obtained in the scanning electron microscope Figure (2) show a fine grain equiaxed ferrite with approximately 10% volume fraction of martensite, as determined by the linear intercept method.[19] The second phase is not equiaxed but aligned with the rolling direction: this probably indicates some influence of the rolling process on recrystallization during the cooling cycle. Table II shows the average grain sizes of the two phases.

(ii) The HSLA 80 Steel

This is a high strength, low carbon, pearlite-free steel which is produced by microalloying with niobium and controlled rolling to produce a fine grain ferrite containing a fine dispersion of niobium carbo-nitrides precipitated during cooling from the hot rolling process. The strength in this steel is obtained by a combination of fine grain size, solid solution hardening by manganese and silicon and the fine dispersion of carbo-nitrides. This steel was selected for comparison purposes because it has similar strength in the completed part to the dual phase steel, and it has been suggested [7] that dual phase steel could be substituted for the HSLA 80 to

obtain better formability at similar strength levels. The chemical composition of the steel is given in Table I. The micrographs, Figures (3) and (4), show a very fine though mixed grain size (see Table II), with some regions of highly elongated ferrite. Some banding of the microstructure is observed at low magnification which may be associated with the higher manganese content. At this level, segregation of the manganese may occur during solidification of the ingot.

(iii) The HSLA 50 steel



This is a medium strength, low carbon fine grained steel which is produced by microalloying with small amounts of zirconium and controlled rolling to produce a fine grain ferrite. The strength in this steel is mostly due to the fine ferrite grain size. This steel was selected for the comparison because its forming behaviour was thought to be similar to that of the dual phase steel [7,16]. The chemical composition of this steel is given in Table I; it is a similar alloy to the HSLA 80 except that the manganese and niobium contents are lower. The micrographs, Figures (5) and (6), show a uniform structure of fine equiaxed ferrite and some pearlite

(see Table II). In both the HSLA steels and the dual phase steel the sulphur content is reasonably low; however cerium or zirconium have been added to prevent the formation of stringer inclusions of manganese sulphide. The inclusion content is low and the shape of the inclusions are generally round except in the case of the HSLA-80 where some stringer inclusions were seen.

(iv) The Interstitial Free Steel

The fourth material is an interstitial free steel, designated I.F. It is a low strength steel, but it was chosen for the comparison because it has excellent formability in most sheet metal forming processes. This steel has very low alloy content (Table I) and the free carbon and nitrogen in the ferrite have been removed by first vacuum degassing and then adding titanium and niobium to form complex titanium or niobium carbo-nitride precipitates. The micrographs, Figures (7) and (8), show the structure to be a uniform distribution of coarse, equiaxed ferrite (Table II).

In subsequent experiments the DPl and high strength low alloy steels could not be used because the thicknesses

were too great for the experimental equipment. So four other dual phase steels and two aluminium alloys were obtained for the tests. The IF steel was also used in the shallow pan tests. The materials are described as follows:-

(v) The Dual Phase 2 (DP2)

This is an experimental dual phase steel supplied by the Republic Steel Company which is produced by the CAPL method. It has similar tensile properties to that of the hot rolled dual phase steel DP1. Mechanical properties are shown in Table III.

(vi) The Hi-form 80d Dual Phase steel (DP3)

This is a commercially available dual phase steel which is produced by the CAL method. Again this material has similar tensile properties to the dual phase steels DP1 and DP2 as can be seen from the mechanical properties in Table III.

(vii) Dual Phase steels DP4 and DP5

These are two experimental dual phase steels with similar properties to the preceding dual phase steels. Mechanical properties also given in Table III.

(viii) The 6010-T4 Aluminium Alloy

This is a higher strength Al-Mg-Si alloy in the solution treated and naturally aged condition. The yield stress is roughly that of the IF steel but the formability is much poorer than that of an IF steel. Mechanical properties are given in Table III.

(ix) The 7146 Aluminium Alloy

This is one of the newer aluminium alloys which is used for automotive parts. The formability of this material is very poor compared to the 6010-T4 alloy. The mechanical properties are given in Table III.

3.2 DESCRIBING FORMABILITY

Formability has been described with the aid of many different tests and indices [20]. Simulative tests such as the Fukui, or the Erichson test [21] have been used to determine formability for some limited geometries. The disadvantages of simulative testing is that the test is only useful when comparing it to a real application of similar geometry and friction conditions. This and other problems have stopped the wide spread use of specific simulative tests. One of the most useful ways of describing material formability is with the use of Forming Limit Curves (FLCs) developed by Backofen, Keeler and Goodwin [22,23]. Forming

limit curves are generated by stretching material over a domed punch under a range of strain conditions. The strain condition in a sheet is described by the ratio of the two principal strains in the plane of the sheet,

$$\epsilon_1 = \beta \epsilon_2 \quad (3.1)$$

It is assumed the process is one of simple proportional straining. The limit strains at necking are then plotted in the principal strain space.

Forming limit curves indicate the peak strains that can be tolerated in a part but do not account for the strain distributing ability of a material. To describe this, various indices based on the tensile test have been used. The simplest way to describe the material work hardening with a single value is the strain index n which is determined by fitting the Ludwik equation to tensile stress strain curves, i.e.,

$$\sigma = K (\epsilon)^n \quad (3.2)$$

The use of instantaneous n values n^* and the normalized slope $\frac{1}{\sigma} \frac{d\sigma}{d\epsilon}$ as functions of strain have also been suggested for describing formability. Even though the strain hardening capability can be described by these parameters

the prediction of strain distribution from these parameters is not possible due to the influence of other factors such as geometry of the tooling and the friction conditions.

There has been little work describing the friction conditions which occur between the punch and the workpiece in a pressing operation and friction coefficients calculated from the usual slider tests may not be appropriate for pressing operations. The work of Duncan et al. [24] suggests that there are other parameters which affect the friction in the pressing type of operation which are not present in slider tests. Clearly more quantitative data on friction in pressing operations is required if material strain distributing ability and formability are to be accurately determined.

3.3 FORMABILITY IN SHALLOW PARTS

In some shallow parts such as the hoods or door panels for automobiles it is necessary to produce the part so that plastic straining occurs throughout the whole region. This is done to control shape and stiffness and to minimize springback problems. This type of part is produced by a pure stretching type of operation. A sheet of material is gripped in a bender or die ring and then stretched over a punch to the required shape. The clamping die is such that any drawing in of the sheet is minimized and carefully

controlled. Draw beads are often used to facilitate the correct amount of draw in. A difficulty in making this type of part is producing enough plastic strain across the face of the punch without having the material fail in the side wall region between the punch and the clamping die. A material must have a certain amount of work hardening to overcome the friction around the punch nose radius and produce the necessary plastic strain over the punch face required for a satisfactory part.

While the forming limit curves will show how much strain a material can undergo before failure in the side wall region of a shallow part there are very few indicators of how well a material can distribute the strain against the friction around the punch nose. Although it is related to the material's work hardening it is very difficult to define this material property. The use of the some tensile test parameters do give some indication but not in as quantitative manner as would be preferred.

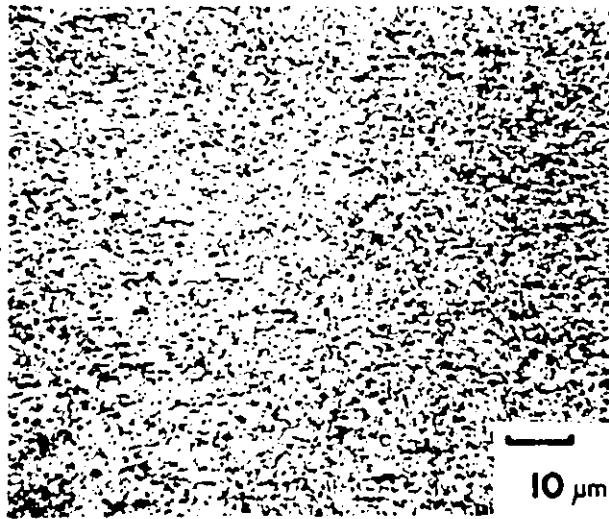


Fig. 1a - Optical Micrographs of the
dual phase steel X120

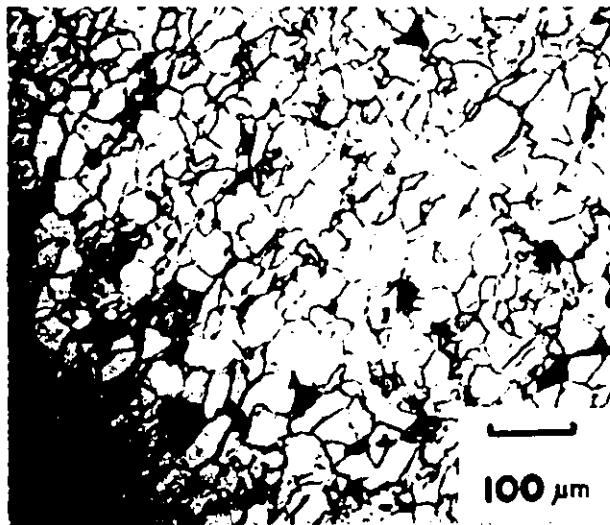


Fig. 1b - Optical Micrographs of the
dual phase steel X900

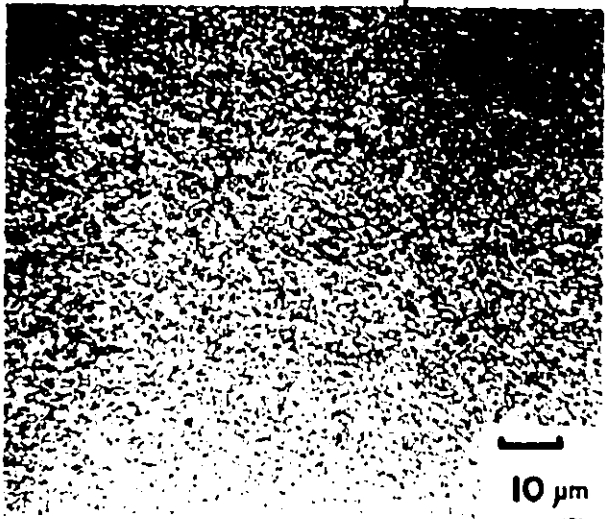


Fig. 2a - Optical Micrographs of the HSLA 50 steel X120



Fig. 2b - Optical Micrographs of the HSLA 50 steel X900

R

A hand-drawn sketch showing a grain boundary or defect structure, consisting of several irregular, interconnected shapes.

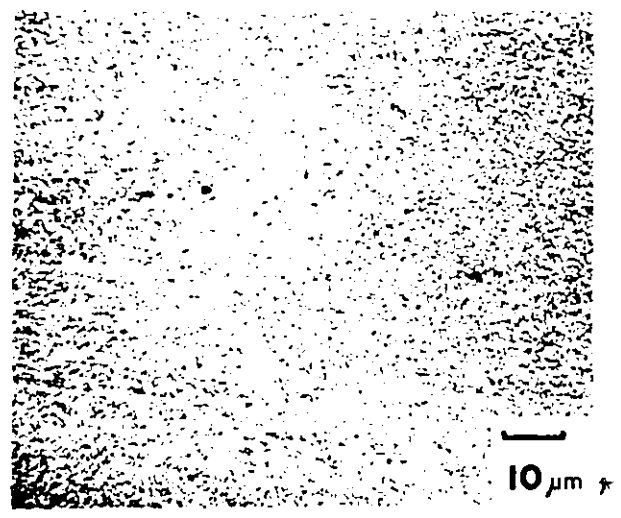


Fig. 3a - Optical Micrographs of the HSLA 80 steel X120

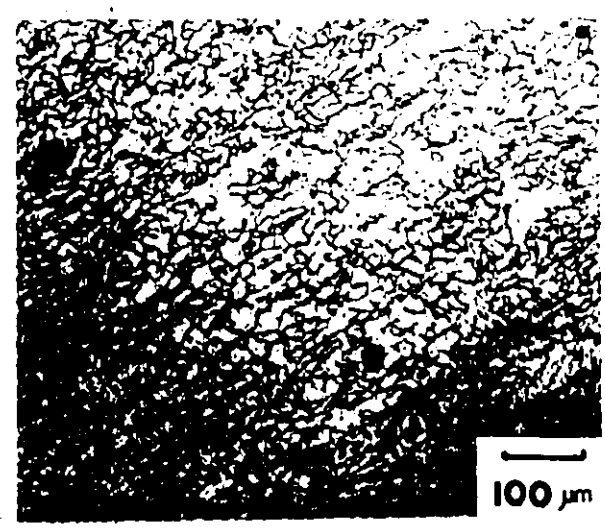


Fig. 3b - Optical Micrographs of the HSLA 80 steel X900

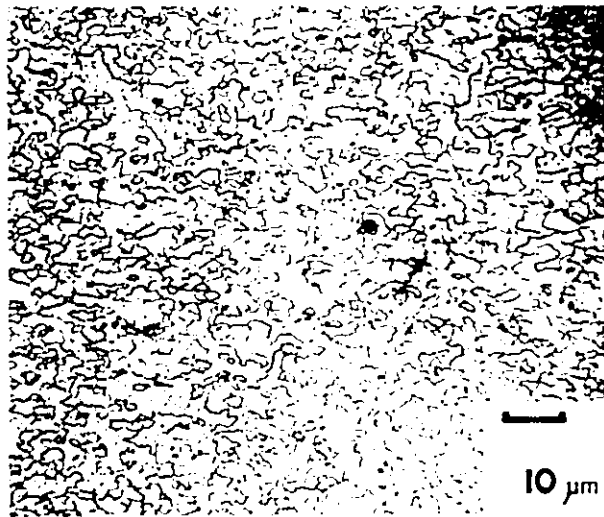


Fig. 4a - Optical Micrographs of the
I.F. steel X120

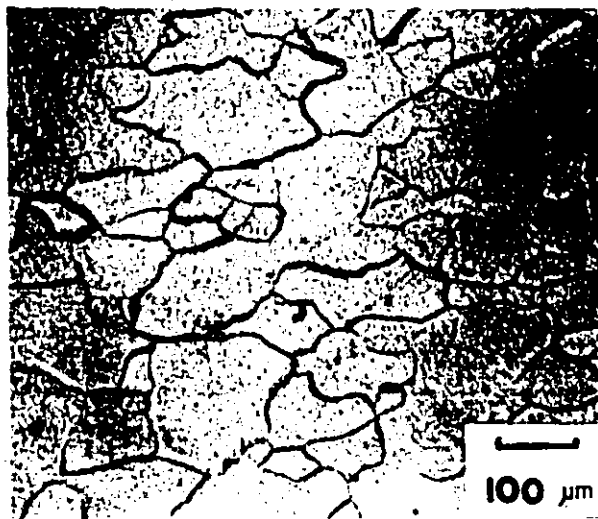


Fig. 4b - Optical Micrographs of the
I.F. steel X900



Fig. 5 - Scanning Electron Micrographs of the D.P. steel

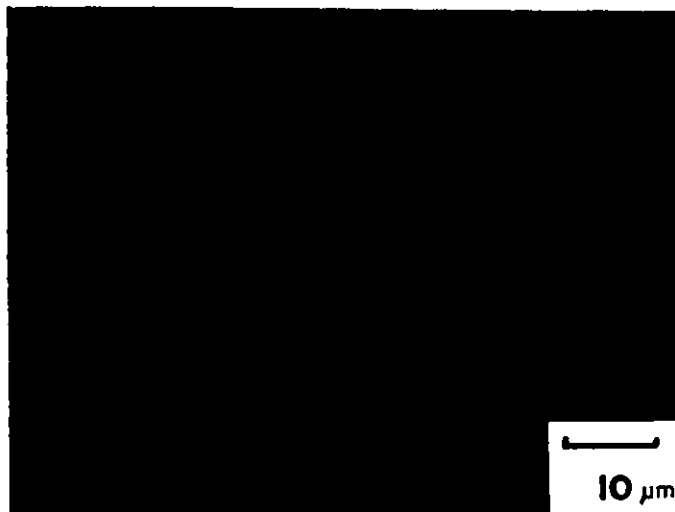


Fig. 6 - Scanning Electron Micrograph of the HSLA 50 steel.

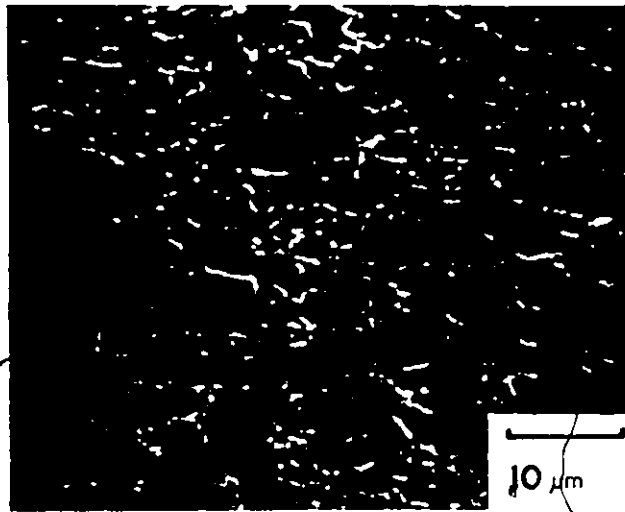


Fig. 7 - Scanning Electron Micrograph
of HSLA 80 steel

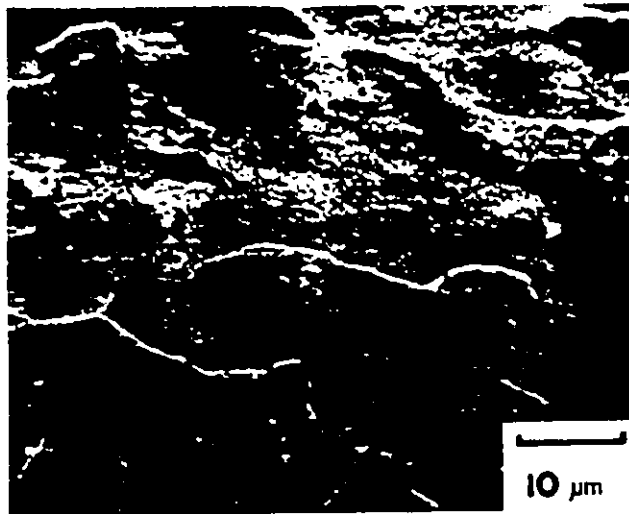


Fig. 8 - Scanning Electron Micrograph
of the I.F. steel

TABLE I
Composition of Materials

	C	Mn	Si	P	S	Nb	Cr	Al	Mo	Ce	N	Zr	Ti
D.P.	.04	1.37	1.37	.021	.010	-	.57	.18	.38	.01	.009	-	-
I.F.	.018	.18	.02	.008	.011	.06	-	.04	-	-	-	.004	.04
HSLA 50	.10	.48	.25	.009	.009	.006	-	.06	-	-	.007	.07	-
HSLA 80	.08	1.51	.27	.008	.012	.08	-	.05	-	-	.011	.09	-

TABLE II
Grain Size*

MATERIAL	SIZE (μm)
D.P.	4.73 (Ferrite)
	1.51 (Martensite)
I.F.	35.0
HSLA 50	4.9
HSLA 80	2.76

*Determined by linear intercept method

TABLE III

MATERIAL	Thickness (inches)	Yield Stress (ksi)				U.T.S. (ksi)	K (ksi)	n	YPE			R.A.	e_{1f}	$\frac{TS}{YS}$	μ	ldo OJc 23
		0.2t	2t	3t	5t				t	t	t					
IF	0.040	16.0	26.1	29.9	35.3	46.7	95.0	.31	0	28	42	91.9	2.51	2.9	0.28	18.0
HSLA 50	0.125	51.3	51.0	55.0	60.1	67.8	114.0	.20	2.2	20	35.7	68.0	1.14	1.3	-	10.6
HSLA 80	0.090	84.5	83.7	85.3	89.7	94.2	142.0	.14	2.8	14	24.5	56.0	0.82	1.1	-	6.3
DP1	0.134	53.3	60.3	74.4	79.7	93.0	160.4	.21	0	20	30	63.7	1.01	1.7	-	12.0
DP2	0.037	38.5	-	-	-	87.5	195	0.31	0	20	-	-	-	2.27	0.15	15.2
DP3	0.046	52.5	-	-	-	87.5	149	.195	0	17	-	-	-	1.67	0.15*	9.5
DP4	0.031	67.0	-	-	-	94.3	152	.163	0	16	-	-	-	1.41	0.20	8.0
DP5	0.030	52.0	-	-	-	93.5	168	.21	0	18	-	-	-	1.8	0.23	11.0
6010	0.042	28.4	-	-	-	47.4	57	.21	0	25	-	-	-	1.67	0.23	7.0
714G	0.084	16.0	-	-	-	26.9	38.7	.116	0	14	-	-	-	1.70	0.30	8.5

* 0.065 with oil and polyethylene lubrication

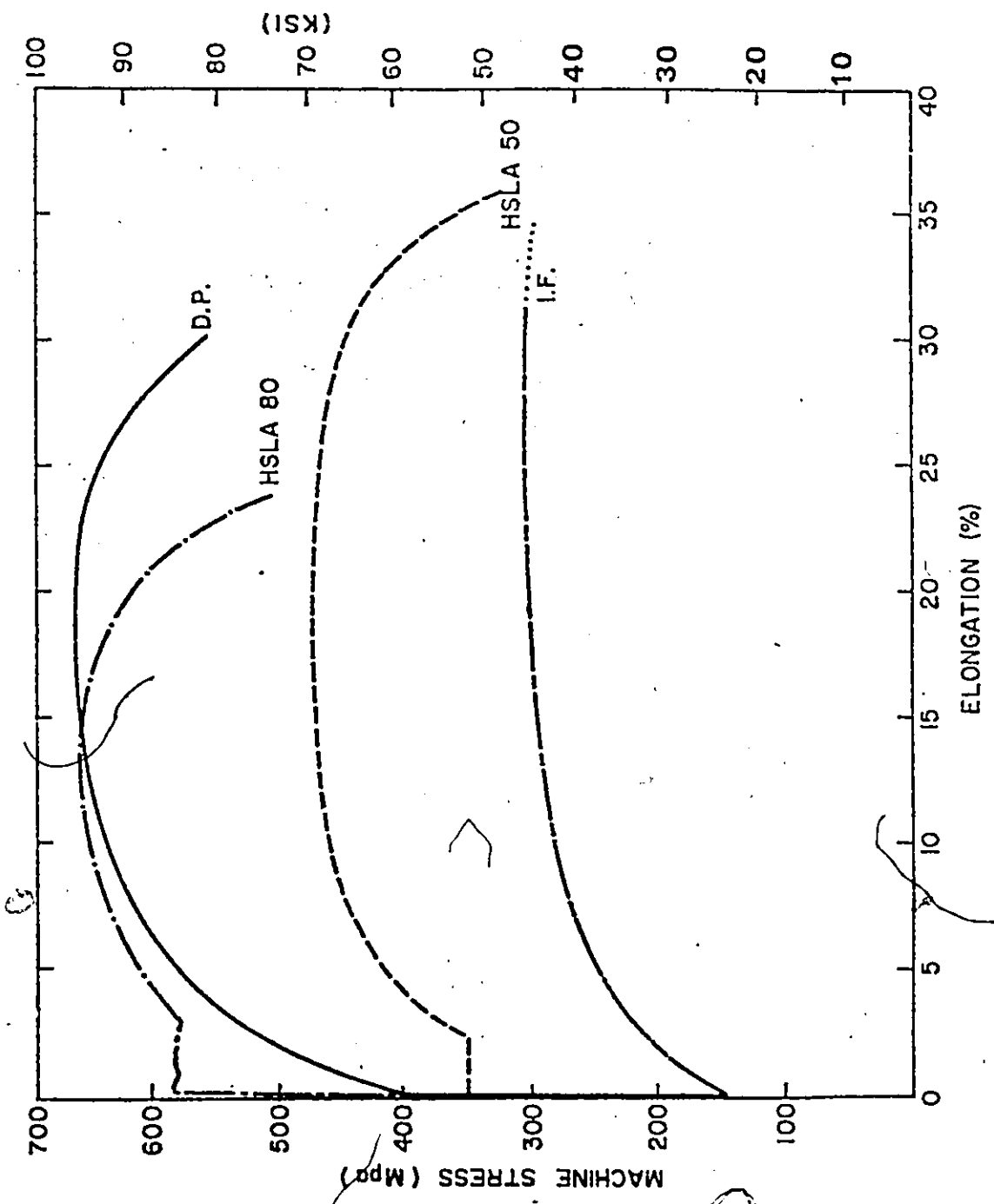


Fig. 9 - Typical load-extension curves

CHAPTER IV
PRELIMINARY WORK

4.1 TENSILE TESTS

Tensile tests were performed on all of the materials except for the dual phase steels DP4 and DP5. The tensile data for these two materials was supplied by the Inland Steel Company. Extensive testing was done on the DP1, the HSLA steels, and the IF steel in preliminary work.

Standard 2" gauge length tensile tests were performed on these materials and the results shown in Figure (9). The crosshead speed was 0.2 in./min. Both the HSLA steels exhibited 3-4% yield point elongation. The IF steel showed a large, 47%, total elongation while that of the dual phase steel was significantly greater than the HSLA 80 but less than the HSLA 50; the dual phase and HSLA 80 had similar tensile strengths.

The tensile parameters are summarized in Table III. The flow stress at various small plastic strains are given as these are required in certain commercial specifications for dual phase steel. In addition, tests were performed in the 0°, 45° and 90° direction and it was found that the planar anisotropy of the dual phase steel was very small.

To assess the variability of the dual phase material, ten tests were performed in the rolling direction. The variation in flow stress in the first 3% of plastic strain was about 15%, while the range in ultimate tensile stress was much smaller.

In addition to measurements of uniform and total elongation, measurements were made of the reduction of area at fracture, R.A.%, by measuring the cross-sectional area of the fracture surface in the tensile samples. The reduction of area for the dual phase steel is greater than that for the HSLA 80, but less than that for the HSLA 50.

The true stress strain curves are shown in Figure (10). The n and K values for the steels were obtained by fitting a power law to the true stress-strain values over the strain range of 0.01 to 0.2; these are given in Table III. The fit was good for the HSLA steels but not for the IF or DP steels, where a "double n " behaviour with a higher n -value at low strains was seen. This has been observed in other dual phase and interstitial free steels [25,26]. The results given are therefore for an average n and K value and illustrate in general the high work hardening behaviour of the interstitial free steel, the similar work hardening behaviour of the HSLA 50 and DP steels and the lower work hardening behaviour of the HSLA 80 steel.

In addition to the conventional single-speed tensile

tests, "step change" tests were performed in which the speed of the tensile test machine was stepped up instantaneously from 0.2 to 2 in./min. and, after a short time, returned to the lower speed. When the speed was increased, the flow stress increased, and from measurements of the flow stress before and after the increase in speed, the strain rate sensitivity, m , was determined, where

$$m = \frac{\log (\sigma_1 / \sigma_2)}{\log (\dot{\epsilon}_1 / \dot{\epsilon}_2)} \quad (4.1)$$

The value of m plotted against strain is shown in Figure (11). It is notable that the dual phase steel shows a considerably higher strain rate sensitivity than the other high strength steels, particularly at small strains.

Tensile tests were also done on the materials used in the shallow pan experiments to be described below. The tensile data for the DP4 and DP5 Dual Phase steels was provided by the Inland Steel Company. The n and K parameters and some other tensile parameters are given in table III. Strain rate sensitivity tests were not done on these materials as the strain rate sensitivity was not used in the modelling work of later sections. Figures (12) to (18) show the true stress strain curves for these materials.

4.2 HYDRAULIC BULGE TEST

In the hydraulic bulge test the material is stretched under biaxial tension by applying a uniform pressure to one side of a circular diaphragm of the sheet. From readings of the pressure applied, radius of curvature and extension at the pole, a plot of membrane stress versus thickness strain is determined [27]. Only some of the materials were tested in biaxial tension, these are the DP1, DP2, DP3, HSLA 80, and the IF steels. For the DP1 Dual Phase steel and the HSLA 80, the original thicknesses (0.134" and 0.090") were too great for the capacity of the bulge tester, so material was ground from each side leaving the middle section of the steel approximately 0.050" thick, before testing. (A tensile sample was also taken from the DP steel to confirm that the grinding process had not significantly altered the properties of the steel.) In Figures (19) to (21) the stress strain curves from the bulge test as well as the tensile stress strain curves are shown.

It can be seen that the bulge test gives stress-strain information at strains far greater than is obtainable with the tensile test, since the tensile test is limited by the formation of a diffuse neck at moderate strains. It can also be seen that the tensile test curve does not always superimpose onto the bulge test curve. This is because the curve calculated from the bulge test is equivalent to the

through-thickness properties of the sheet while the tensile test measures strain in the plane of sheet, in the direction of the applied load. The difference between the two curves is thus due to the normal anisotropy of the material [28]. The results indicate that the HSLA 80, DP2, DP3, and IF steels are stronger in the thickness direction than in the plane of the sheet, however in the case of the HSLA 80, the tensile curve is for a full thickness sample.

While an increase in the strength level is observed in some bulge tests as compared to tensile tests, the shape of the stress strain curve does not alter very much. From this it is assumed that the plane strain stress strain curve is similar in shape to that of the simple tension condition. A common method of characterising the stress strain curve is to fit the data to the Ludwik equation, see equation (3.2). The strain hardening index n is quite often used to describe the shape (work hardening) of a stress strain curve. The tabulated values of n in table III were calculated using a curve fitting program on the computer from the tensile data but the statistical analysis of the fit showed the results to be a poor fit. This was due to the small range of strain found in the tensile test.

4.3 WORK HARDENING AND STRAIN DISTRIBUTING ABILITY

As well as using the strain index n to describe work hardening plots of normalized slope, $1/\sigma \, d\sigma/d\epsilon$ and the instantaneous n value, n^* as functions of strain are shown in Figures (22) and (23) to (25) respectively for the DP1, DP2, DP3 steels using the bulge test results. The two parameters, $\frac{1}{\sigma} \frac{d\sigma}{d\epsilon}$ and n^* can be shown to be related as follows

$$n^* = \epsilon / \sigma \, d\sigma / d\epsilon \quad (4.2)$$

It can be seen from the n^* curves that the n -value is not a constant for all materials and therefore the use of the Ludwik equation (3.2) is not a suitable description of the stress strain curve if an accurate fit is required. Figure (26) shows the comparison of the IF, DP1, and HSLA 80 normalized slope. The higher the curve the better the formability so the IF material has the highest formability and the HSLA 80 has the lowest of the three.

4.4 RANKING OF MATERIALS

In shallow parts strains range from a few percent to 40% throughout the part and it is not always known what section of the normalized slope curve or the n^* curve is related to the strain distributing ability of the material in

this type of part. To form a satisfactory shallow part it is usually necessary to have a minimum of two percent plastic strain throughout the part to get the required stiffness and shape control while minimizing springback problems.

Because these parts are produced by stretching over a punch as described in chapter three it is also necessary that the material have a high rupture strain in the side wall as well as the strain distributing ability necessary to generate the 2% or more strain over the face of the punch. Forming limit curves can be used to determine the material's rupture strains in the side wall, but the strain distributing ability of materials has yet to be characterized properly.

There are several parameters based on the tensile test which can be used as indicators of material strain distributing ability. The most commonly used parameter is the strain index n from the Ludwik equation (3.2). Another common parameter used is the uniform strain, ϵ_u or strain at maximum load as taken from the load extension graph of the tensile test. The uniform strain is very convenient to measure and from the Considère analysis should be equal to the strain index n . Another parameter is the U.T.S./Y.S. ratio from the tensile test which is also easily determined. There is some experimental correlations between all three of these parameters and the press performance of materials.

Though the correlation indicates that as the n value, the uniform strain ϵ_u and the U.T.S./Y.S. are increased there is better performance from a material; the scatter of experimental results is such that only a very general rating of materials is possible. A possible rating index could be derived from the normalized working hardening curves; for example the value of normalized work hardening at some particular strain. Just what strain to use is not known but a value of 2% seems to be a reasonable guess since this is the minimum strain required over the punch face.

Figure (27) shows the four parameters, the n value, the uniform strain ϵ_u , the U.T.S./Y.S. ratio and the $\frac{\epsilon dg}{\sigma de}$ value at 2% strain as bar charts for all the materials examined. As can be seen from the graphs there is disagreement between the four parameters as to the relative ranking of materials.

Several interesting points can be observed regarding the various parameters for the dual phase ~~table~~. While the DP2 steel appears to have an n value similar to that of the IF steel this may be misleading. The plot of instantaneous n , n^* for the bulge test shows a drop in value at higher strains. The high n value from the tensile test is due to the extremely high work hardening in the first few percent, and the fact that tensile strain range is too small for a good fit of the Ludwik equation (3.2).

This material is a good example of the danger of relying only on tensile data. The DP4 steel is another case where the n value may be misleading; bulge data not shown here indicate higher n values at higher strains.

While it would be possible to look at other tensile parameters such as Reduction in Area for rating materials these are not considered since there is no evidence indicating any direct connection between strain distributions and these parameters. One exception is the strain rate sensitivity, n which does have a minor effect on strain distribution as shown by the work of Conrad [29] and Ghosh [30].

The usefulness of the various rankings in Figure (27) is questionable since each parameter has some disadvantages; these are:

For the U.T.S./Y.S. ratio only the yield point, 0% plastic strain and the strain at maximum load ϵ_u are used to determine the value of the U.T.S./Y.S. ratio. Neither of these strains are directly related to the straining in a shallow pan.

The uniform strain parameter is only one point on the stress strain curve which also does not directly relate to the straining in the part. To measure the uniform strain accurately is difficult

in some materials as can be seen from the load extension graphs in Figure (9). The strain rate sensitivity also effects the value of the uniform strain.

The value of the normalized work hardening parameter, although taken at a strain related to the strains in a shallow part, is still only taken at one strain. The influence of the strain in the side wall is not allowed for.

The n value is an averaging parameter over the strain range 0% to 20% but may not be a good fit and does not take account of strains higher than those in the tensile test which occur in the side wall regions of shallow parts.

Friction plays a part in determining the amount of face strain but none of the above parameters include the influence of friction.

There is some change in the ranking for some materials (6010, 7146, DP1, DP5) depending on the parameter used. Since the parameters are measured differently and suffer from the disadvantages described above discrepancy

among the rankings is not unexpected. There is the question as to which one of these parameters is the better indicator of shallow pan formability and just how accurate is it.

What is required is some indicator which includes the influence of friction, minor changes in the shape of the stress strain curves over the range of strains that are seen in shallow parts, and is directly related to the amount of face strain found in a shallow part. A test which simulates a shallow pan and in which the bottom strain is measured experimentally and used as an indicator for ranking material would be a good method of determining shallow pan formability.

It would be advantageous to know how the geometry, friction and material parameters interrelate to influence the amount of face strain. For a better understanding of the interrelationship of these parameters an analytical modelling technique was developed and is described in the following chapter.

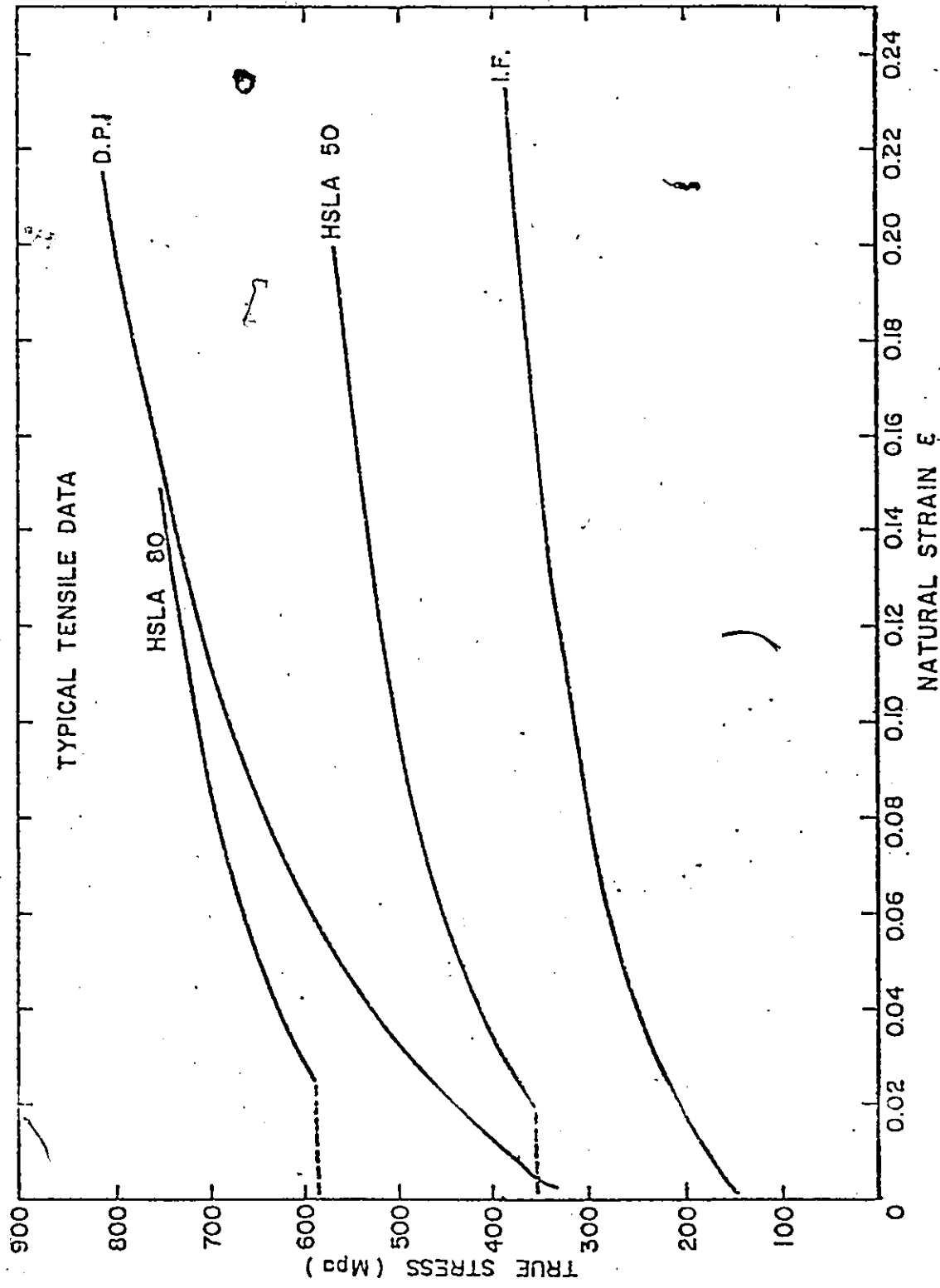


Fig. 10 True-Stress - strain curves from tensile tests

f

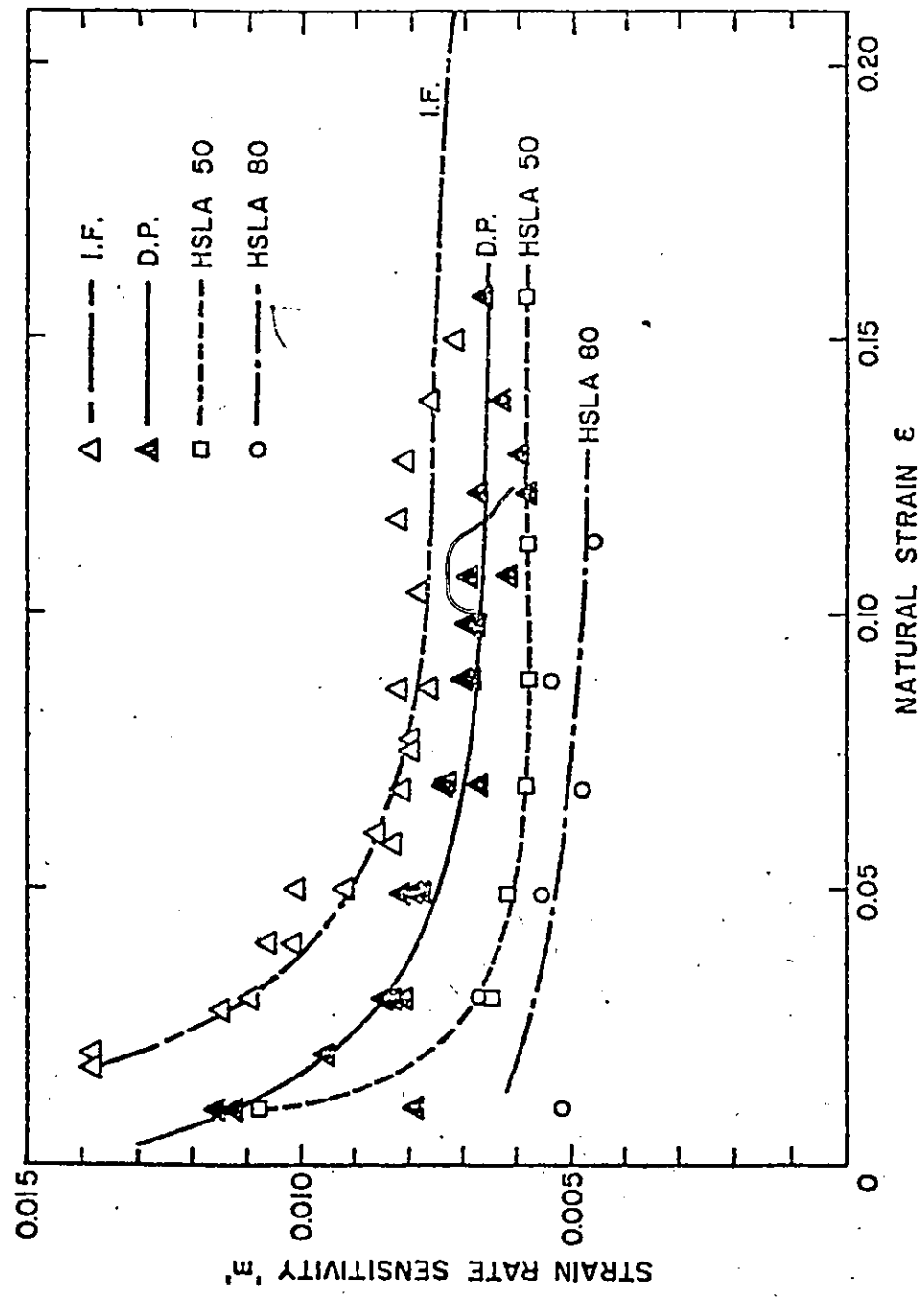


Fig. 11 - "m", strain rate sensitivity versus strain

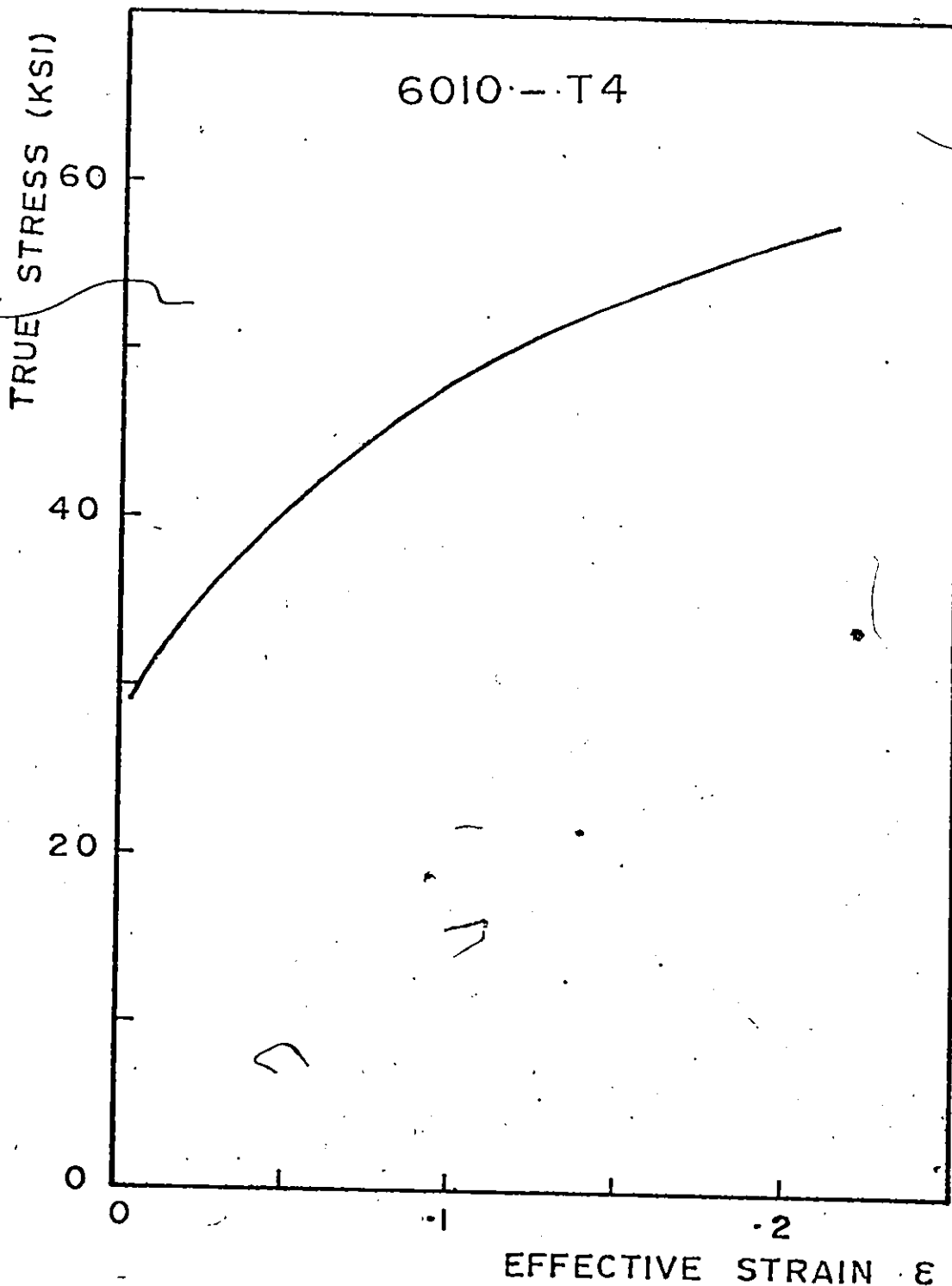


Fig. 12

- True Stress-Strain curve for the 6010-T4 material

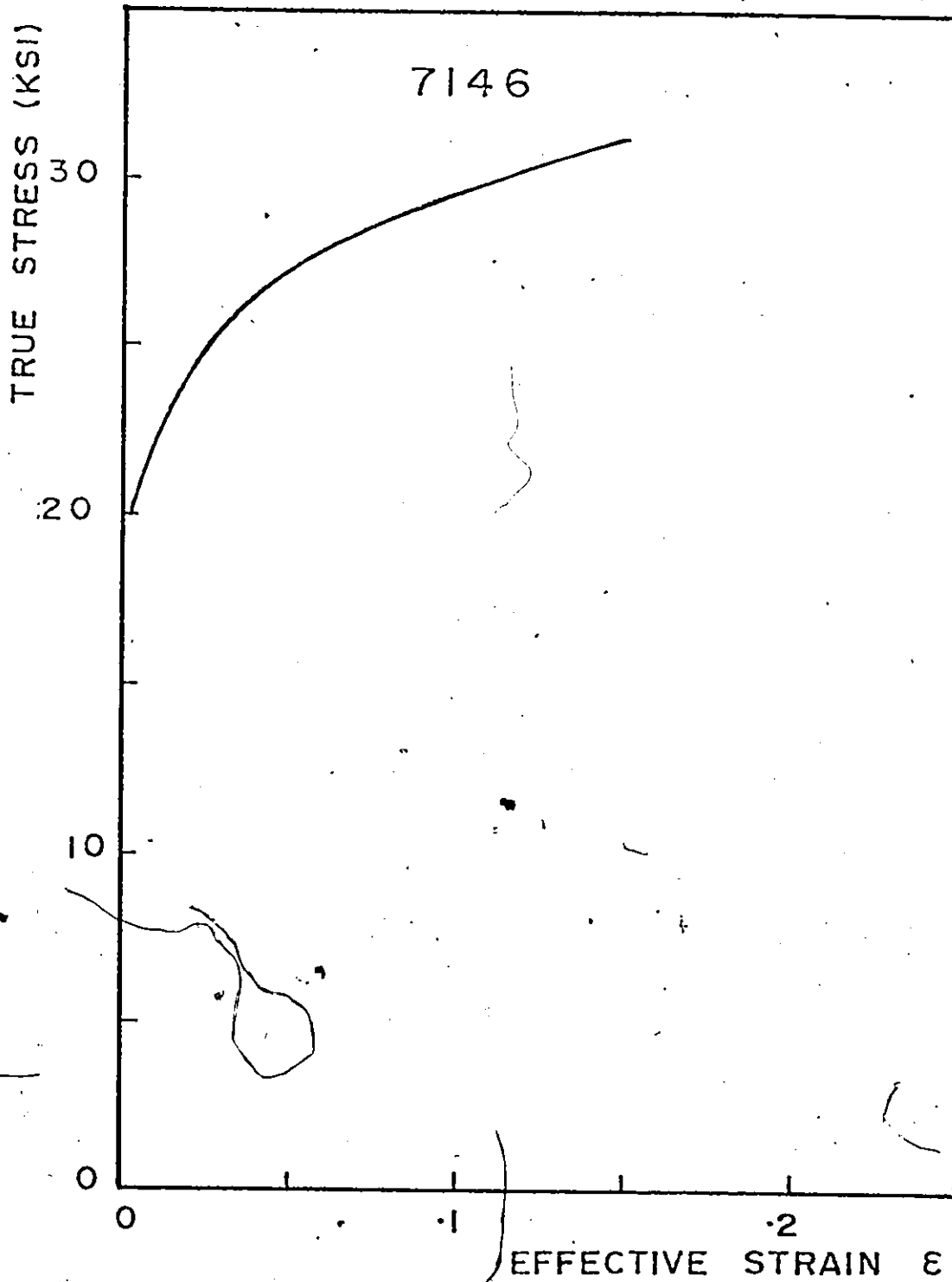


Fig. 13

- True Stress-Strain curve for the
7146 material

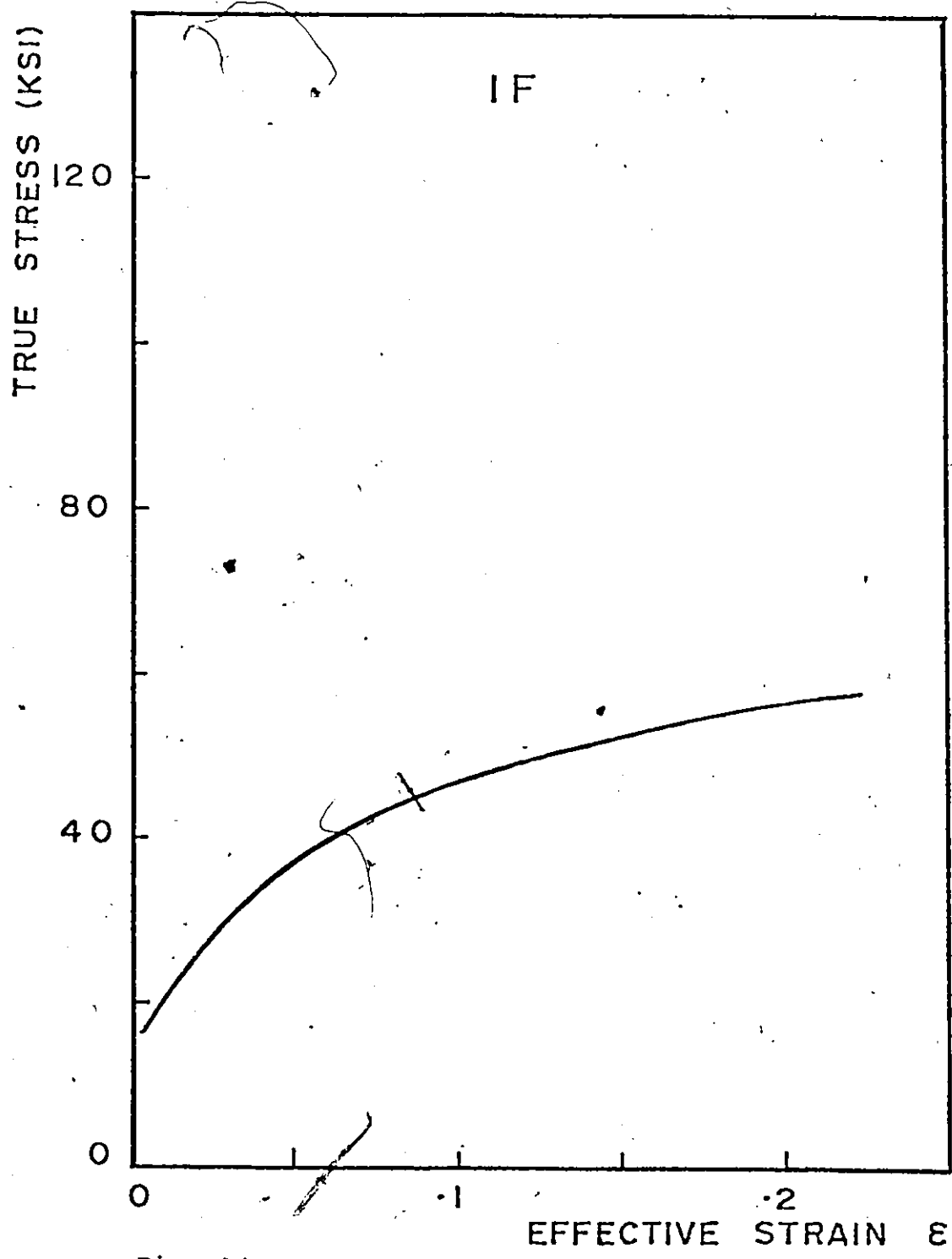


Fig. 14 - True Stress-Strain curve for the IF material

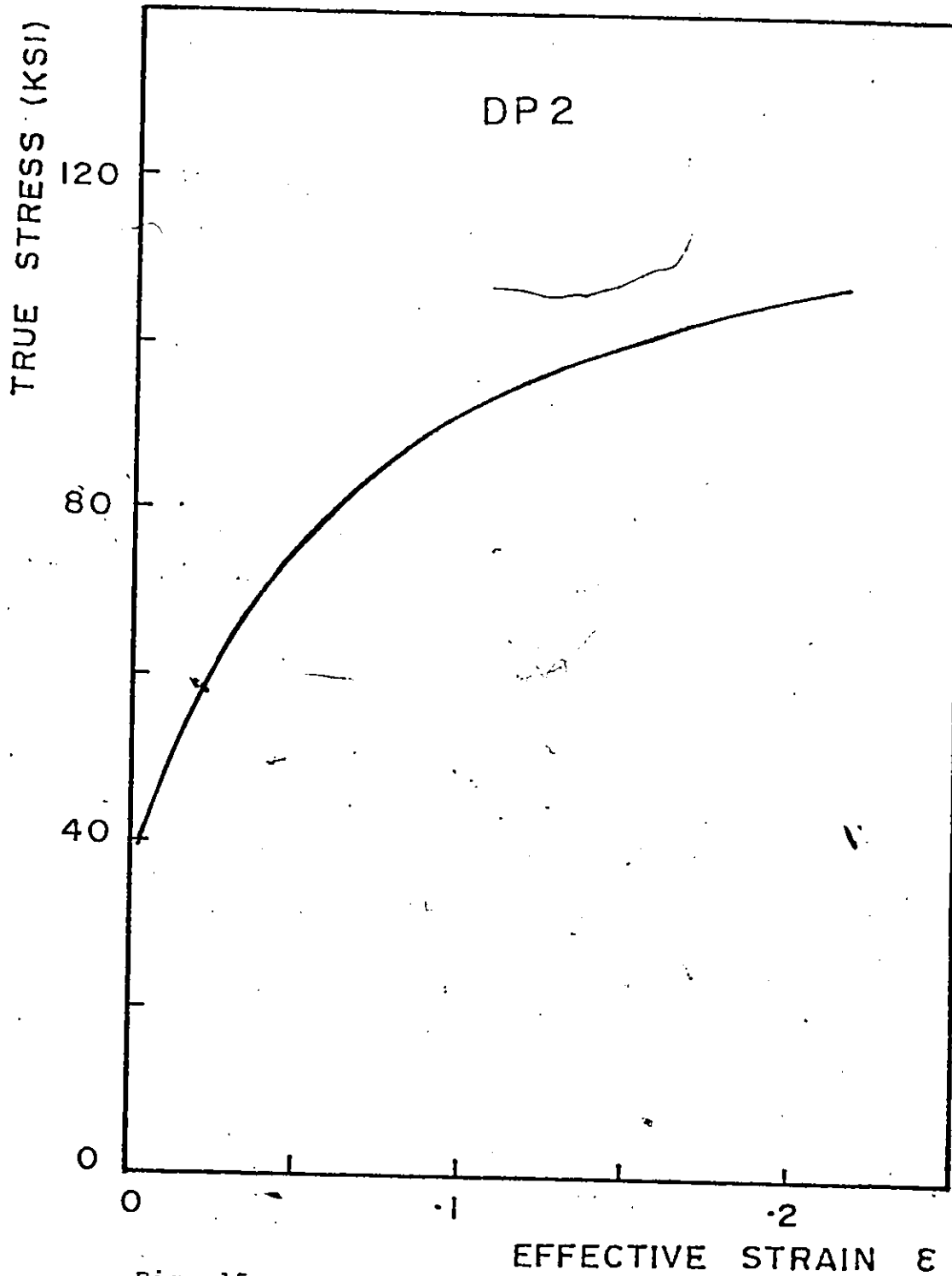


Fig. 15 - True Stress-Strain curve for the DP2 material

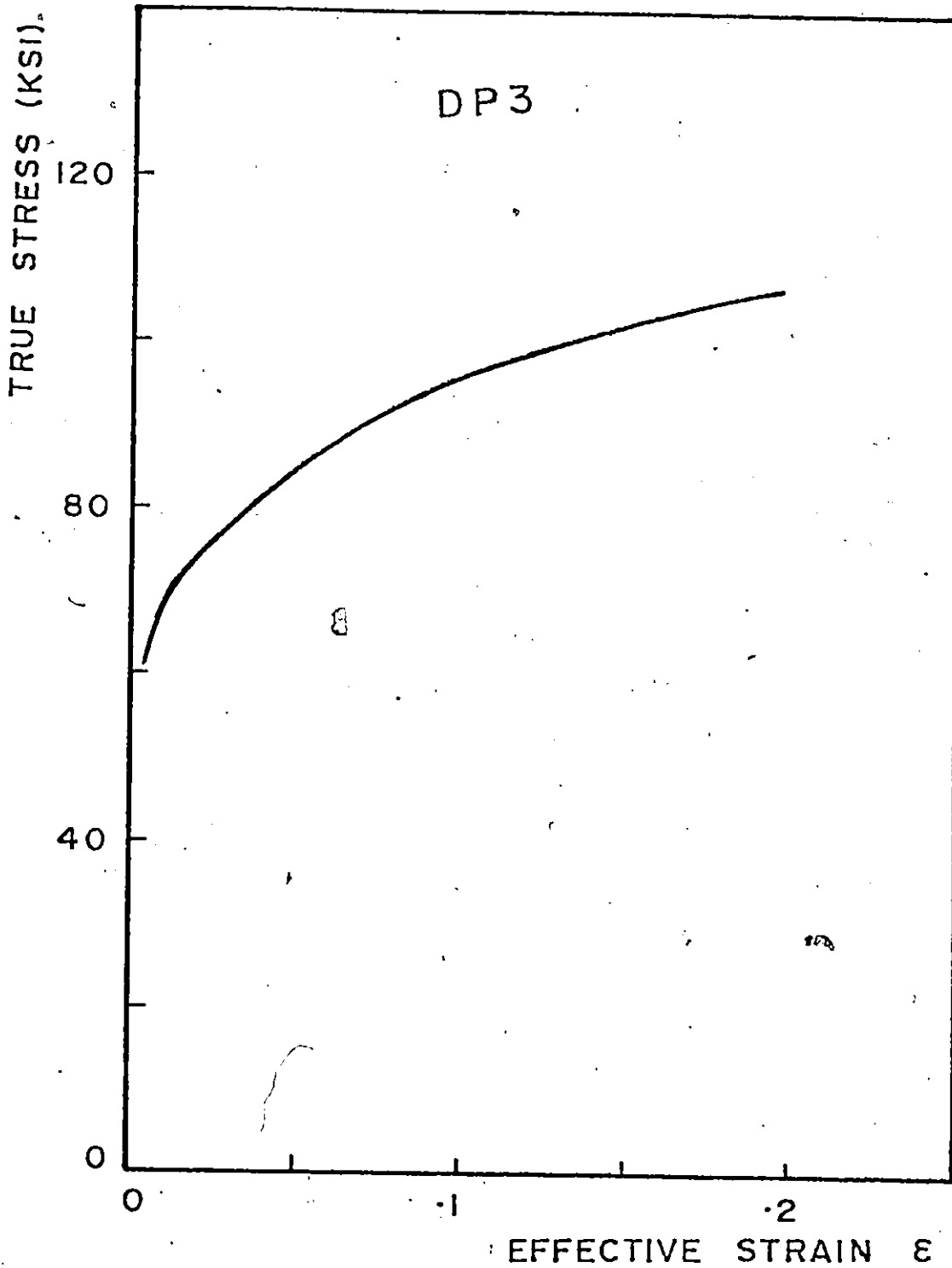


Fig. 16

- True Stress-Strain curve for the DP3 material

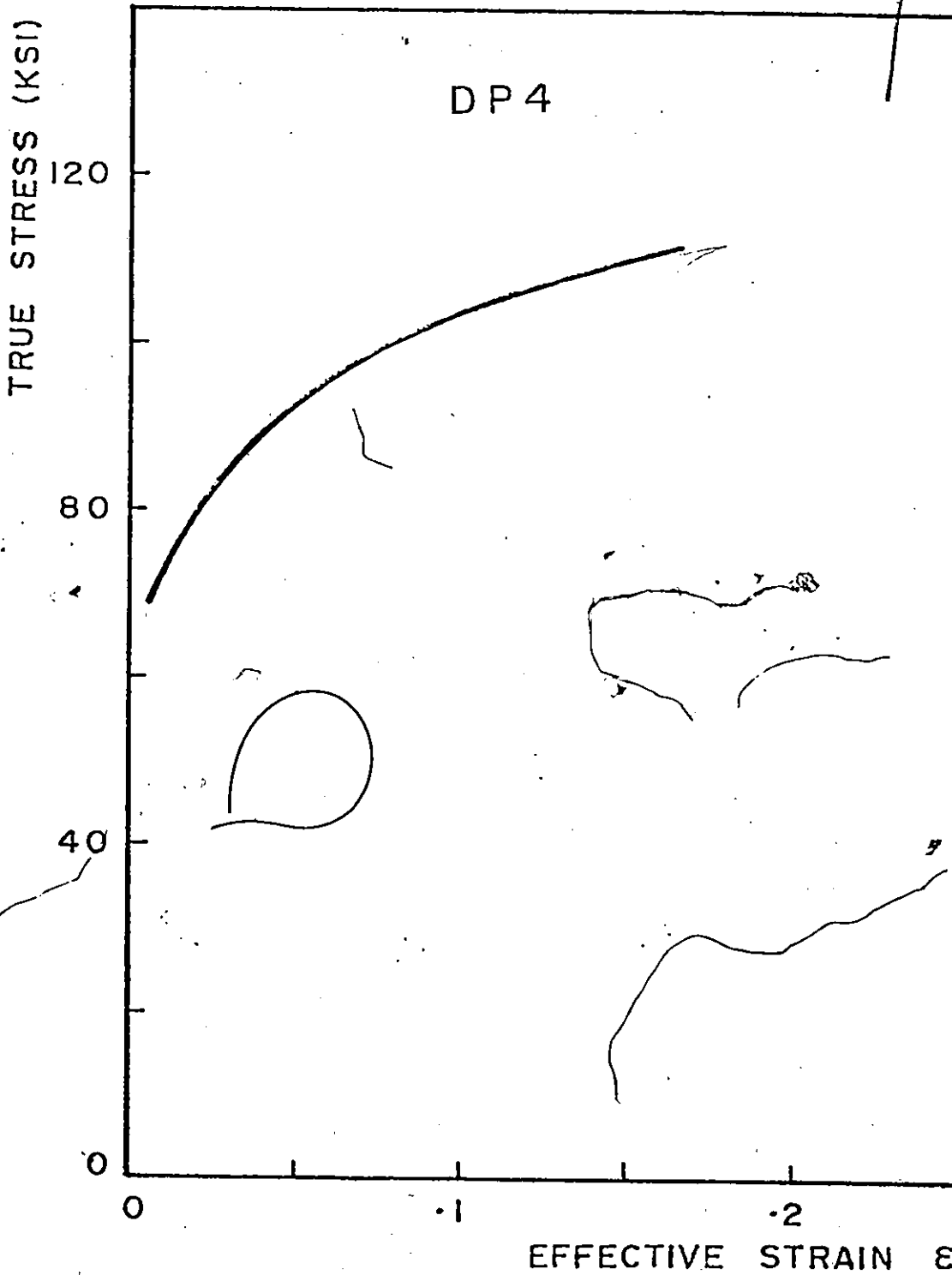


Fig. 17

- True Stress-Strain curve for the DP4 material

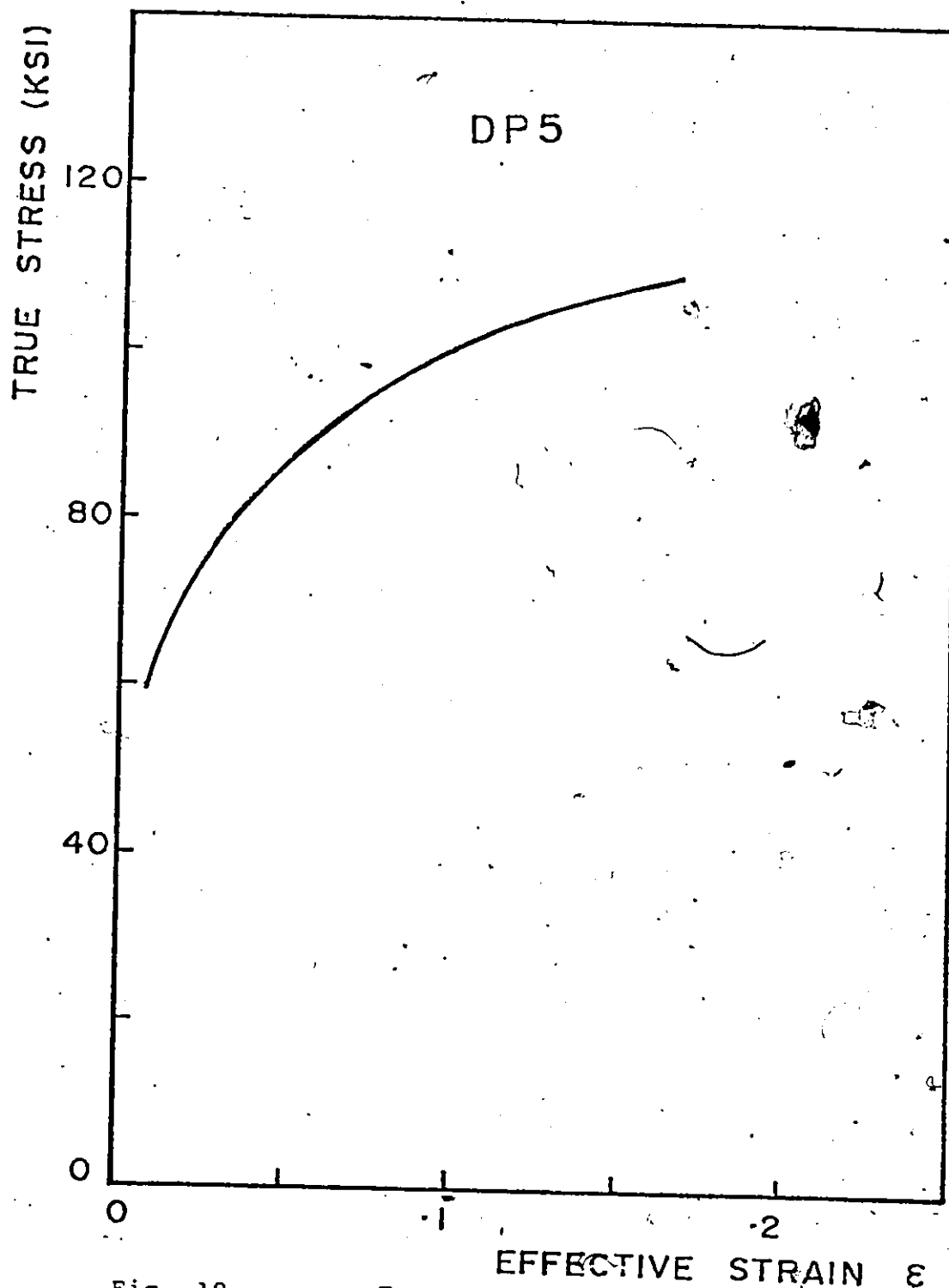


Fig. 18 - True Stress-Strain curve for the DP5 material

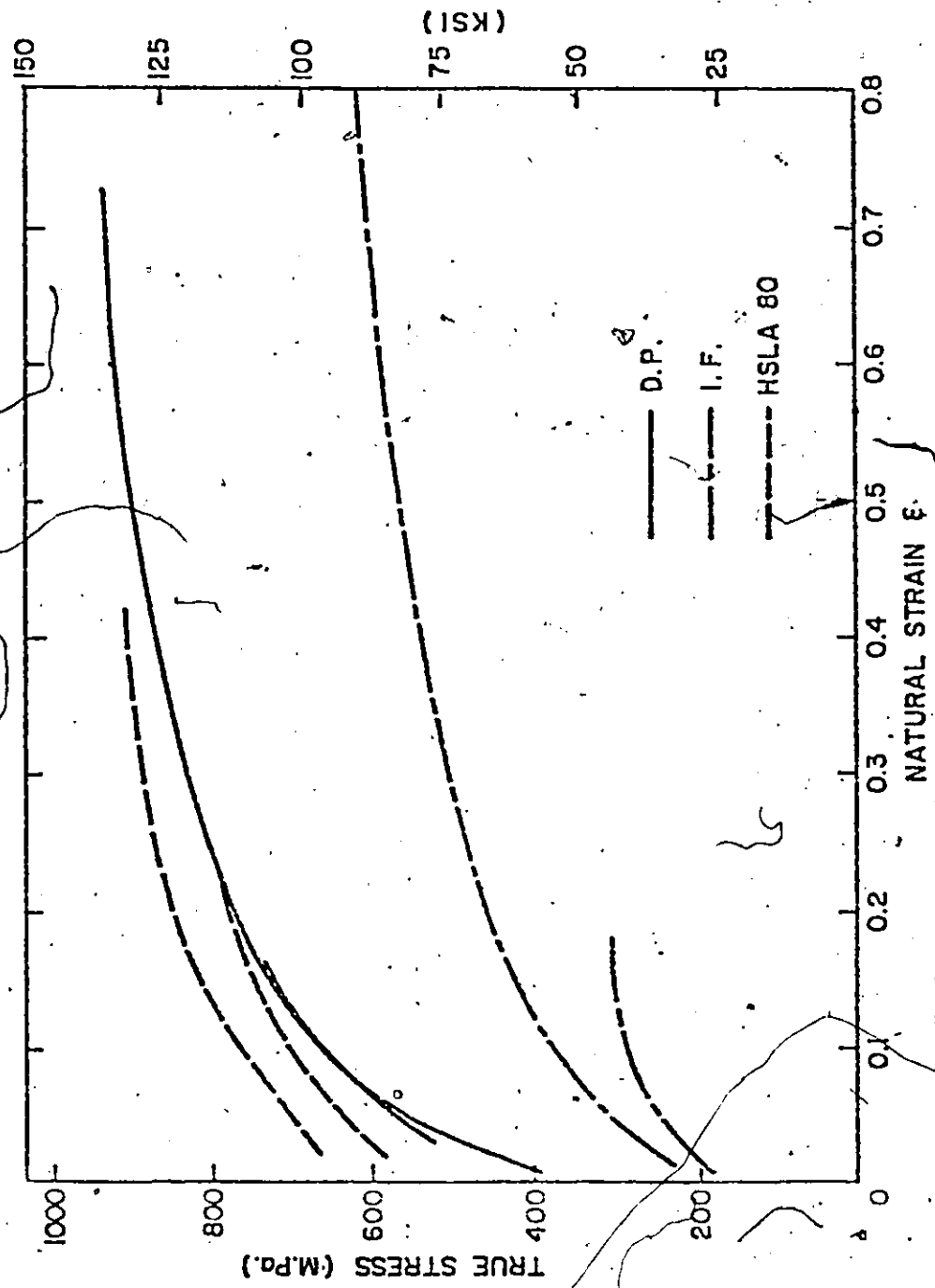


Fig. 19 - Stress-Strain curves from the bulge test for the D.P., I.F. and HSLA 80 steels. Lower curves are tensile test curves.

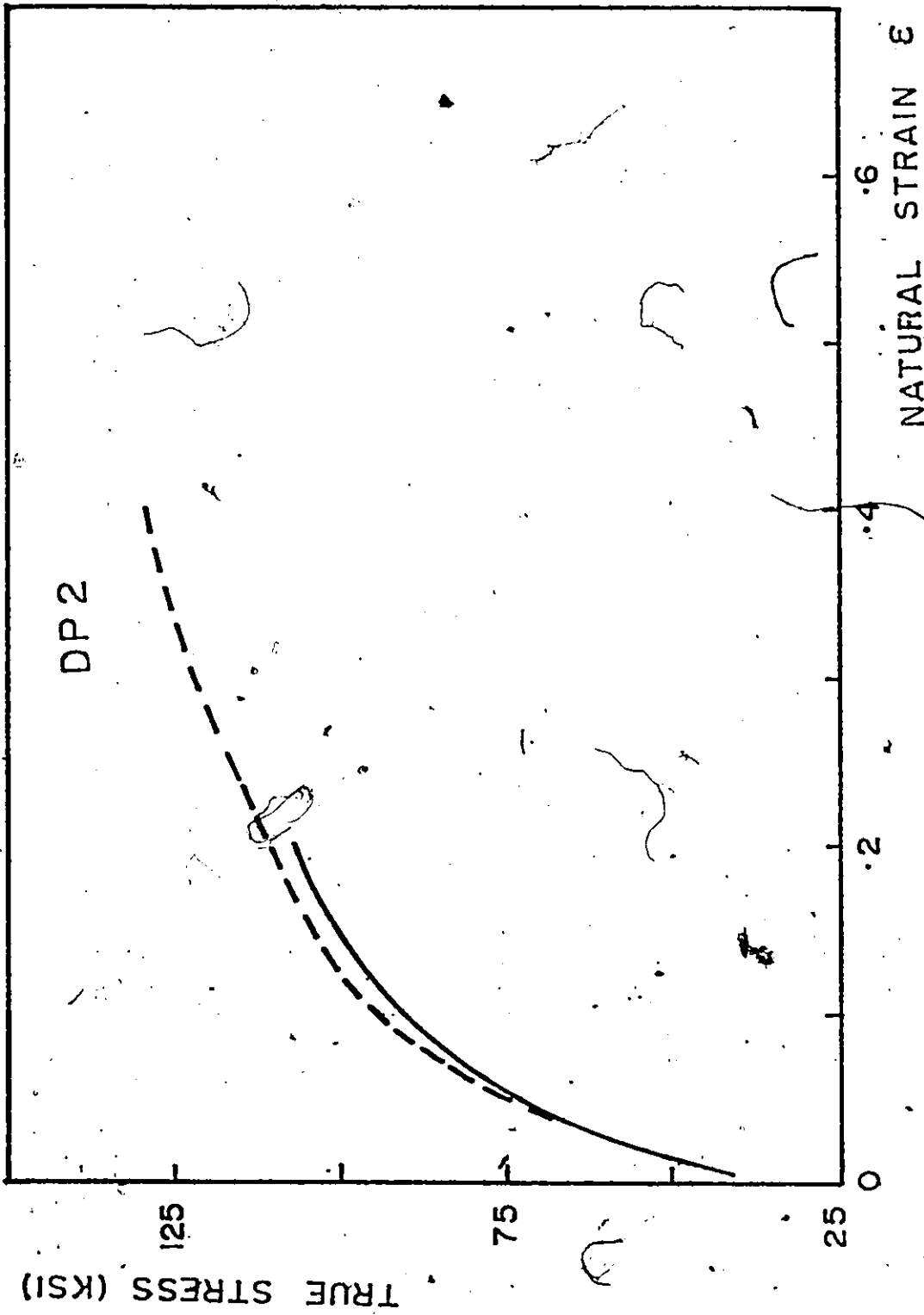


Fig. 20 - Stress-Strain curve from the bulge test for the DP2 steel

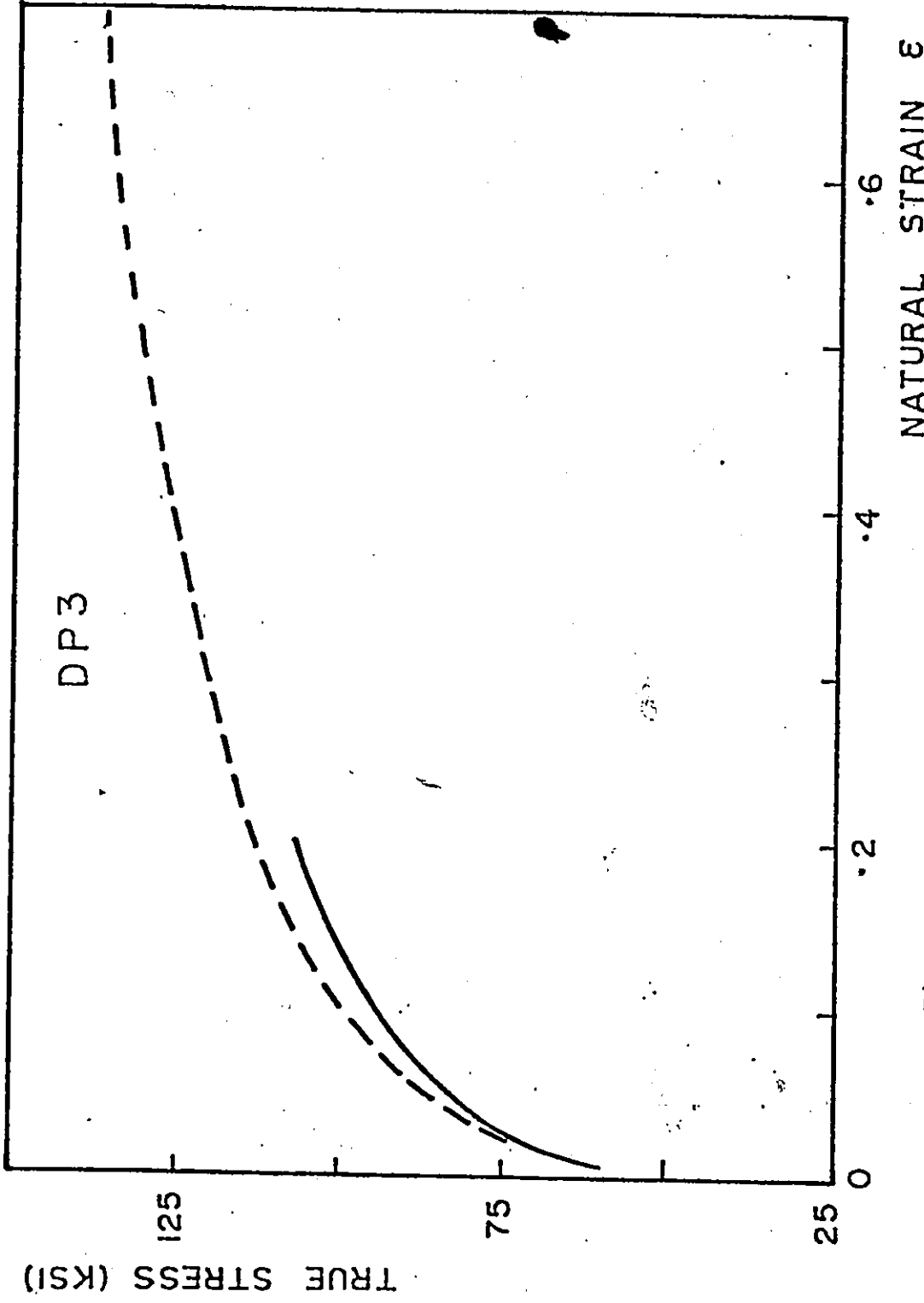


Fig. 21 - Stress-Strain curve from the bulge test for the DP3 steel

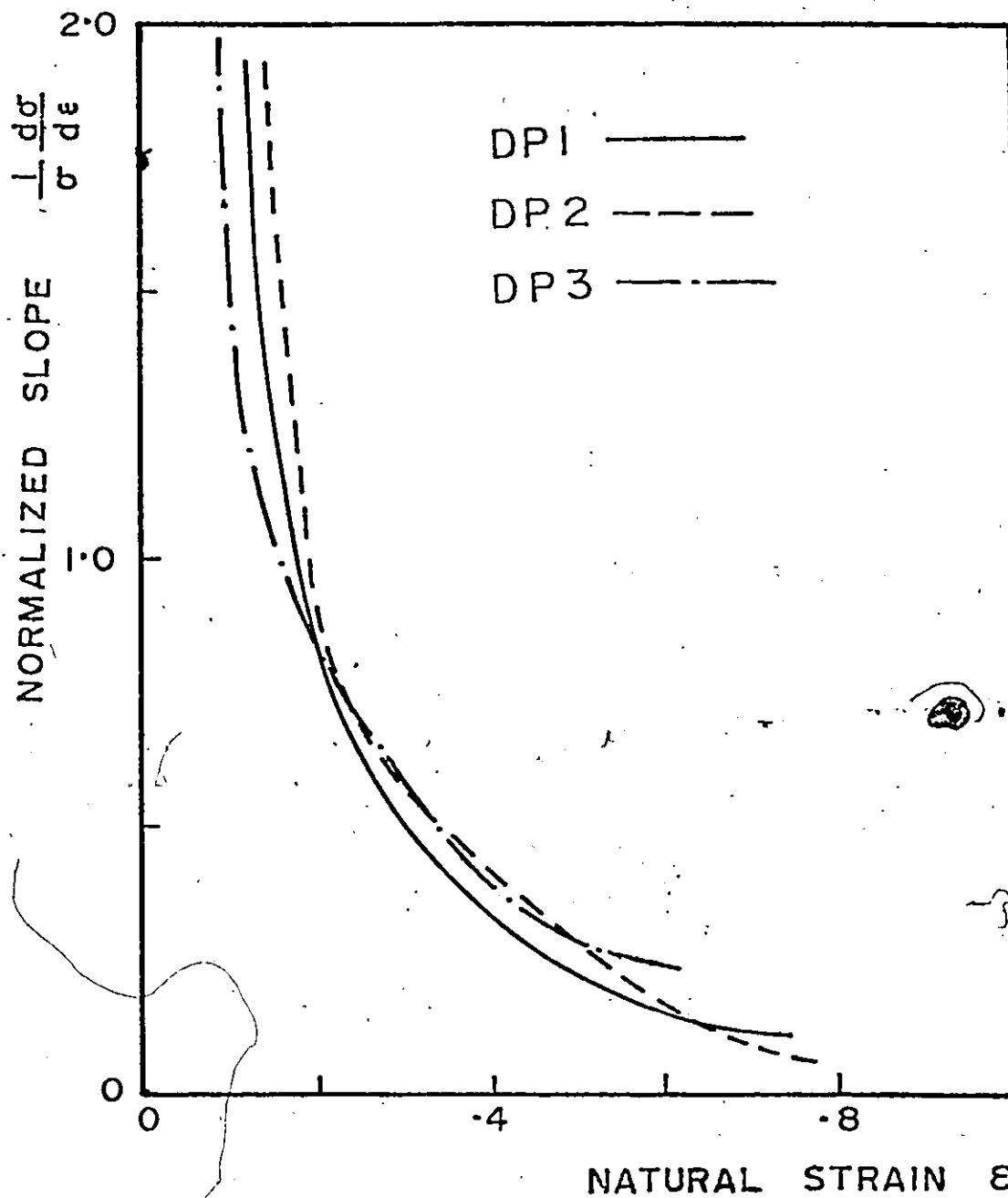


Fig. 22

- Normalized Slope, $\frac{1}{\sigma} \frac{d\sigma}{d\epsilon}$ curves for DP1, DP2, and DP3 steels

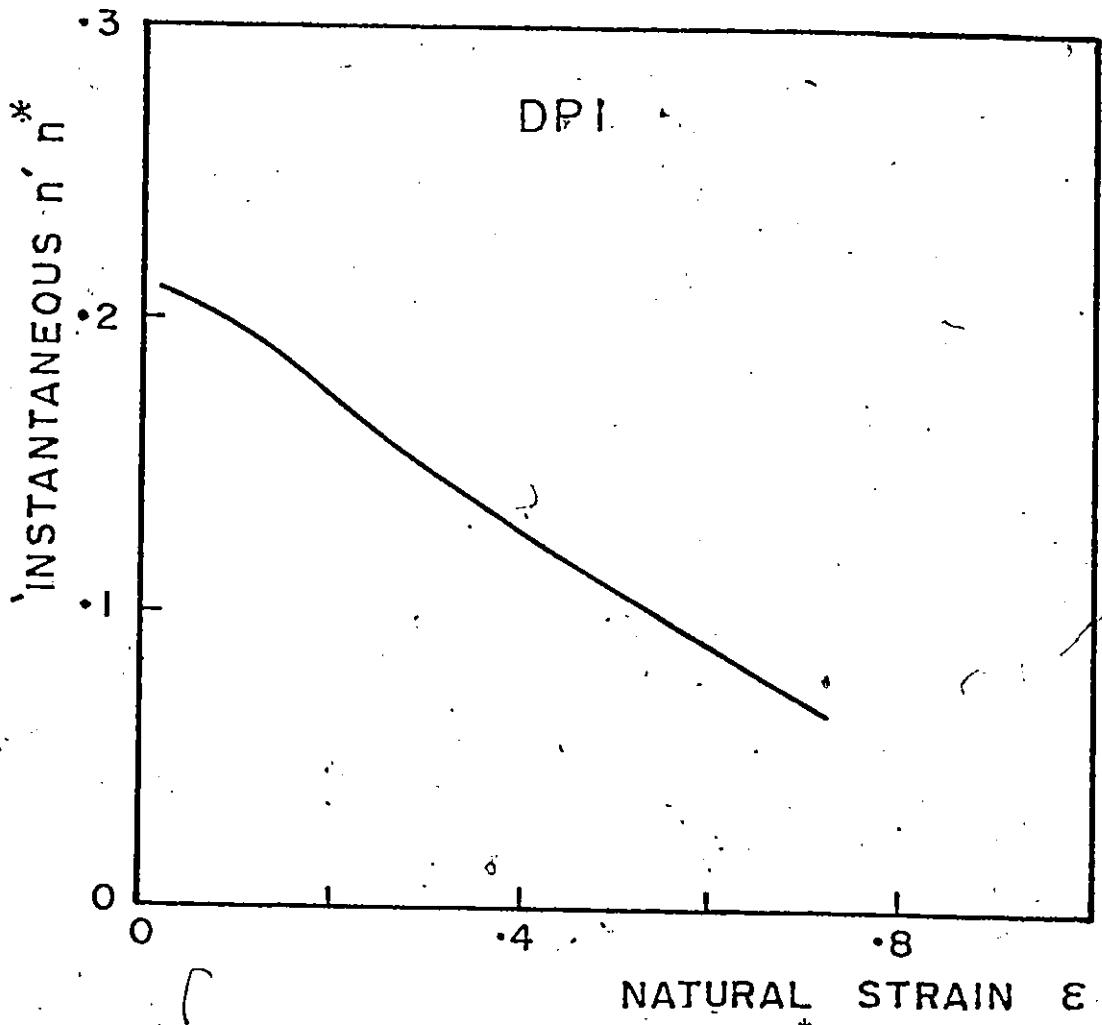


Fig. 23

- Instantaneous n, n^* curve for DPl steel

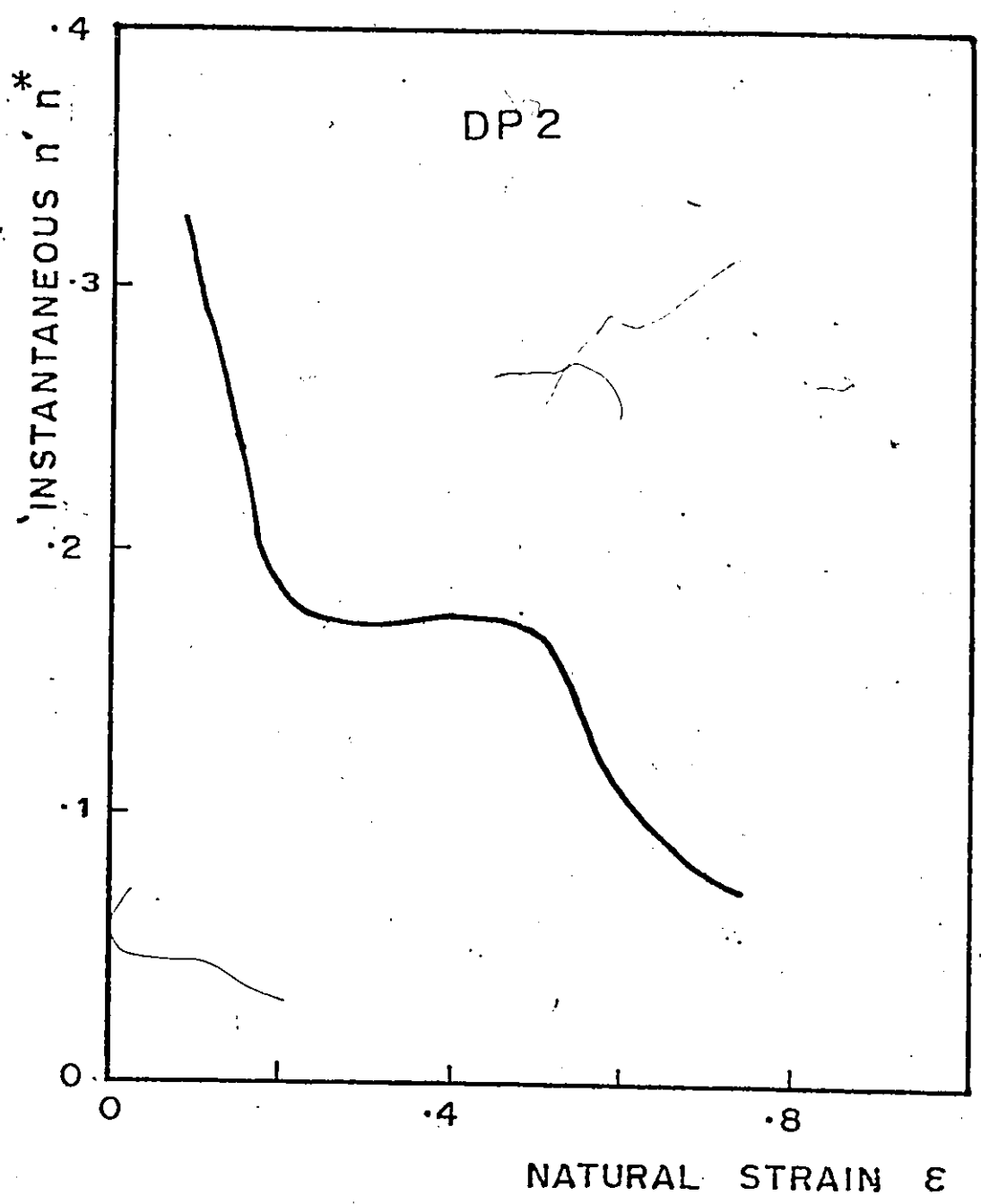


Fig. 24 - Instantaneous n, n^* curve for DP2 steel*

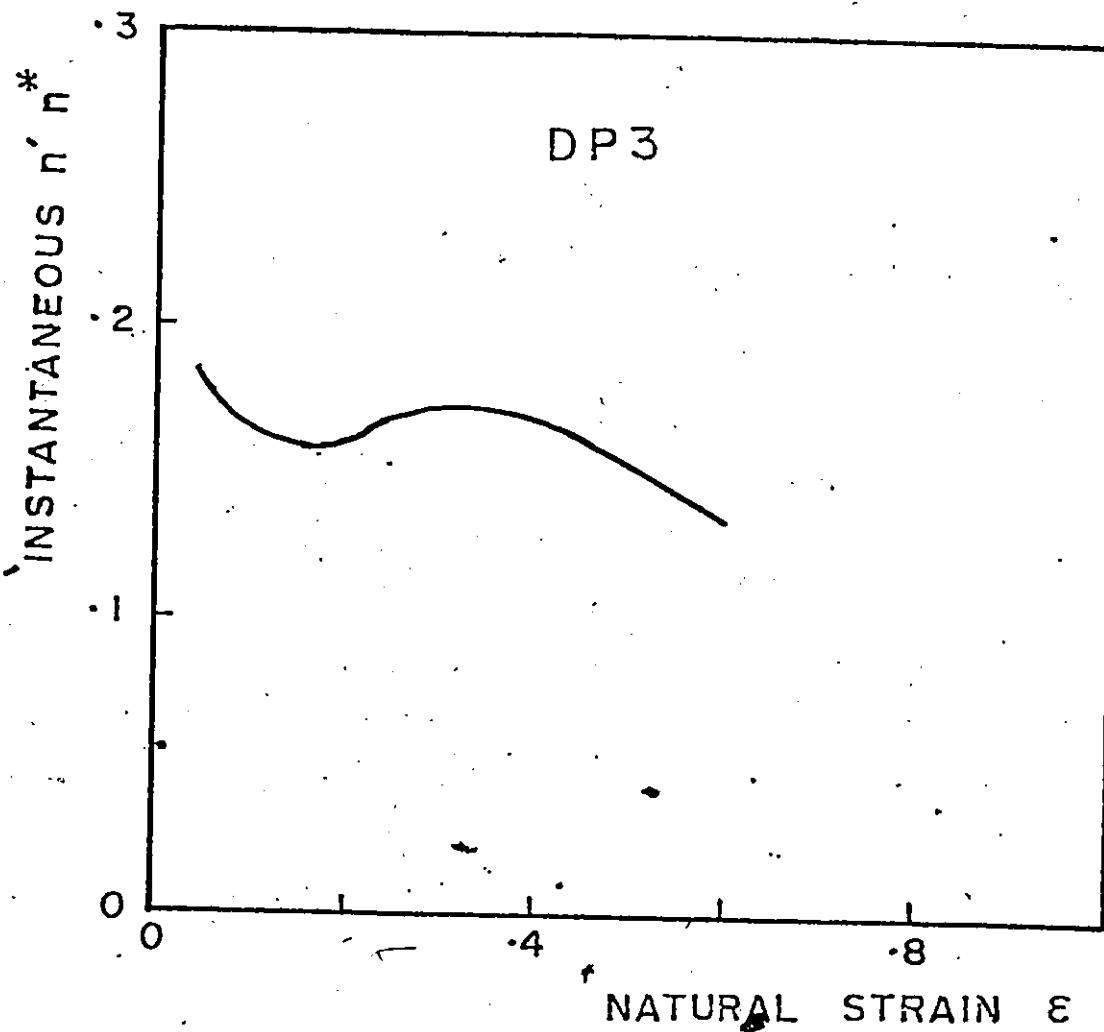


Fig. 25 - Instantaneous n, n^* curve for DP3 steel

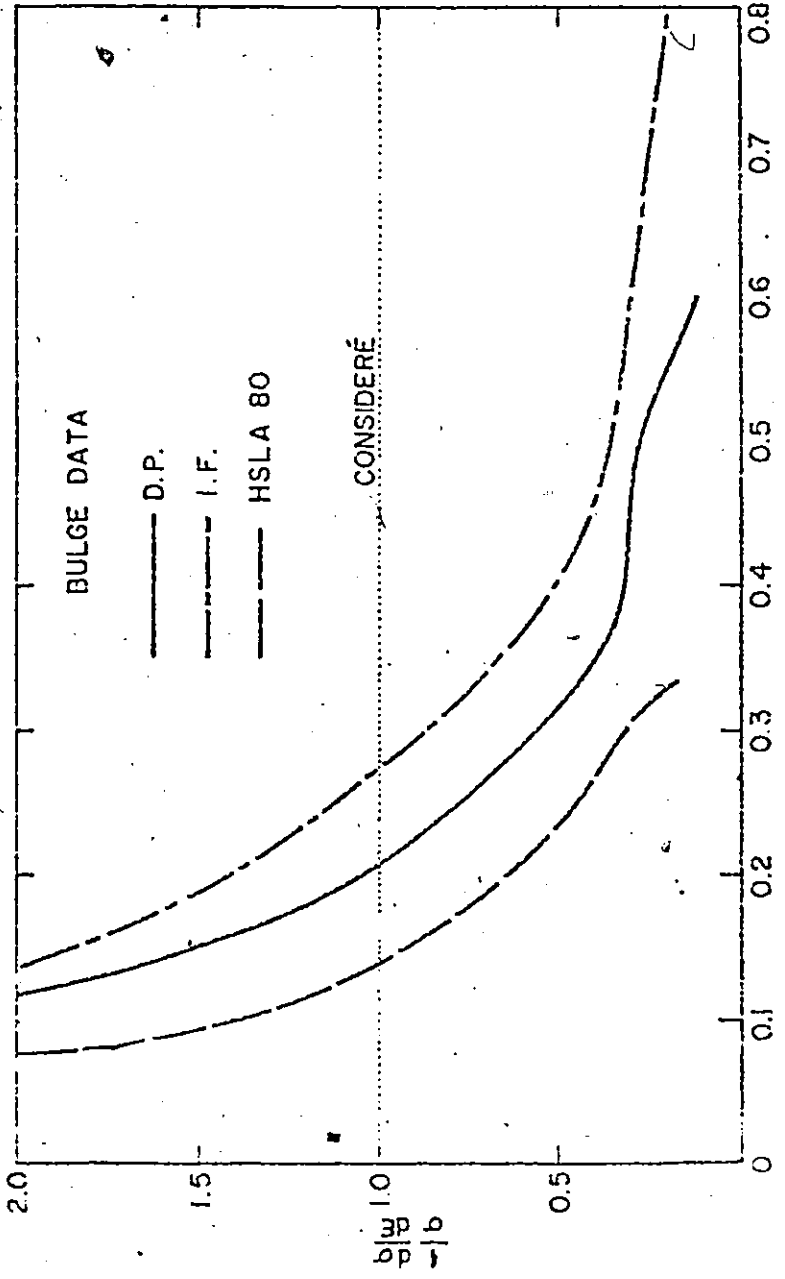


Fig. 26 - Normalized Slope, $1/\sigma \frac{d\sigma}{d\epsilon}$ curves for D.P., I.F., and HSLA 80 steels



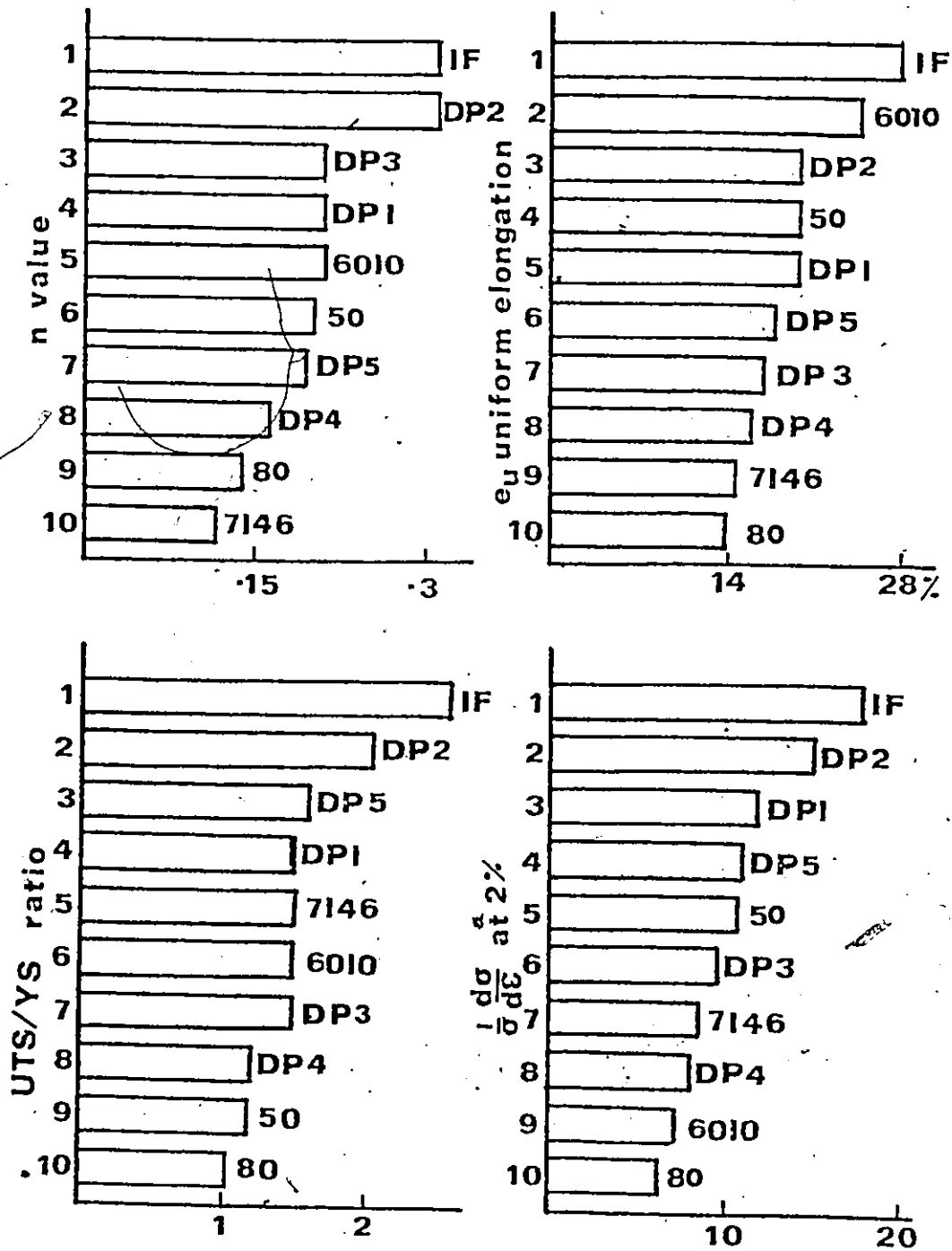


Fig. 27 - Bar Chart of Material Ranking from Tensile Parameters

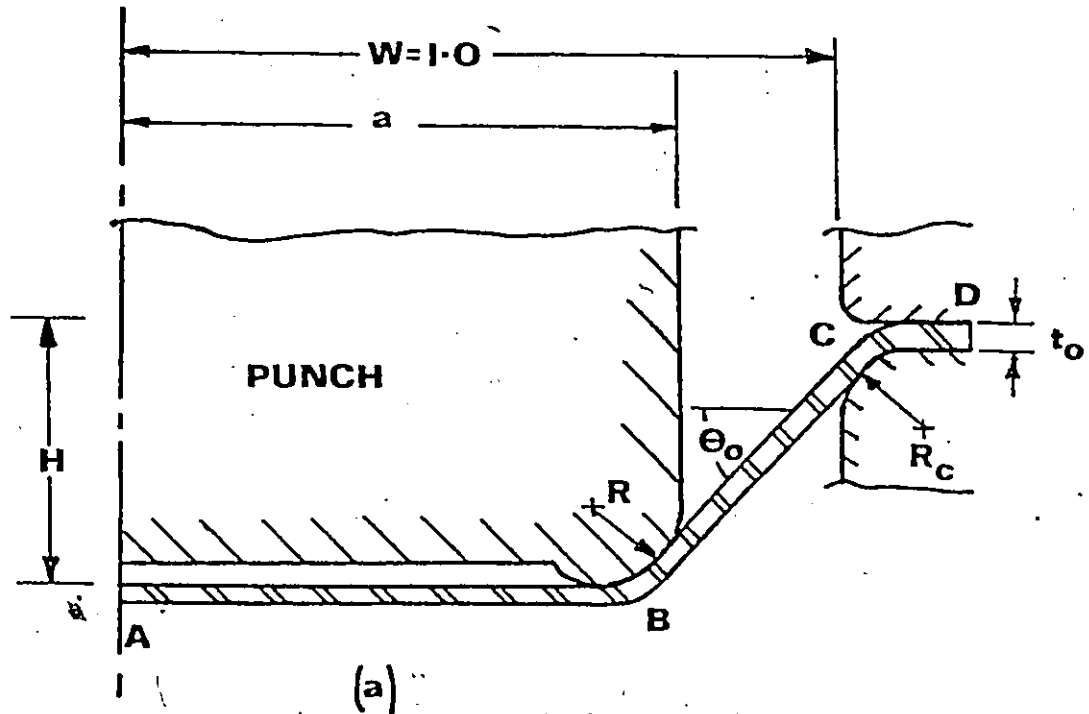


Fig. 28(a) - Schematic of a shallow pan part

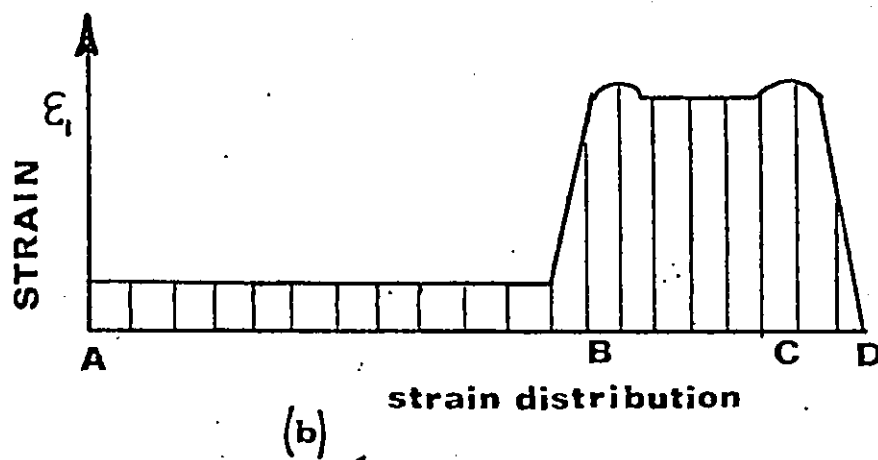


Fig. 28(b) - Typical strain distribution in shallow pan

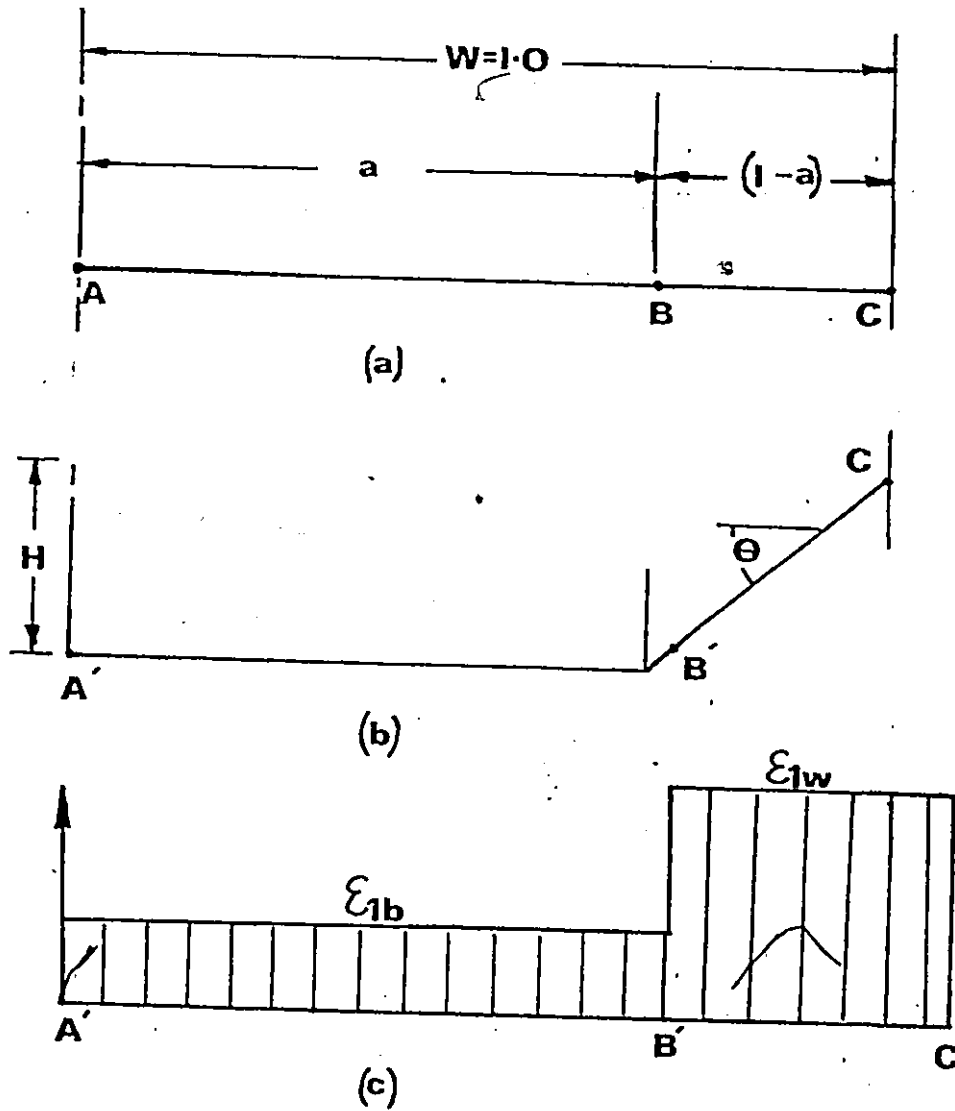


Fig. 29(a) - Idealized part before pressing

29(b) - Idealized geometry of shallow pan
at a depth H

29(c) - Idealized strain distribution

CHAPTER V

ANALYTICAL MODEL

5.1 SIMULATIVE MODELLING

It is well known that the strain distribution and limits of forming in these components depend on the geometry of the part, the tooling and the blank, on friction at the tool/workpiece interface and on material properties. In the absence of any satisfactory modeling technique, the detailed nature of the interaction between these variables is not known, or at least not known well in a quantitative manner. The only available modelling techniques at present are based on Finite Element Modelling (FEM).

Finite element modelling is now being used in some applications which involve the prediction of material formability for given part geometries. The finite element modelling technique suffers from several disadvantages which inhibit its wide spread use. The major disadvantage is that the accuracy of finite element modelling is very poor for modelling in the plastic region of the stress-strain curve unless a very lengthy computational technique is employed. The larger the plastic strain the poorer the accuracy. Thus it is not particularly suited to applications in sheet metal

forming which involve large plastic strains.

To get the best accuracy from finite element modelling it is necessary to have expertise in numerical methods and in finite element modelling. The "black box" approach is not really appropriate in metal forming applications where the variables can change drastically from one application to the next. The amount of computer time required for any finite element modelling is also very large, though with the introduction of larger and faster computers this may not be a problem in the future. The final problem with finite element modelling which would be common to all possible techniques is the lack of information concerning material properties and the workpiece/tool friction conditions.

With finite element modelling the interaction of the various parameters, material, geometric, and friction can only be observed from the modelling results. It would be advantageous to develop a modelling technique whereby the interaction of the parameters could be observed in the form of equations as well as from the modelling results. A model which is simpler to understand and use, as well as requiring less computer time could be put to beneficial use. To this end an analytical modelling technique was developed which included all of the above mentioned parameters.

5.2 ANALYTICAL MODELLING

This technique is similar to finite element modelling but employs a very small number of elements. In this modelling several assumptions are made about the strain conditions and a macroscopic approach to the equilibrium equations is used. In the approach adopted here, complex stampings are first idealized to the extent that they can be analyzed by simple techniques without losing those features on which the interaction of the variables depend. The model is then used to generate theoretical curves which indicate the influence on forming of changes in particular variables. The model is as described below.

Figure (28) shows a schematic of a shallow pan part and the typical strain distribution found throughout the part. The strain, ϵ_1 is the strain in the plane of the sheet parallel to the plane of the diagram. The geometry is described by the following dimensions; the die half width, W ; the punch half width, a ; the punch nose radius, R ; the clamping radius, R_c ; and the material thickness, t_0 . To simplify the description the die half width is taken as unity, $W=1.0$ so that all other dimensions, including the depth, H become ratios with respect to the die half width.

The shallow pan part is assumed to be two dimensional having a width in the direction perpendicular to the plane of figure (28) equal to unity. The strain condition is

assumed to be plane strain so that the strain perpendicular to the plane of the figure ϵ_2 is zero. Thus the strain ratio, β as defined by

$$\beta = \epsilon_2 / \epsilon_1 \quad (5.1)$$

is also zero. In the final model, the value of β could be varied from the plane strain condition. The plane strain condition is chosen since this is a common strain condition where failure occurs.

The next step is to idealize the geometry. Referring to figure (28b) it can be seen that there are two major levels of strain, that in the wall section, BC and that on the face of the punch, AB. Note the slight increase in strain level at points B and C due to the superposition of the bending strains over the radii. The bending strains are ignored in this modelling since it is found in practice that bending strains are negligible if R/t ratios greater than 4 or 5 are used in the tooling. The idealization of the part is to reduce the radii B and C to corners connecting the two sections AB and BC; we assume that material can slide around the corner at B. Figure (29a) shows the idealized part before the punch has penetrated, while figure (29b) shows the part at a depth H and figure (29c) shows the strains in the two sections. The original

lengths of the sections AB and BC as can be seen from figure (29) are

$$AB = a \quad ; \quad BC = (1-a) \quad (5.2)$$

The bottom section AB undergoes a strain of ϵ_{1b} while the wall section BC undergoes a strain of ϵ_{1w} , so that the final lengths of the sections are

$$A'B' = a \cdot \exp(\epsilon_{1b}) \quad (5.3)$$

$$B'C' = (1-a) \cdot \exp(\epsilon_{1w})$$

The total length of the strip which is the sum of A'B' and B'C' can be related to the side-wall angle and initial geometry, i.e.

$$a \cdot \exp(\epsilon_{1b}) + (1-a) \cdot \exp(\epsilon_{1w}) = a + \frac{(1-a)}{\cos \theta} \quad (5.4)$$

This relates the two levels of strain to the angle θ , and the angle can in turn be related to the depth, H as follows

$$H = (1-a) \cdot \tan \theta \quad (5.5)$$

Another equation relating the strains ϵ_{1b} and ϵ_{1w} is necessary before the strains can be determined as functions

of the depth H or the angle θ . This equation is found from the equilibrium conditions. Figure (30) shows a detailed view of the punch nose at and from consideration of equilibrium between the punch load P and the tractions T_w and T_b in the two sections the following equations can be derived.

$$P = 2 T_w \sin \theta \quad (5.6)$$

$$T_b = T_w \exp(-\mu\theta) \quad (5.7)$$

The term μ is the friction coefficient for the material sliding around the corner. The tractions can also be expressed as follows

$$T_1 = \sigma_1 t_1 \quad (5.8)$$

The current thickness t_1 can be expressed in terms of the original thickness t_0 and the strains as follows

$$t_1 = t_0 \exp(-(1+\beta)\epsilon_1) \quad (5.9)$$

The stress, σ_1 can also be expressed in terms of the strain using the Ludwik equation (3.2) and laws of plasticity

$$\sigma_1 = \phi K \epsilon_1^n \quad (5.10)$$

The term ϕ is a constant which relates stress, σ_1 and strain, ϵ_1 to the effective stress $\bar{\sigma}$ and effective strain $\bar{\epsilon}$ in the Ludwig equation (3.2).

Substituting equations (5.8), (5.9) and (5.10) in the equation (5.7) yields

$$(\epsilon_{1w}/\epsilon_{1b})^n = \exp [(1+\beta)(\epsilon_{1w}-\epsilon_{1b})+\mu\theta] \quad (5.11)$$

This equation with equation (5.4) is enough to allow the strains ϵ_{1w} and ϵ_{1b} to be calculated for an input value of H (or θ). The calculation must be done by an iterative process. The value of the input H can be incrementally increased from zero and the strains calculated at each value of depth until some end criteria is reached.

5.3 END POINT CRITERIA

The model is only valid if the strains remain uniform within each section, so a possible limiting criteria is when necking in the wall segment begins. The criteria for diffuse necking is when the force in the segment reaches a maximum; F is given by

$$F = \sigma_1 A \quad (5.12)$$

where

$$A = A_0 \exp(-\epsilon_1) \quad (5.13)$$

Differentiating equation (5.12) and equating to zero gives the strain at which the force is a maximum and is

$$\epsilon_{1w} = n \quad (\text{diffuse}) \quad (5.14)$$

But this criteria is not applicable to this case since diffuse necking does not develop in continuous sheets because of the geometric constraints in a lateral direction.

Localized necking can occur when maximum tractions are reached; this is a better end criteria. By differentiating equation (5.8) with respect to strain the following equation giving the strain at which necking occurs can be developed.

$$\epsilon_{1w} = n/(1+\beta) \quad (\text{local}) \quad (5.15)$$

It is this criteria for maximum traction which is used to terminate the theoretical simulations for all of the results present in this chapter. Some of the theoretical results are presented which give some understanding as to how the geometry, friction and material parameters interact to influence the depth of part and the amount of strain occurring in the bottom.

5.4 RESULTS OF ANALYTICAL MODELLING

Figure (31) shows the theoretical relations for a particular set of variables. The simulation was allowed to run beyond the limit of maximum traction to illustrate the behaviour of the simple model.

The following conditions were used in the calculations:

punch half width, $a = 0.46$
 punch radius, $R = .114$
 clamp radius, $R_c = .114$
 material thickness, $t_o = .0071$
 friction coefficient, $\mu = 0.2$
 strain condition, $\beta = 0.0$
 strain index, $n = .21$
 strength index, $K = 38.0$

Referring to figure (31) it can be seen that the tractions and the strains increase with increasing depth and that there is a gradual divergence between the traction and strain in the wall and the traction and strain in the bottom. This divergence is due to the increasing θ which has its effect in equation (5.7). Note that the bottom strain reaches a maximum before any other variable for this set of input conditions. The strain then remains at the maximum level since it is irreversible plastic strain.

The reason that the bottom strain reaches a maximum is due to the fact that the increase in wall traction is no longer able to offset the decrease in the exponential term, $(-\mu\theta)$ so the value of T_b calculated in (5.7) begins to decline. The bottom traction cannot be calculated beyond the point of maximum bottom strain since equation (5.7) no longer holds as an equality but becomes

$$T_b < T_w \exp(-\mu\theta) \quad (5.16)$$

The strains, load and tractions are plotted beyond the maximum wall traction as dotted lines since these are not realistic because local necking would occur in the wall segment.

The solid lines beyond the maximum traction indicate what would be expected to occur due to the necking. Note that the maximum punch load, P does not reach a maximum until after the wall traction reaches a maximum. Again this is due to the influence of the increasing angle θ in equation (5.6).

5.5 INFLUENCE OF GEOMETRY

By plotting the depth H and maximum bottom strain, ϵ_{1b} at the point of maximum wall traction for various geometries, the effect of geometry can be observed. It was

found that the thickness, t_0 and the radii, R and R_c did not have much effect on the depth of the maximum bottom strain so long as these parameters were very small when compared with the die half width.

$$R \ll W, R_c \ll W, t_0 \ll W \quad (5.17)$$

This left only the punch half width, a as the only geometry parameter with any large influence on the results. Figure (32a) shows the effect of a on the depth of a part. Figure (32b) shows the effect on the maximum bottom strain. While reducing the punch width does improve the depth and the bottom strain the actual value of a is not usually a variable but is prescribed by the shape of the pressing.

The basic analytic model presented here is a very simple model and does have some gross simplifications and assumptions. In the calculations a more sophisticated model which has some improvements to overcome some of the objections to the simple model was used. These include the inclusion of the effects of the radii on the various lengths, the possibility of the strain condition varying from the plane strain case and being different in each section, the influence of the strain rate sensitivity and the use of a digitized stress-strain curve instead of the Ludwig equation (3.2). It was also possible to study the

effect of pre-strain ϵ_0 in the material by using the following equation for the material:

$$\sigma = K(\epsilon_0 + \epsilon)^n \quad (5.18)$$

The results of using this equation are shown in the figure (33).

The results indicate that pre-strain has a large detrimental effect on the depth and the amount of strain in the bottom of the pan. This is expected since the inclusion of ϵ_0 changes the limit strain which lowers the wall strain at which necking occurs.

$$\epsilon_{1w} = n/(1+\beta) - (3/4(1+\beta+\beta^2))^{0.5} \epsilon_0 \quad (5.19)$$

All of the calculations done with both the basic model outlined in this chapter and the final more sophisticated model in the appendix one gave results which were continuous and smooth within the limits of computational error. There is only a small difference in the results of the two models which also implies that the effect of the radii on the results is a minor influence. A comparison of the results for the two models is given in figure (34).

5.6 INFLUENCE OF FRICTION AND MATERIAL

In figures (35) and (36) the influence of the friction coefficient, μ and the strain index, n on the depth and the maximum bottom strain are shown. Clearly the higher the n value or the lower the friction the more bottom strain will occur and hence a greater depth. The lower the value of friction the more sensitive the bottom strain and depth are to changes in friction or n value.

Changes in n and μ are reflected more strongly in the bottom strain ϵ_{1b} than the depth. This is because the friction and the n value directly affect the bottom strain while their influence on the depth is indirect. The depth is mainly due to the wall strain and only a small part (<30%) is due to the strain in the bottom for this geometry. The influence of the μ and n on the depth is through the bottom strain and so only partially affects the depth. As the geometry is changed so that the punch width is increased towards unity then the more influence the bottom strain has on the depth and hence the more influence μ and n will also have on the depth.

The reason n has more influence on the depth than the friction μ while they both have roughly the same amount of influence on the bottom strain is due to the influence n has on the limiting strain in the side wall which is a major factor in determining depth.

This influence of n on the limit strains is seen in the equation (5.15). As the punch half width, a is increased then the influence of μ becomes more important relative to the influence of the n value, and since most real applications for shallow pans have the punch half width, a close to unity the friction will be important.

Because of the greater sensitivity of the ϵ_{1b} over the depth H and the fact that in shallow pan type parts it is the face strain and not the depth of part which is important, the maximum bottom strain ϵ_{1b} is chosen as the parameter by which materials should be ranked regarding their formability in shallow pan type parts.

Figure (36) can be used to give an idea of what n and μ values are required to get a certain amount of bottom strain. For example if a bottom strain of .04 is required and the friction μ is 0.25 then to get the strain a material with an n value greater than 0.195 must be used. If the friction was 0.35 instead then the n value would have to be greater than 0.23. Note that the friction values which give reasonable strains and n values appear higher than those values commonly believed to occur in pressing operations. The model implies that for the strains and corresponding n values found in actual shallow pans the actual friction coefficient must be high, say around 0.2 to 0.3. Clearly it would be advantageous to have the actual

values of friction determined but this is extremely difficult to measure in practice. If a simulative test of the shallow pan geometry could be made then the accuracy of the modelling could be checked, some estimate of the friction conditions could be made and materials could be ranked for their formability in shallow pans.

An experimental rig was constructed to simulate a shallow pan. In the design, provision was made for measuring the bottom strain as well as several other parameters. This rig was used to test some of the materials described in chapter three to check the analytical model and to see if the bottom strain as an indicator of formability agreed with the other indicators described in chapter four. In the next chapter, the rig and experimental procedure are described and some experimental results are presented.

In the above analysis the die half width, W was taken as unity to allow the geometry to be described in terms of depth H , punch radius R , die radius R_c , and punch half width a . In the next chapter the parameters used to describe the geometry are the ratios H/W , R/W , R_c/W , and a/W . Strain rate sensitivity and differing strain ratios in the bottom and wall had been included into the modelling but were not used in the model for the computer simulations.

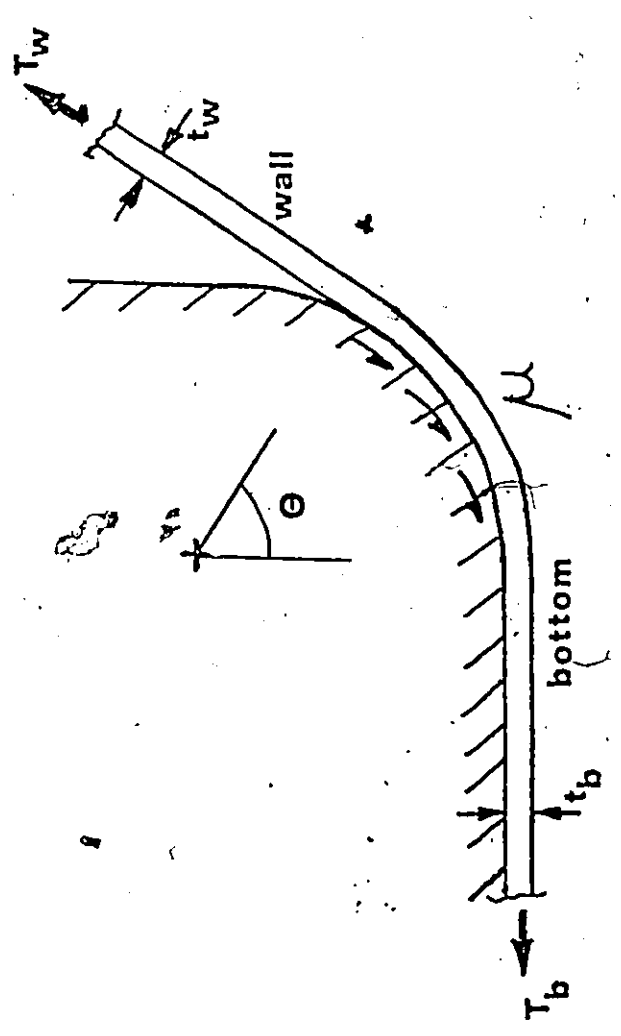


Fig. 30 - Detail of tractions around punch corner

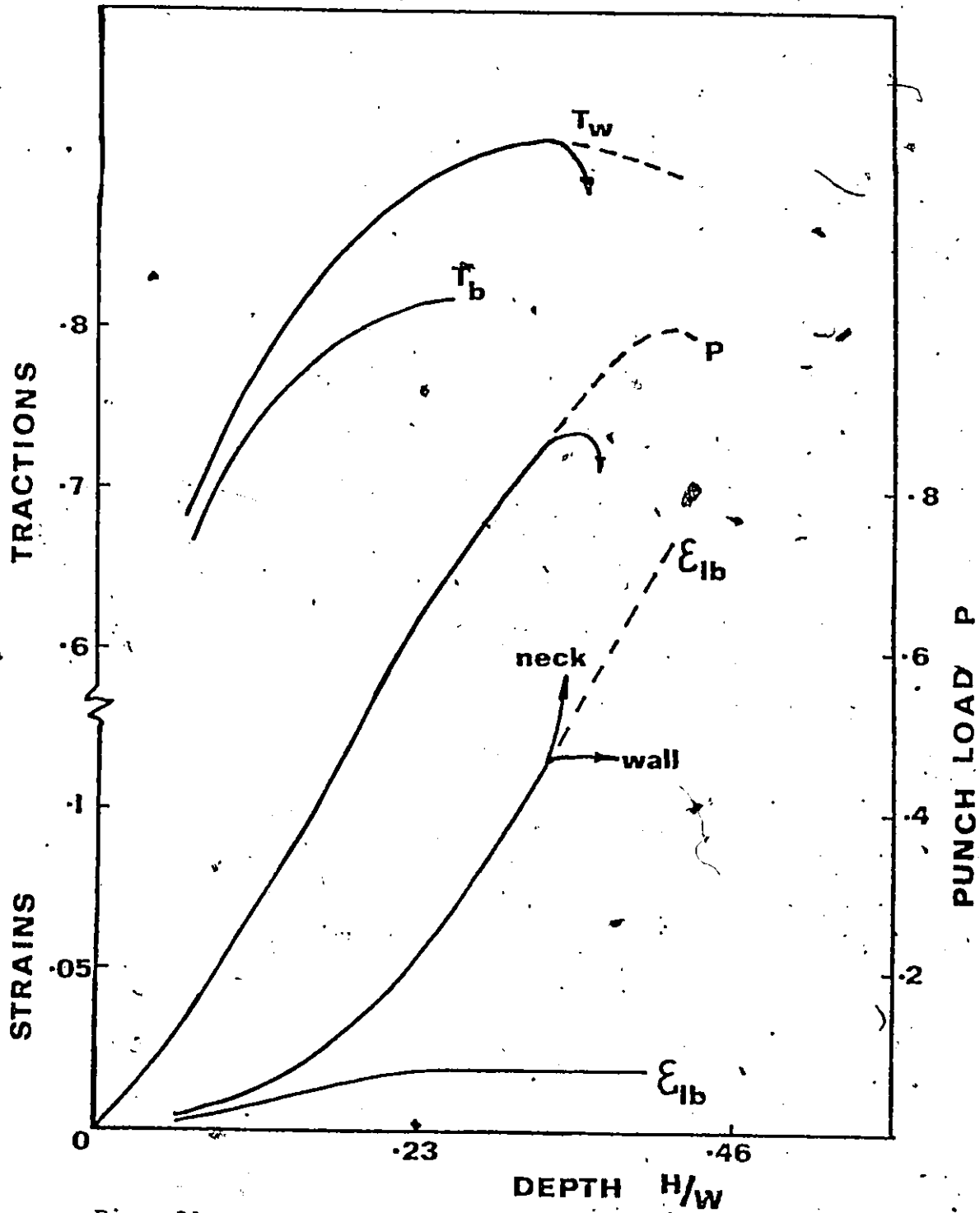


Fig. 31 - Results of one theoretical simulation of a shallow pan

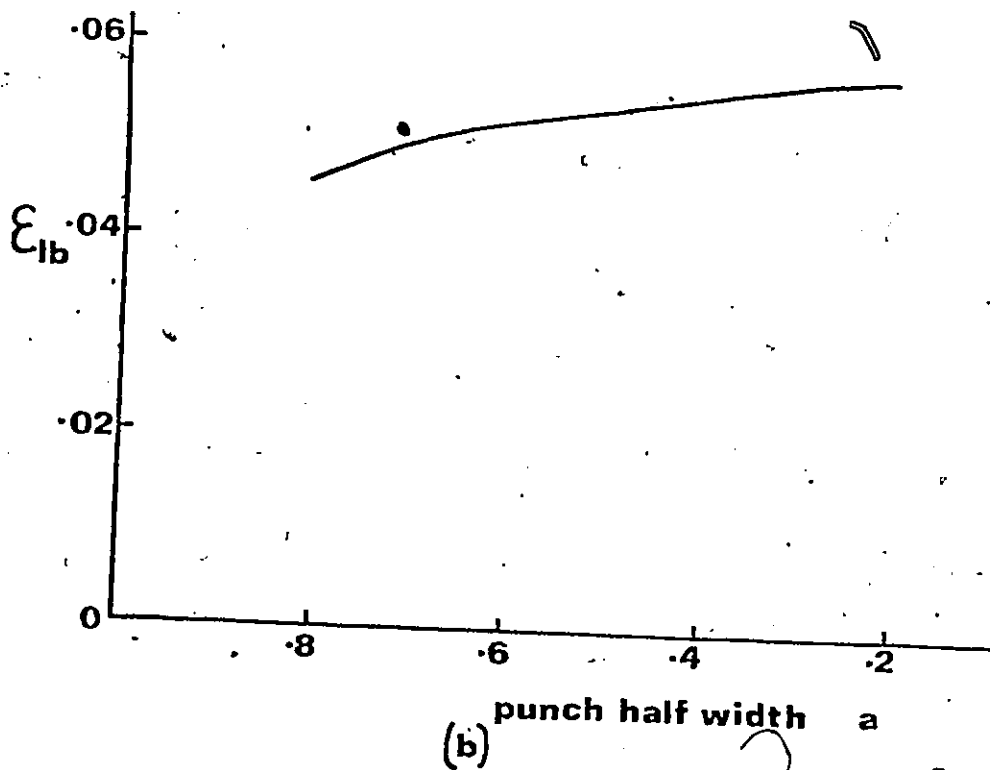
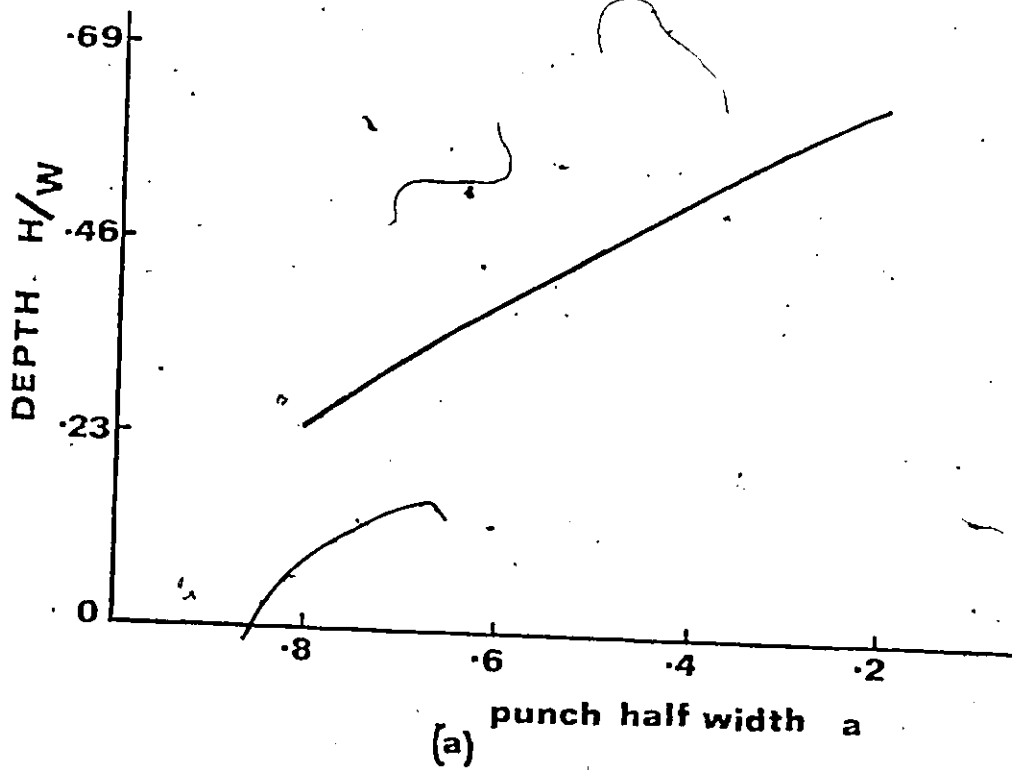


Fig. 32(a) - Depth as a function of punch half width, a

32(b) - Bottom strain as a function of punch half width, a

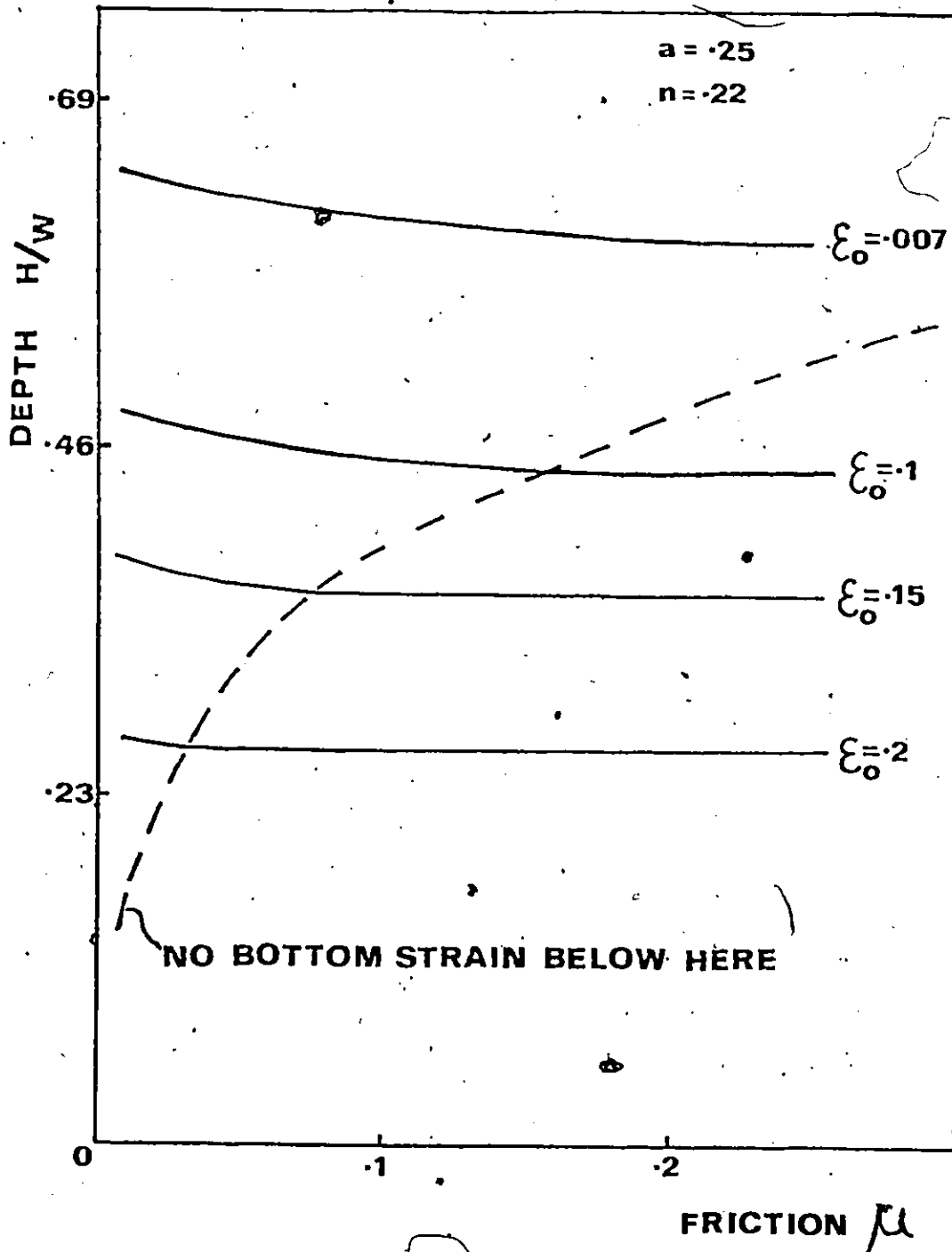


Fig. 33

- Depth against friction μ showing the effect of pre-strain ϵ_0 .

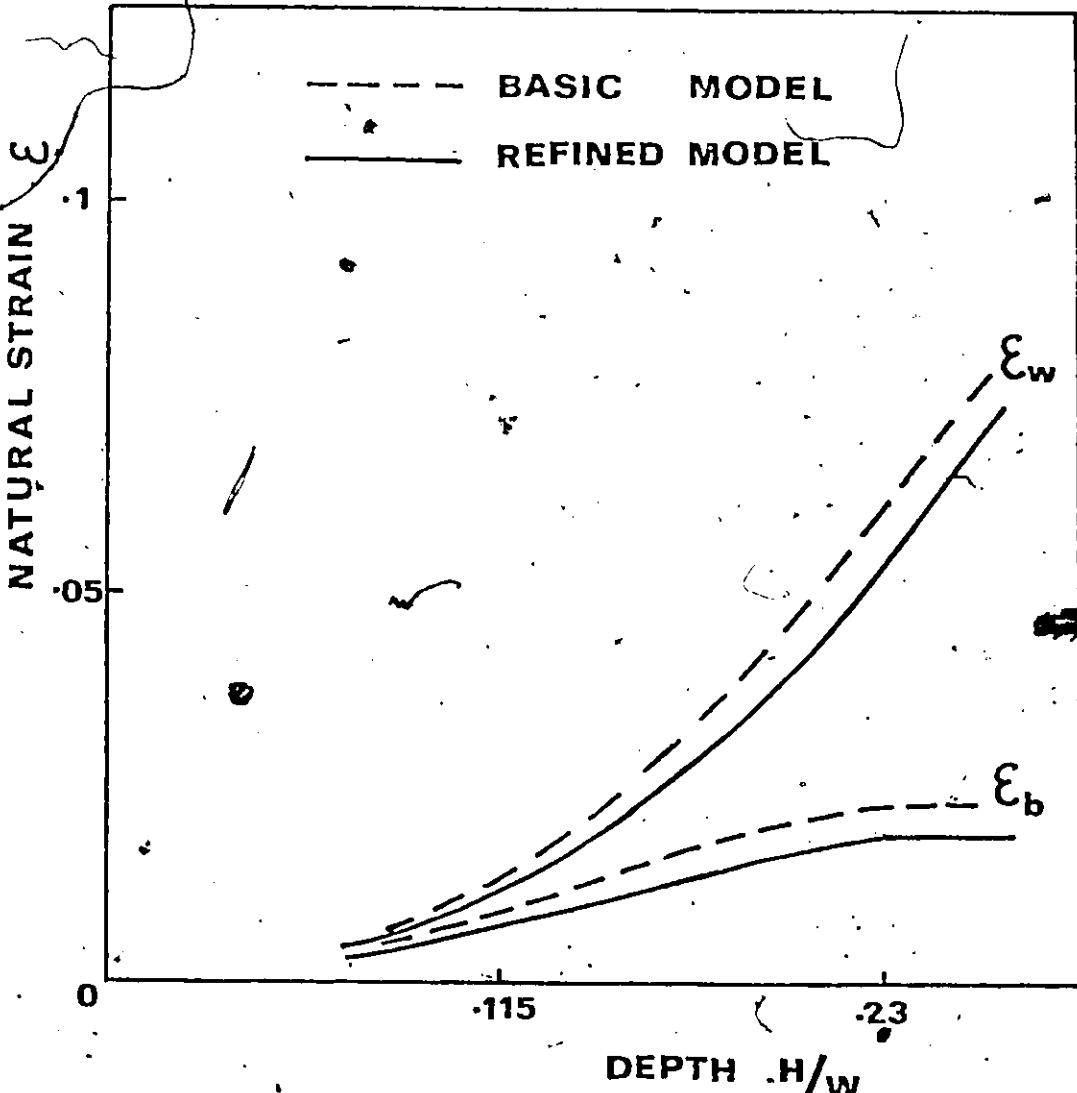


Fig. 34 - Comparison of the computed strains for the basic and refined models

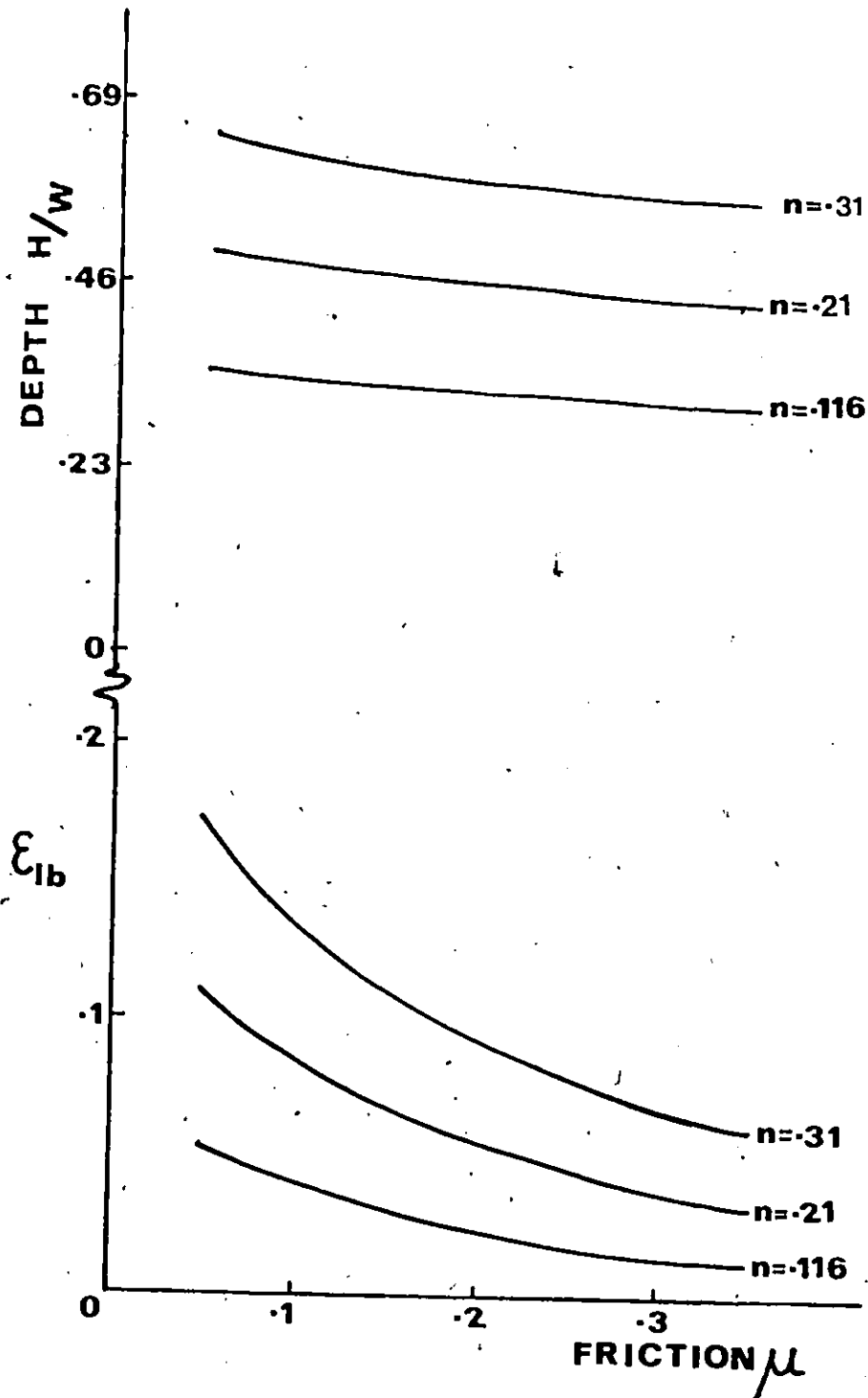


Fig. 35 - Theoretical depth, H and bottom strain ϵ_{1b} as a function of friction for several n values

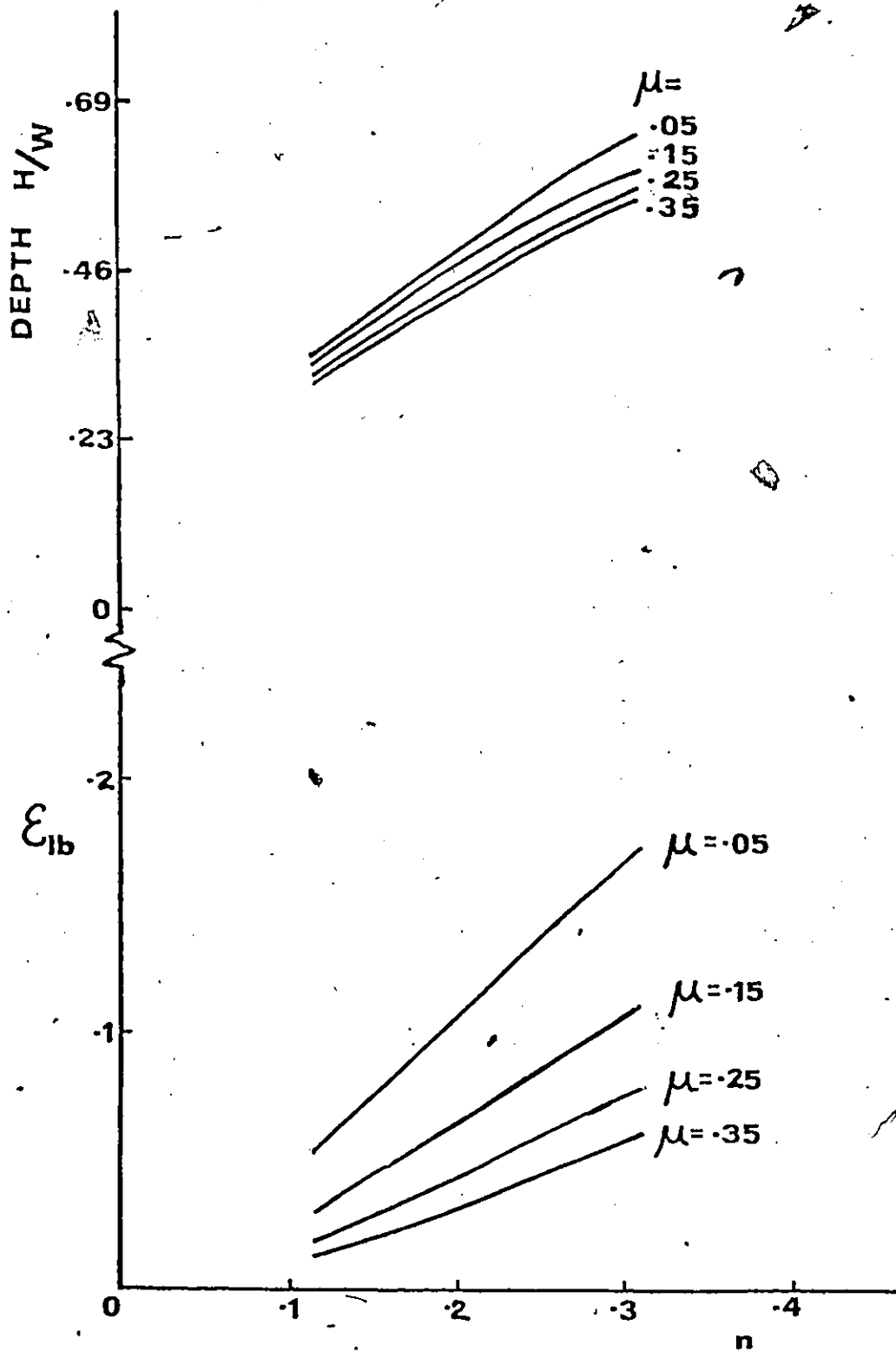


Fig. 36

- Theoretical depth, H and bottom strain ϵ_{1b} as a function of n value for several values of friction

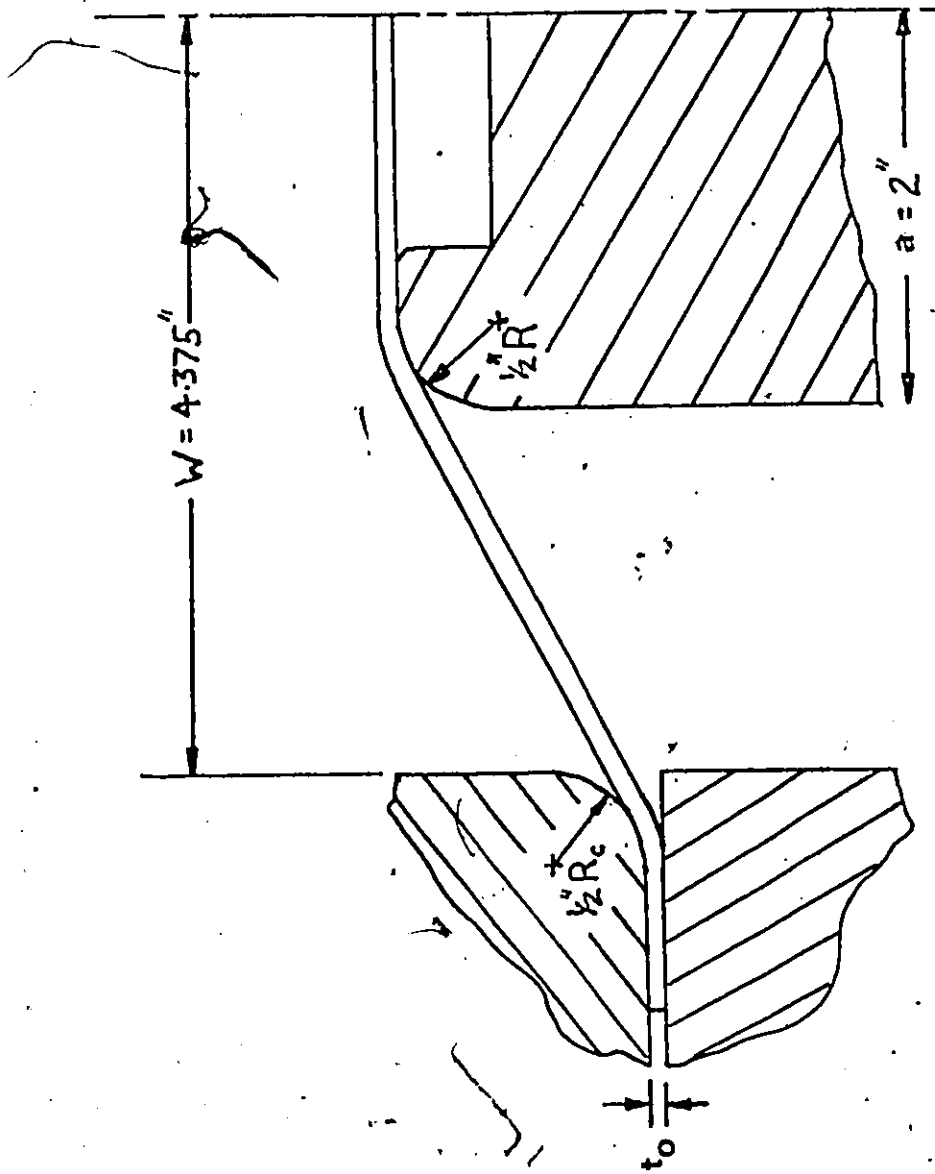


Fig. 37 - Schematic of experimental rig showing dimensions



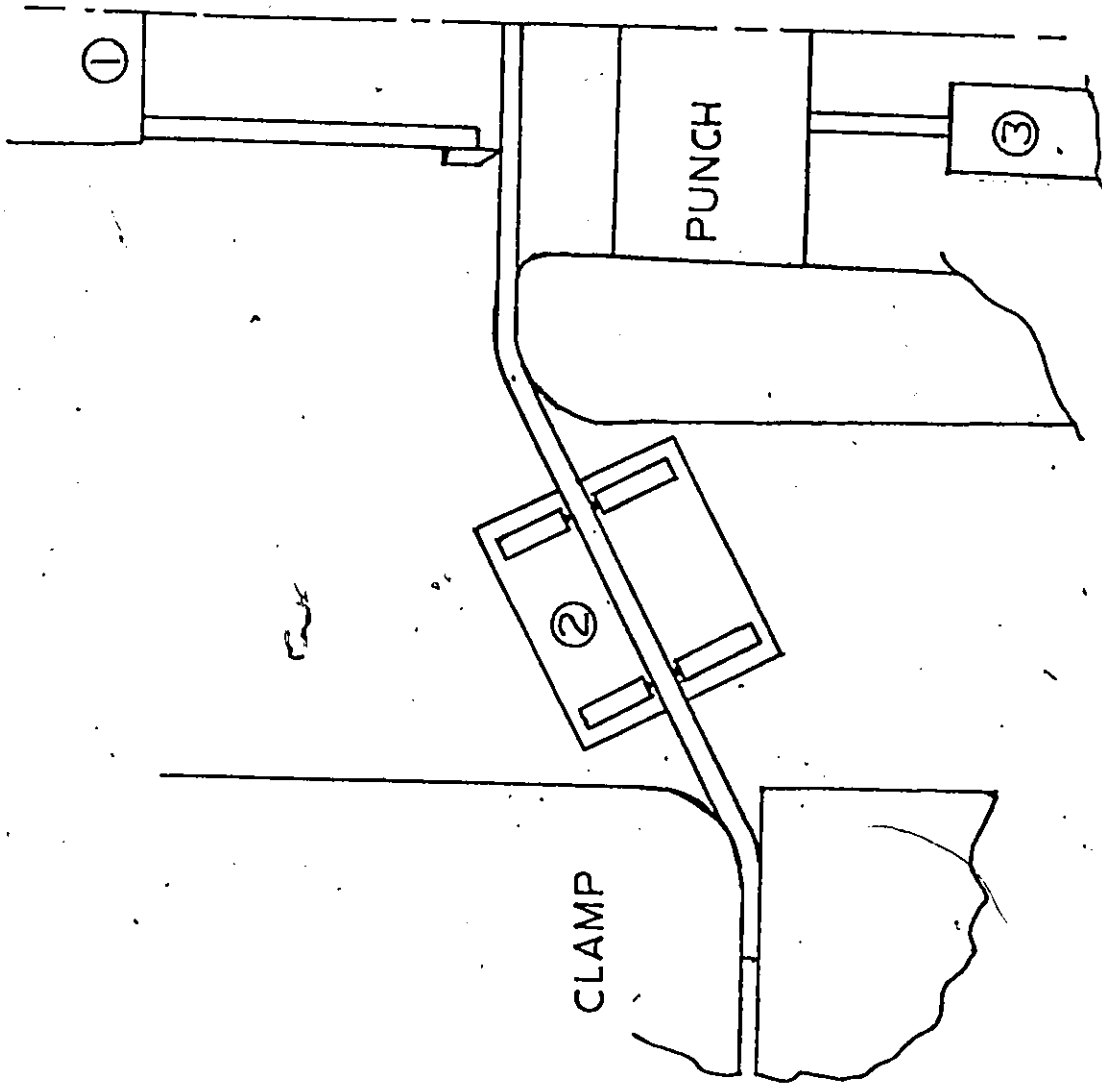


Fig. 38 - Extensometer layout for the experimental rig

CHAPTER VI
SHALLOW PAN TESTS

6.1 EXPERIMENTAL RIG

The next section of work entailed the design and construction of experimental apparatus to check the validity of the theoretical modelling developed in the last chapter. Figure (37) shows a schematic of the experimental rig built to simulate a two dimensional section of a shallow flat bottomed pan. The rig was designed and built so that it was possible to vary the three non-dimensional parameters developed in the theoretical modelling; the punch-to-die width ratio, a/W ; the punch radius-to-die width ratio, R/W ; and the material thickness-to-die width ratio, t/W . These parameters could be set to a number of discrete values so that the effect of geometry could be studied. In this work it was not possible to complete a comprehensive set of experiments covering all the possible range of geometries and friction conditions.

The geometry selected for the experiments had the following dimensions;

die half width $W = 4.375$ "
punch half width $a = 2.0$ "
punch radius $R = 0.5$ "
clamp radius $R_c = 0.5$ "

This gives two of the non-dimensional geometry parameters as $a/W = 0.426$ and $R/W = 0.061$. The third parameter, the material thickness to die width ratio, t/W varied due to the range of material thicknesses used from 0.007 to 0.02. The dimensions of the test pieces were 3" by 10.5" with sheared edges.

The width of the strips of material tested was selected as three inches so as to approximate a plane strain condition as closely as possible; this is the strain condition most commonly found at failure sites in real applications. Measurements were taken to see how closely this condition was approached. Referring to figure (38) it can be seen that space limitations made the measurements of the wall strain impossible with conventional extensometers. Two cross-blade extensometers of McMaster design were modified to fit the experimental rig as shown in figure (38). Extensometer (1) is used to measure the strain in the bottom of the pan while extensometer (2) measures the strain in the side wall. The transducer (3) shown in figure (38) is used to measure the depth of the part. The rig was then

assembled in the McMaster-Mand 200 ton press. Punch load was measured with the load cells incorporated in the press. All instruments were then connected to X-Y recorders so that autographic records could be made of the punch load, the strains in the bottom and side wall of part as functions of the depth of the part.

6.2 EXPERIMENTAL PROCEDURE

The width of all the test specimens was first measured so that when the final widths were measured the width strains could be calculated. The two extensometers were then attached to the specimen after being calibrated and the test piece was then placed in the rig and clamped with the secondary hydraulics of the press. The clamping pressure was set to give a total clamping force of 30 tons. Before each test the extensometers and the displacement transducer were calibrated using calibration jigs. Several preliminary tests were done in order to check the test rig and the accuracy of the measurements made. For this purpose test specimens were gridded with 0.1" circles electro-etched onto the surface. These circles were then used to determine the final strains in the deformed test pieces. The strains were then used to check the final strains measured by the extensometers. The error in measuring strains with the extensometers was found to be ± 0.005 natural strain, i.e.

1/2% strain. The wall extensometer was the least accurate of the two extensometers.

When the test specimen was clamped there was a small amount of flexing in the specimen which affected the measurement of depth. To compensate for this the depth was determined by taking the final depth of the transducer measurement as equal to the final depth as measured with a vernier and working backwards on the autographic record. In all cases the flexing produced an increase in depth of no more than 0.15". Using the above compensation for flexing the error in measured depth was estimated to be less than 0.125" ($H/W = 0.0163$). An exception is the DP5 material in which the flexing was bad and there was some drawing in at the beginning of the test. This has the effect of changing the strain curves as can be seen by comparing the results of DP5 with the other dual phase steels.

The error in the punch load^B was ± 150 lbf. and was mainly due to the friction in the press. The punch speed was set at 1.2 inches/minute although it was recognized that this was several orders of magnitude lower than speeds in actual pressing operations.

The end of the test was taken as when a drop in the load was observed or when failure in the test piece occurred. Some tests had to be stopped prematurely because the wall extensometer came into contact with the die.

For all the tests performed except one the lubrication condition consisted of the liberal application of SAE 80 All PURPOSE EXTREME PRESSURE LUBRICANT to the clamp and punch radii. The radii had been cleaned with a cloth and no other special preparations were made. In the one other test a different lubrication condition was used where 0.004" thick polyethylene was coated with the SAE 80 oil on both sides and used on the punch radii. No measurement was taken of the surface condition of the punch or the test materials though this was recognized as a factor which could influence the friction coefficient between the punch and the work piece.

In all tests the strain measurements below a depth of half an inch ($H/W = 0.115$) were considered inaccurate and are not shown. The errors in the strain and depth measurements and the fact that the bending over the punch radii may not have become fully plastic are the reasons for disregarding the results under half inch depth.

6.3 EXPERIMENTAL RESULTS

Figure (39) shows the load and strains measurements for the 6010-T4 material as functions of depth. The load has been normalized with respect to the original cross-sectional area and the ultimate tensile strength of the material. The normalized load, P^* , is then given as

$$P^* = P/UTSx A_0 \quad (6.1)$$

The graph in figure (39) has not been plotted against depth, but against the non-dimensional depth parameter, H/W which is used in chapter five. The test was stopped when a drop in the punch load was observed. The experimental results for the other materials tested are shown in the figures (40) to (46). Tests were stopped on the IF, DP2, and DP3 (oil only lubrication) materials because of the wall extensometer coming into contact with the clamping dies.

All test materials that failed except the 7146 alloy, did so by localized shear in the middle of a side wall, indicating that the bending strains could be safely neglected for most materials where the R/t ratio of the bend is large. The 7146 alloy failed prematurely by fracture at the clamp radii. This is most likely due to this material's sensitivity to sharp radius bends and its poor formability.

6.4 STRAIN CONDITION IN TEST PIECES

The strain condition in the bottom and the side wall of the shallow pan specimens was calculated by measuring a width strain, ϵ_2 from the initial and final width dimensions of the bottom and walls, and then using the final strains recorded by the extensometers a value for the strain ratio, β could be determined.

TABLE IV

STRAIN CONDITION IN TEST PIECES

MATERIAL	β_{wall}	β_{bottom}
6010	-.4	-.35
7146	-.27	-.33
IF	-.5	-.5
DP2	-.5	-.3
DP3	-.5	-.49
DP3*	-.42	-.5
DP4	-.42	-.41
DP5	-.33	-.5

* oil and polyethylene lubrication

Table IV shows the values of the strain ratio, β for all the specimens tested. All of the specimens had strain ratios between the plane strain condition, $\beta = 0.0$ and simple tension, $\beta = -0.5$.

The straining that occurred in the test specimens was not uniform for either the wall or the bottom. Figure (47) shows an exaggerated schematic of the strain non-uniformity in the test specimen.

For the bottom the non-uniformity of the strain was very small (10-15%) while the wall strain non-uniformity was (21%). From the arrangement of the extensometers the experimentally measured strains would be slightly higher (5%) than the average strain in the section.

6.5 FRICITION

The friction on the punch radii can be calculated for each test by using the experimental results, and the material stress-strain curves. The stress strain in tension is assumed to describe the strain hardening experienced by the test piece. This can be justified since the straining conditions in the test pieces are close to simple tension. Also in the analysis used here only the shape of the stress strain curve is important and the von Mises and Hill models of the yield surface predict only a change in strength level and not in the shape of the curve when the straining

condition is changed from simple tension to plane strain.

Because there was slight differences in the widths of the wall and bottom sections due to the slight differences in strain condition the following equation relating forces over the punch radius was used instead of equation (5.7)

$$F_{\text{wall}} = F_{\text{bottom}} \times \exp(\mu\theta) \quad (6.2)$$

By using the stress strain curves, see figures (12) to (18) for determining the stress and the following equation for the force

$$F_1 = \sigma_1 \times A = \sigma_1 \times A_0 \times \exp(-\epsilon_1) \quad (6.3)$$

then the friction coefficient is given by

$$\mu = \left(\ln(\sigma_{\text{wall}}/\sigma_{\text{bottom}})^{-\epsilon_{\text{wall}} + \epsilon_{\text{bottom}}} \right) / \theta \quad (6.4)$$

The value of the wrap angle, θ is a function of only the geometry and figure (48) shows the plot of θ as a function of depth H/W for the geometry used. The friction coefficients calculated from equation (6.4) are presented as functions of depth in figures (49) to (55), for all materials. The scatter in the readings is high presumably due to the assumptions made and the errors in the measure-

ments. An estimate of the effective friction coefficient was made and is shown as the dotted lines in the figures. It should be noted that the coefficient is approximately 0.22 for most of the materials. Although very little information is available in the literature, this value appears greater than that generally assumed in press forming calculations. In figure (56) the friction coefficient for the 6010-T4 material is graphed against the percentage of strain occurring in the pan bottom. The friction coefficient results of Duncan, Shabel, and Gerbase [24] for the 6010-T4 coefficient are also shown in comparison. There is good agreement.

These estimated effective friction coefficients could now be used in the modelling of chapter five to generate theoretical results which should correspond to the experimental results. This was done using the refined model which included the digitizing of the stress-strain curves. Figures (57) and (58) show examples of the modelling and experimental results for the 6010 and DP3 materials respectively. These curves are typical of all the comparisons between the modelling and experimental results. All tests gave close agreement between the modelling and experimental results up to a depth of $H/W = 0.34$. Beyond this depth there was a consistent discrepancy in all tests indicating that the value of effective friction used in the

modelling was too low. This is further evidence that the friction does increase after a certain amount of sliding around the punch nose has occurred.

These results indicate that using a constant value of friction for modelling purposes is not accurate and that having the friction as a function of depth or bottom strain would be better. The modelling could be used to more accurately determine the friction coefficient as a function of depth from the experimental results. This was not done in this work. Figure (59) shows the effect of changing the friction μ for the theoretical simulation of the strains for the IF material.

6.6 EFFECT OF LUBRICATION CONDITION

Figure (53) shows the friction coefficient for the DP3 material with two different forms of lubrication. As well as the oil only lubrication, the results for oil plus polyethylene sheet are plotted. Clearly the use of polyethylene sheet reduces the friction coefficient by a large amount. In figure (60) the strains for the DP3 material are plotted against depth for the two lubrication conditions. It can be seen that at any one depth the bottom strain for the oil and polyethylene sheet test is higher than for the oil only test. Correspondingly there is a decrease in wall strain for the oil and polyethylene test.

A better indication of the friction effect is the amount of increase in depth that can be obtained with the same amount of wall strain. If the wall strain limit is taken as 0.16 then the depth increases from $H/W = 0.40$ to $H/W = 0.43$ which is approximately seven percent increase in depth. For the 6010-T4 alloy the friction coefficient was also calculated from the Ludwik equation (3.2) using the n and K values shown in table IV instead of the digitized tensile stress-strain curve. Resulting values of friction were slightly higher than those calculated by the digitized stress-strain curves.

6.7 EFFECT OF STRAIN INDEX ON THE BOTTOM STRAIN

In order to show the effect of the n value on the strain distribution in shallow pans the experimental wall and bottom strains for two materials with different n values were compared; the DP4 material, $n=0.1635$ and the IF steel, $n=0.31$. These two materials are compared since the n values for these materials is different while the terminal friction coefficients are similar. Figure (61) shows the experimental strains, from which it is evident that the higher n value increases the bottom strain while decreasing the wall strain, as would be expected from the modelling on the previous work done in chapter five.

6.8 SHALLOW PAN FORMABILITY

In figures (62) the maximum bottom strain, ϵ_{1b} is plotted as a function of the n value and the experimentally determined friction coefficient μ for the experimental results. Figure (63) shows the same figure replotted in a different form.

The previously estimated constant values of friction were used even though the modelling indicates these are underestimates of the actual values that occur when the maximum bottom strain is reached. While the IF, DP2 and DP3 tests were stopped before failure examination of the experimental strains showed that the bottom strains were very close to their maximum values for all three of the materials, so the final strains are plotted as the maximum bottom strains. A plot as the theoretical modelling bottom strains as functions of n and μ are also plotted with the experimental strains.

In the plots the 7146 test is included though the mode of failure of this material is not the same as the other tests. The DP3 test with oil and polyethylene lubrication is also included; while this is a different lubrication condition it should be accounted for by the friction terms.

There are two sources of error in these diagrams. One is that the n values for the materials which are used in

the modelling do not accurately reflect the strain hardening behaviour; this was discussed in chapter four and the graphs illustrate this point. The second source of error is the friction. The experimental values plotted in figures (49) to (55) were based on several assumptions and also had considerable scatter due to the errors in measuring the experimental strains.

The greatest source of error is in the estimation of the constant effective friction. The theoretical and experimental strain comparisons of section 6.5 show that the constant friction coefficients used in the modelling were inaccurate. While the actual value of the friction is subject to error the relative ranking of the friction coefficients should be more accurate since the same method was used to determine the values. If the values of friction are taken to be relatively correct then figure (62) suggests that the DP2 steel really has a lower effective n value, closer to the n value of the DP5 steel, while the DP4 has a higher effective n , also close to the value of the DP5 steel. This is what was observed in chapter four from the indications of the n curves and bulge test data for these materials.

The 6010 and the DP3 steel with oil only lubrication show some discrepancy from the theoretical predictions. This probably is due to errors in both the n index and the

friction but it is impossible to separate the two sources of error. The work of Duncan et al [24] on the friction of 6010 material indicates that the friction coefficient used here may be slightly high. All other materials, IF, DP5, DP3 (oil and polyethylene) and 7146 fall very close to the theoretically predicted values.

In figure (64) the materials are ranked according to the experimental bottom strain as well as the n value. The DP3 material tested with oil and polyethylene is not included since it would be unfair to compare tests having different lubrication conditions. The DP4, DP3 and 6010 materials have changed their ranking. The 6010 material moves from the fourth position to the third position with a considerable increase in its relative formability when the bottom strain is used instead of the n value for ranking. The DP4 material moves from sixth to fifth position and its relative formability increases to roughly that of the DP5 steel. The DP3 material loses some of its relative formability and drops from fifth position to sixth position for the bottom strain ranking. The IF and DP2 still retain the first two rankings with very high relative formability. The figure (62) indicates that the DP2 steel maintains its ranking because the lowering of the effective n value is offset by having a lower friction coefficient.

The modelling could be used in conjunction with the

experimental results plotted in figure (62) to determine the actual effective value of friction but this would require the materials to fit the Ludwig equation (3.2) perfectly so that accurate n values could be used.

Since the bottom strain from the simulative test takes account of friction, and the relevant features of the materials' stress strain which may not be reflected in the n value, it would be a better method of ranking materials for formability than n values or any other tensile parameter.

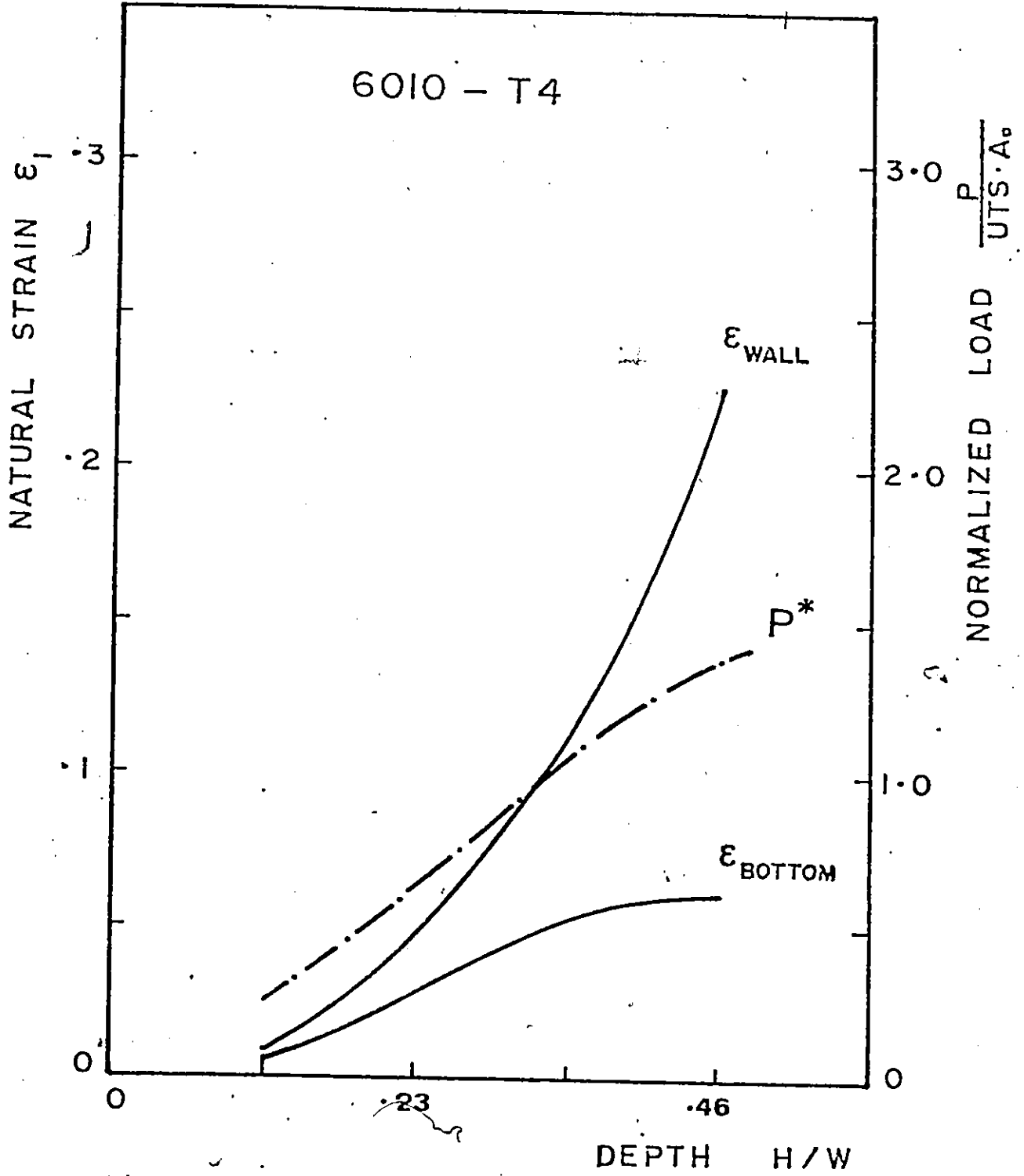


Fig. 39

- Experimental strain and load results for the 6010-T4 material

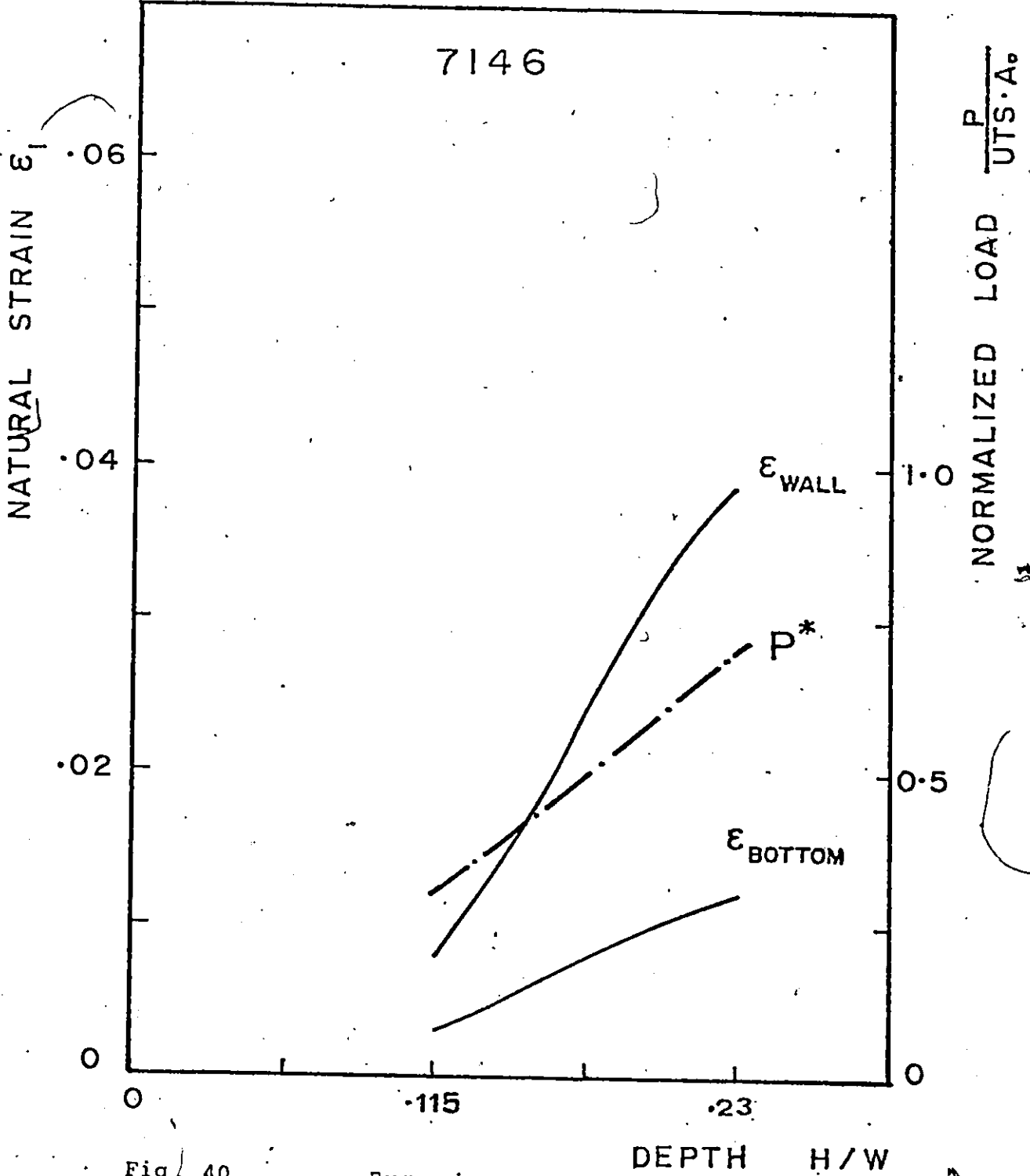


Fig. 40

- Experimental strain and load results for the 7146 material

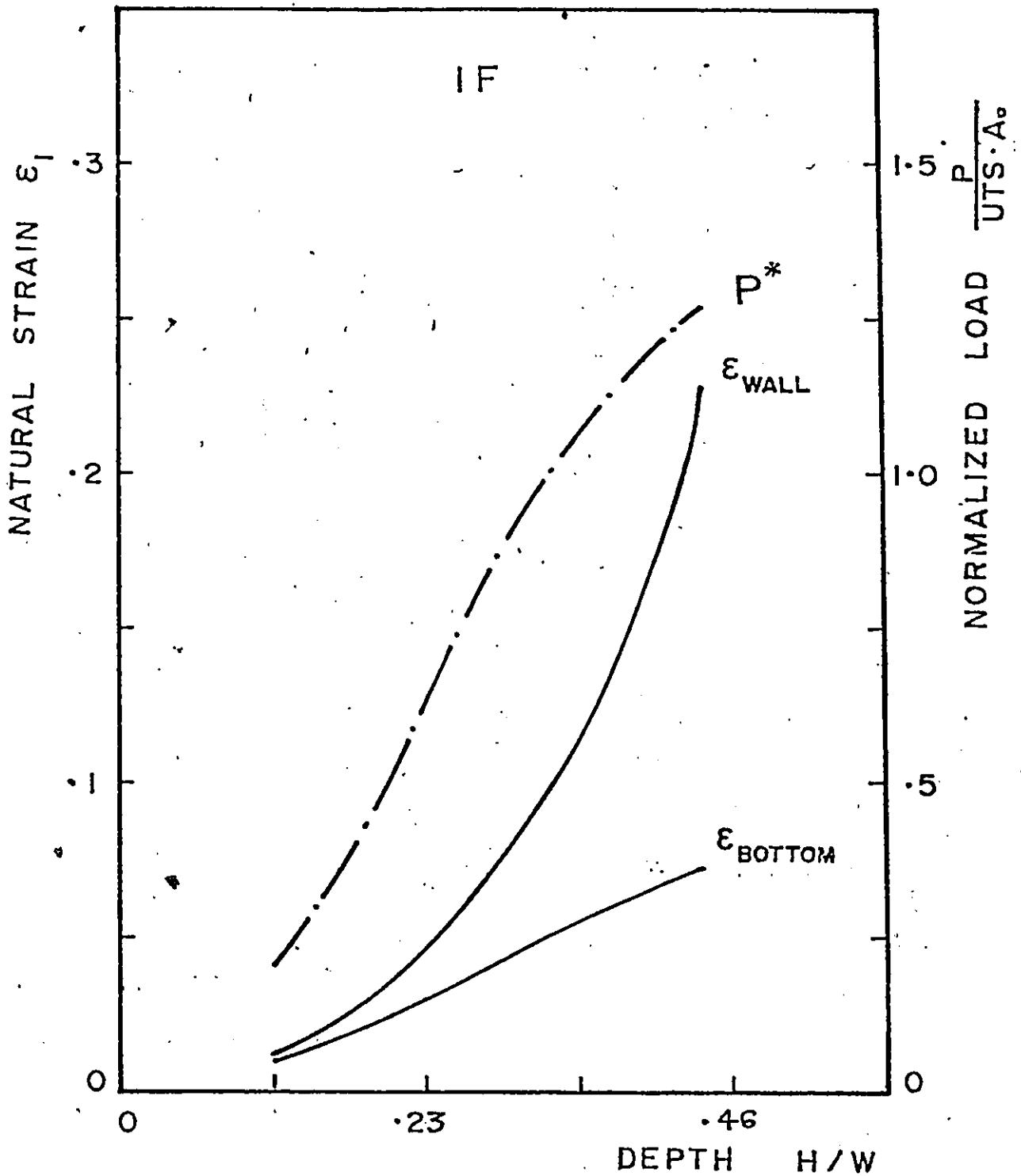


Fig. 41 - Experimental strain and load results for the IF material

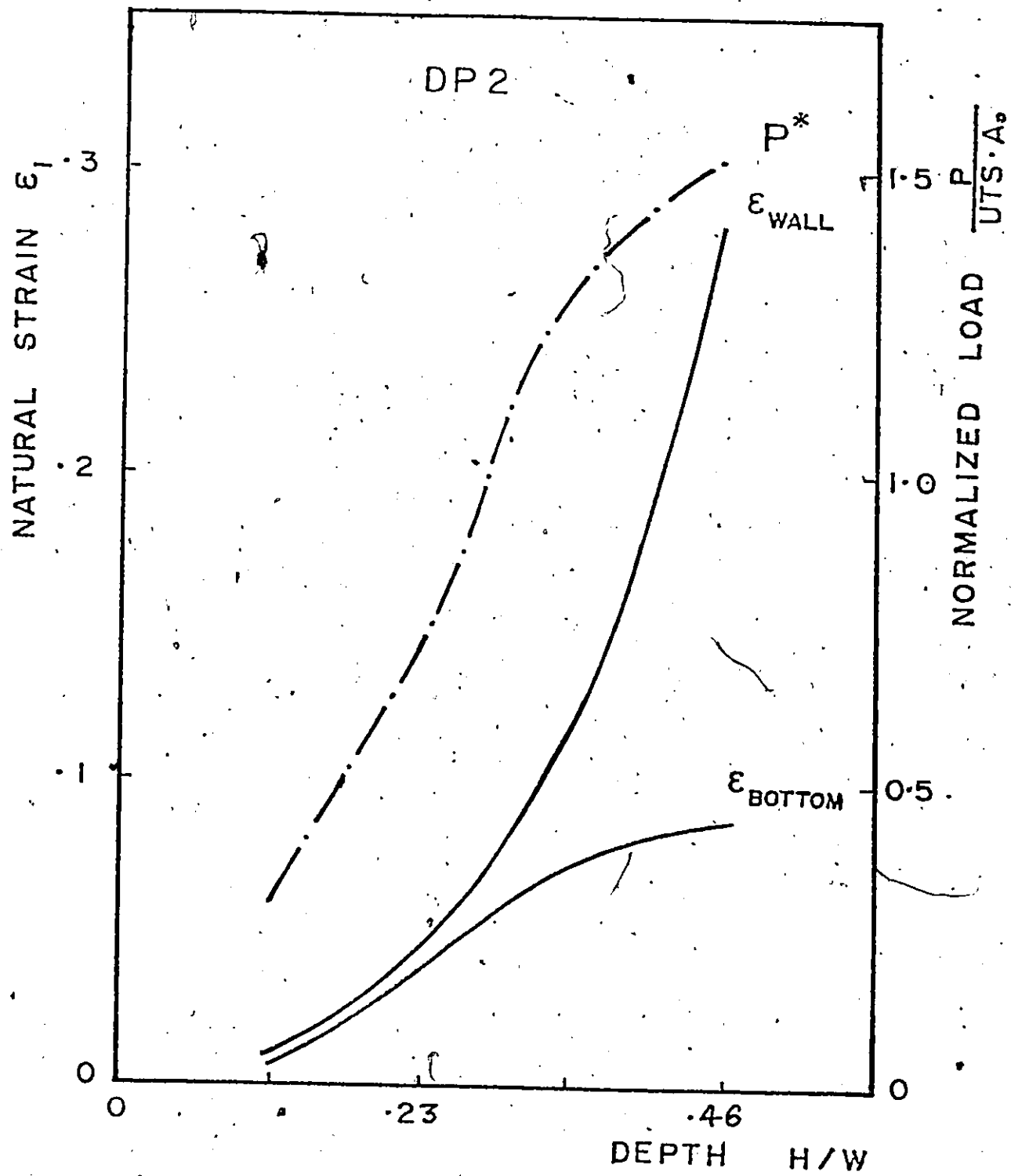


Fig. 42 - Experimental strain and load results for the DP2 material

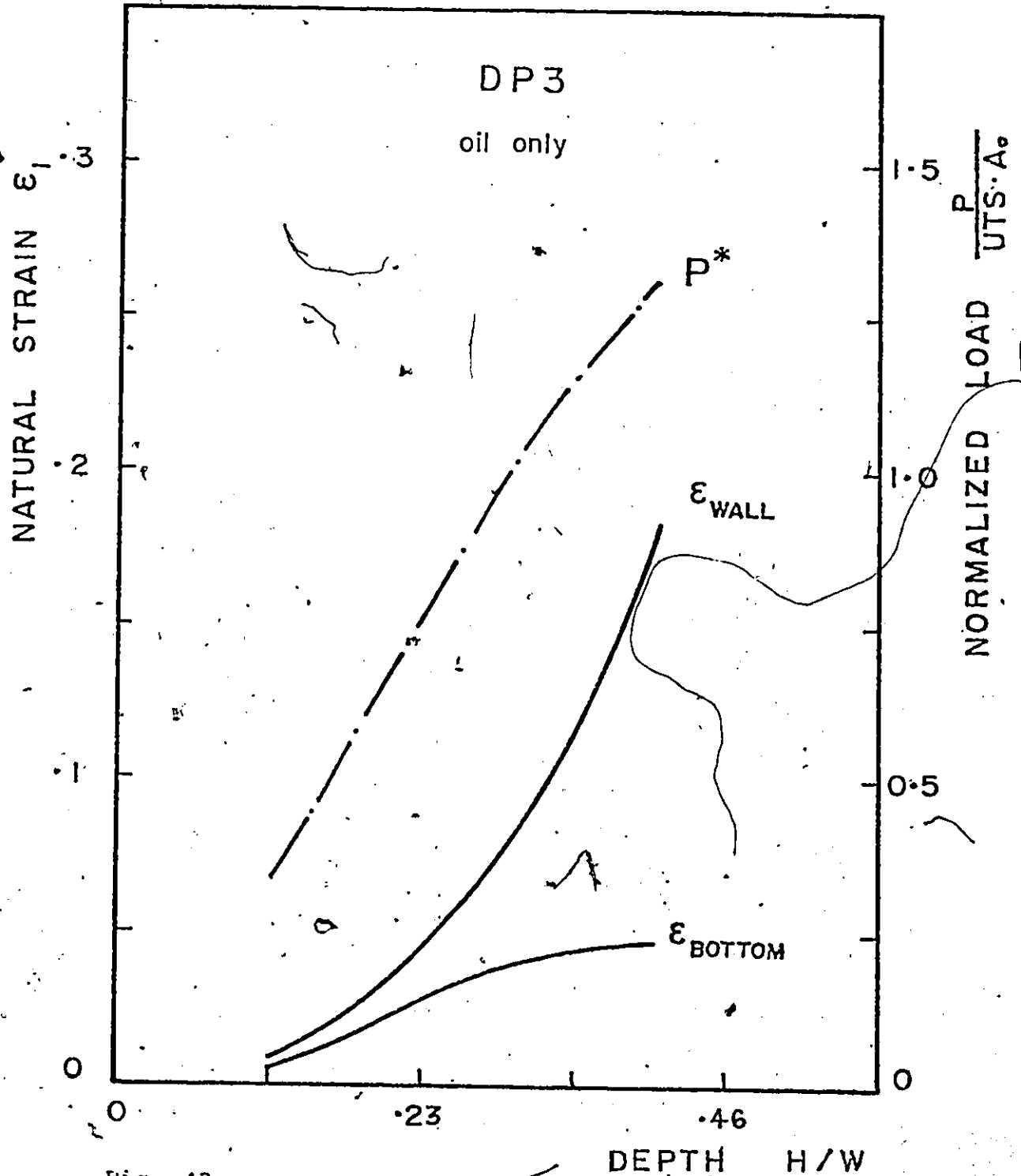


Fig. 43

- Experimental strain and load results for the DP3 material, oil only lubrication

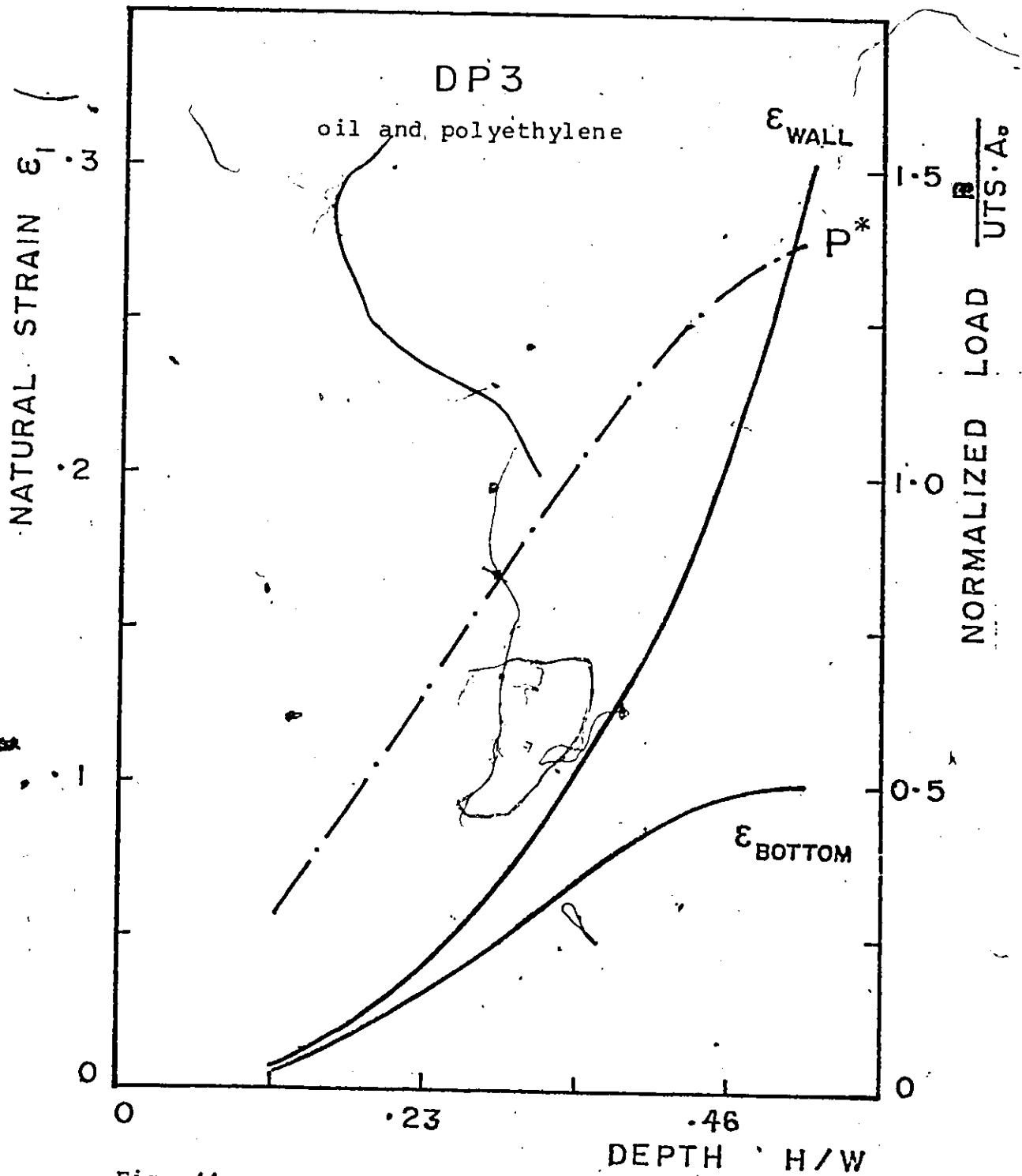


Fig. 44

- Experimental strain and load results for the DP3 material, oil and polyethylene lubrication

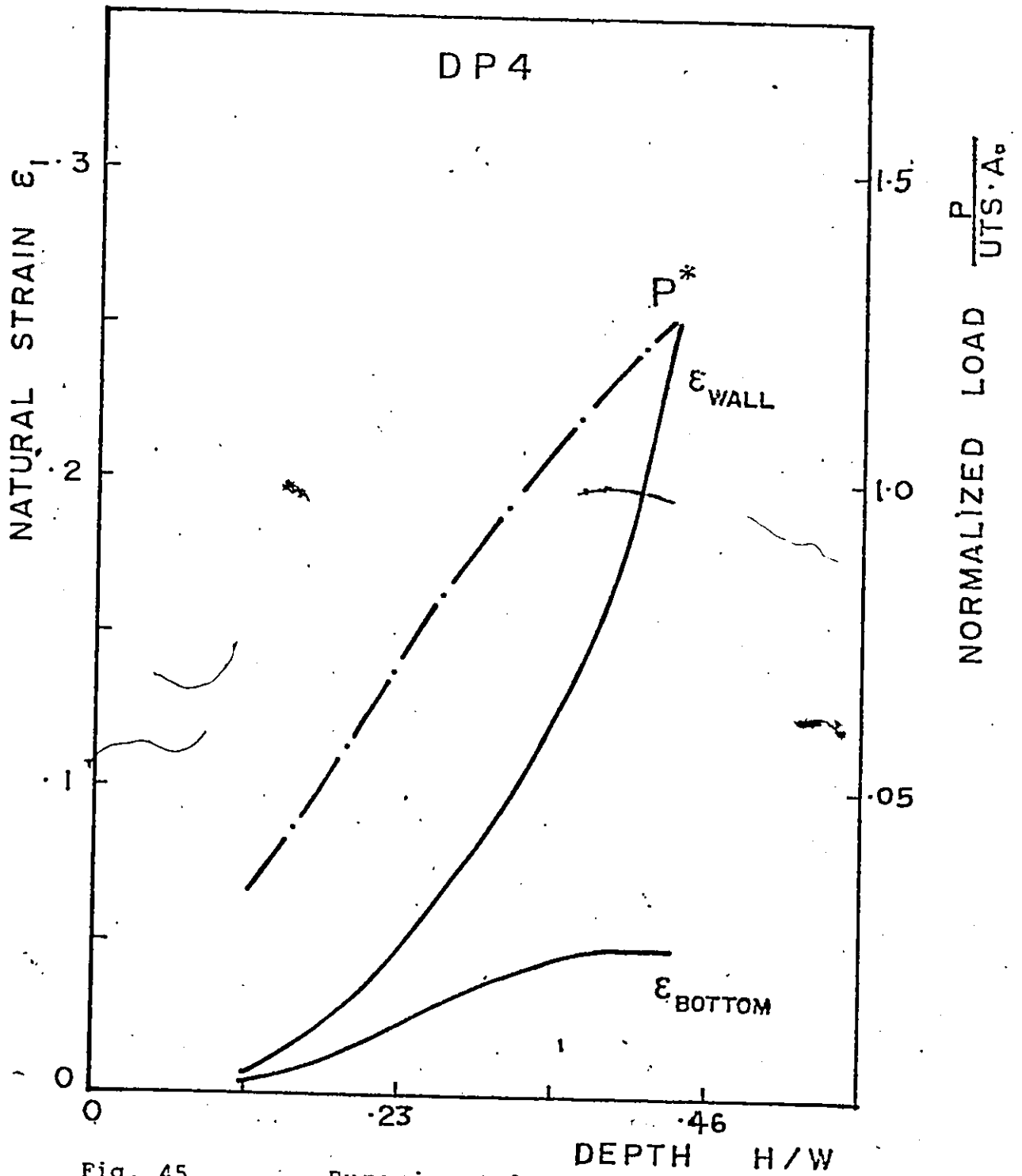


Fig. 45 - Experimental strain and load results for the DP4 material

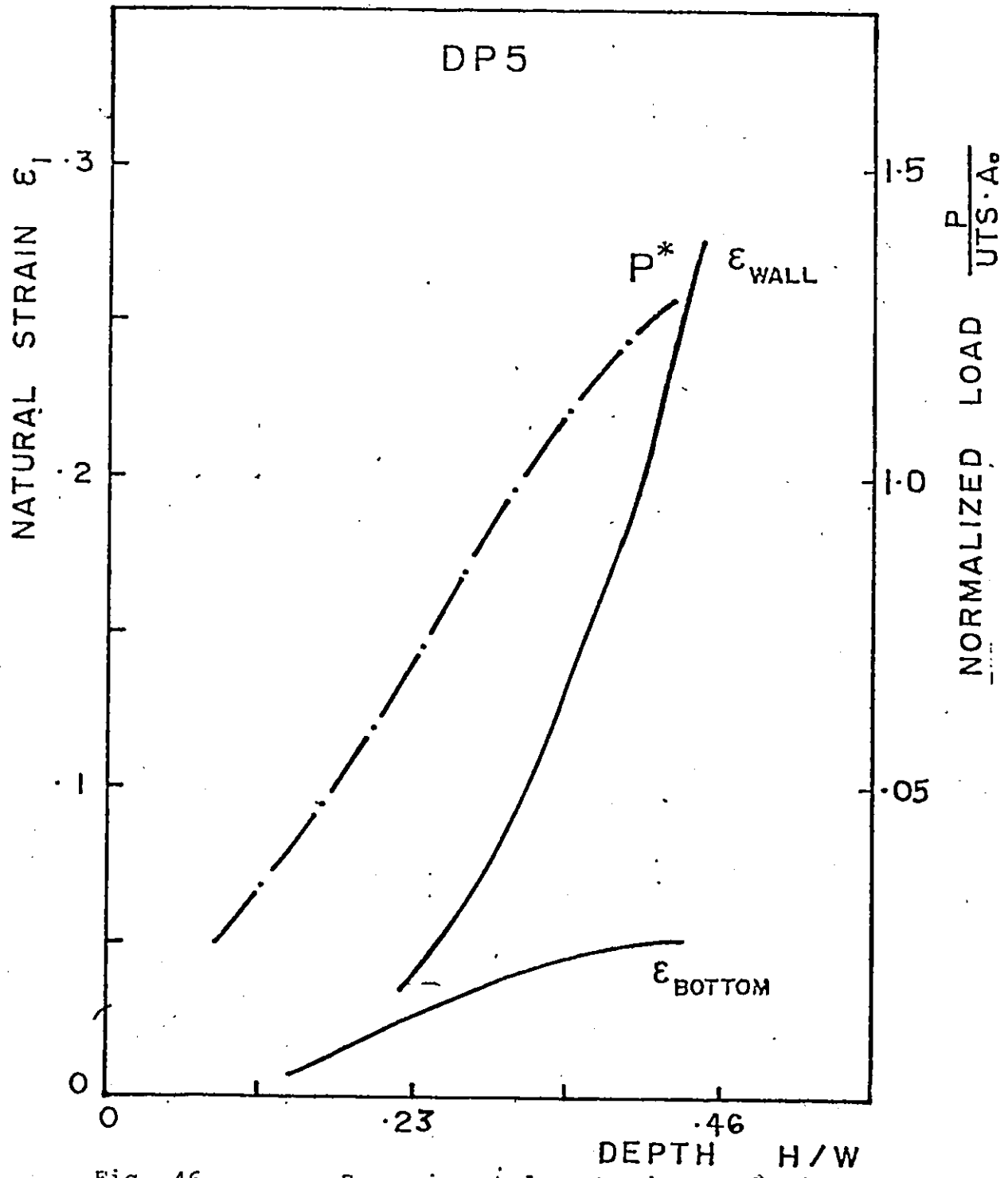


Fig. 46 - Experimental strain and load results for the DP5 material

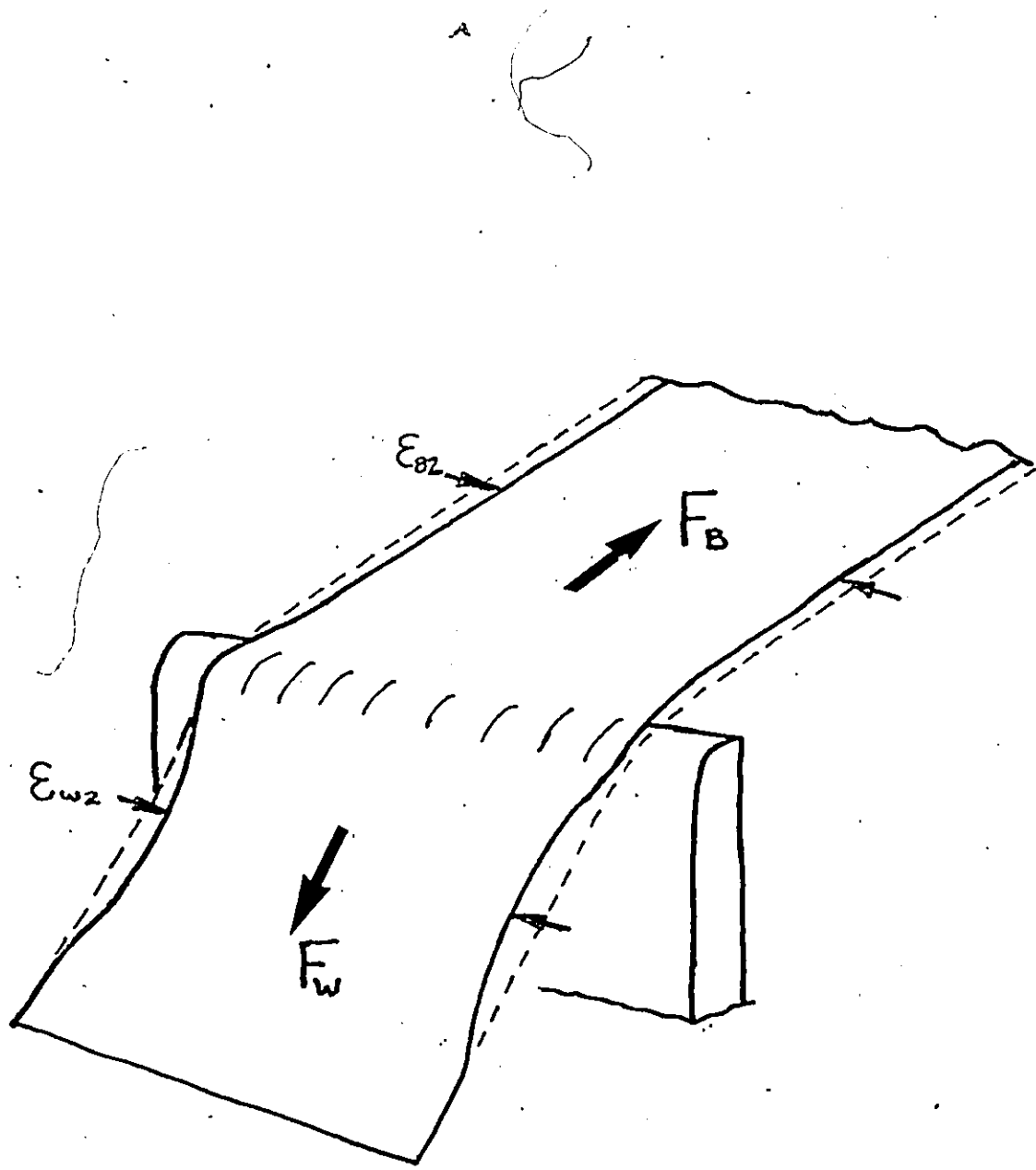


Fig. 47

- Exaggeration of strain non-uniformity in test pieces

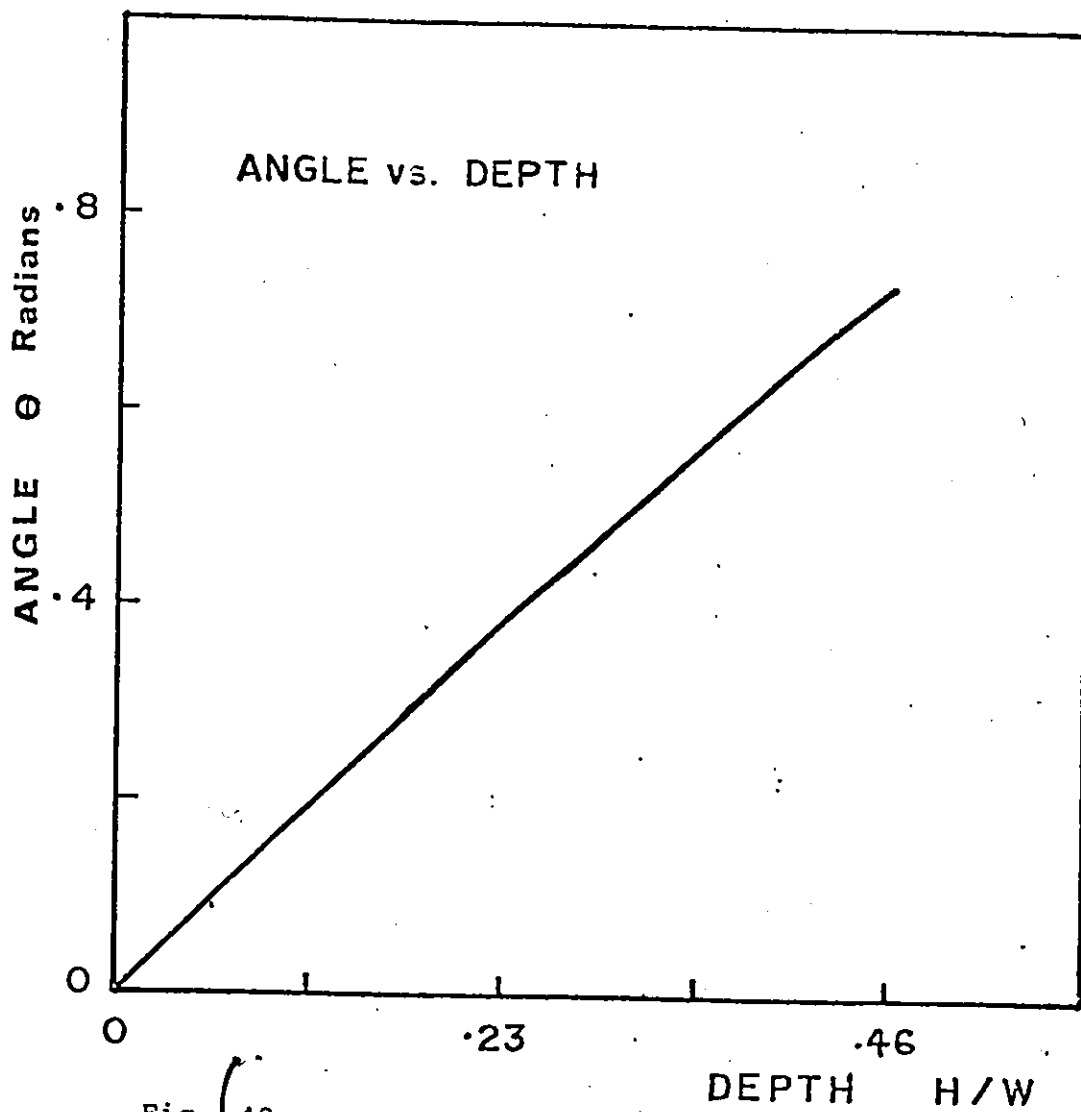


Fig. 48

- Side wall angle θ versus depth

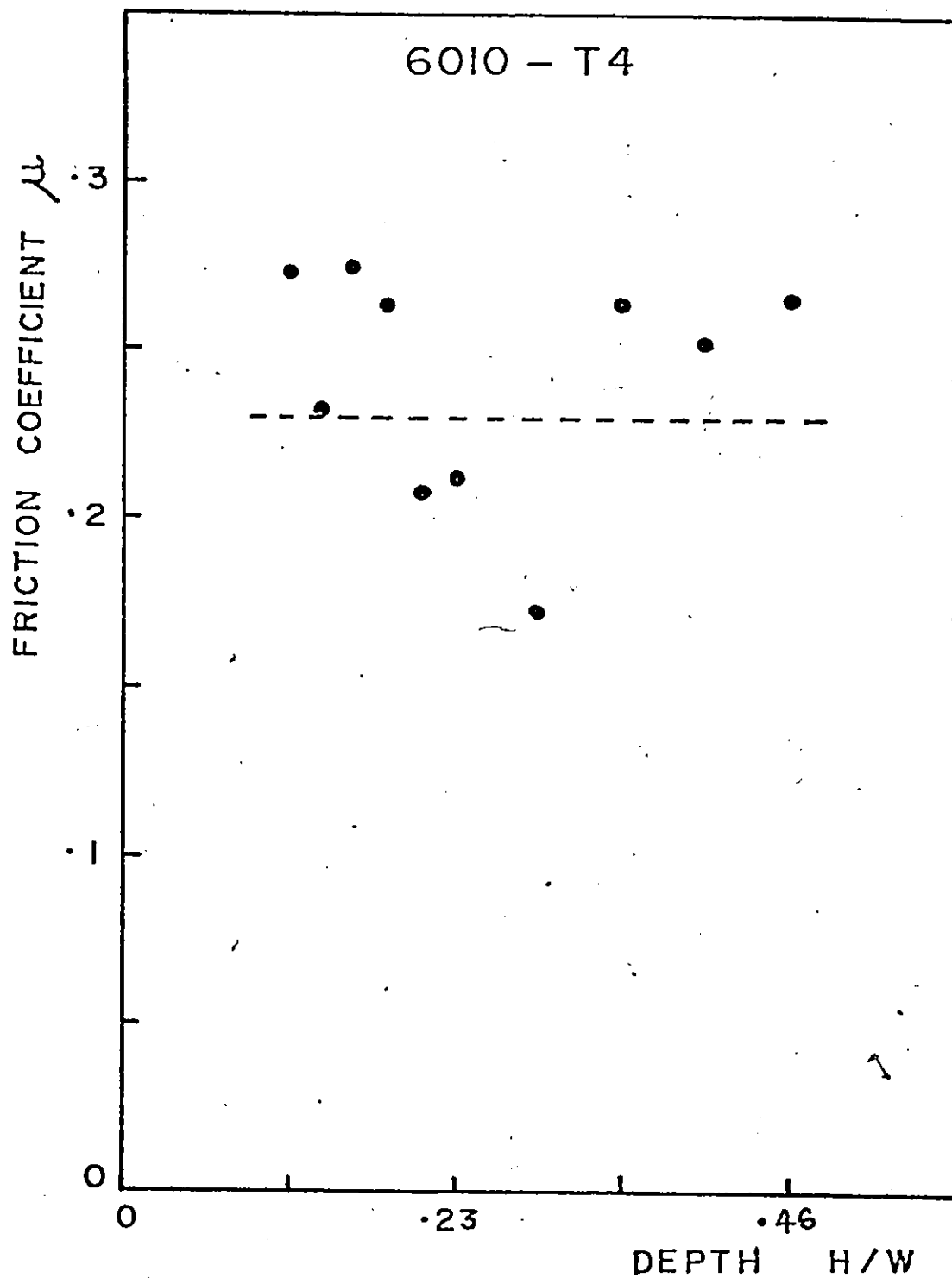


Fig. 49

- Friction coefficient μ calculated from experimental strains for 6010-T4 material

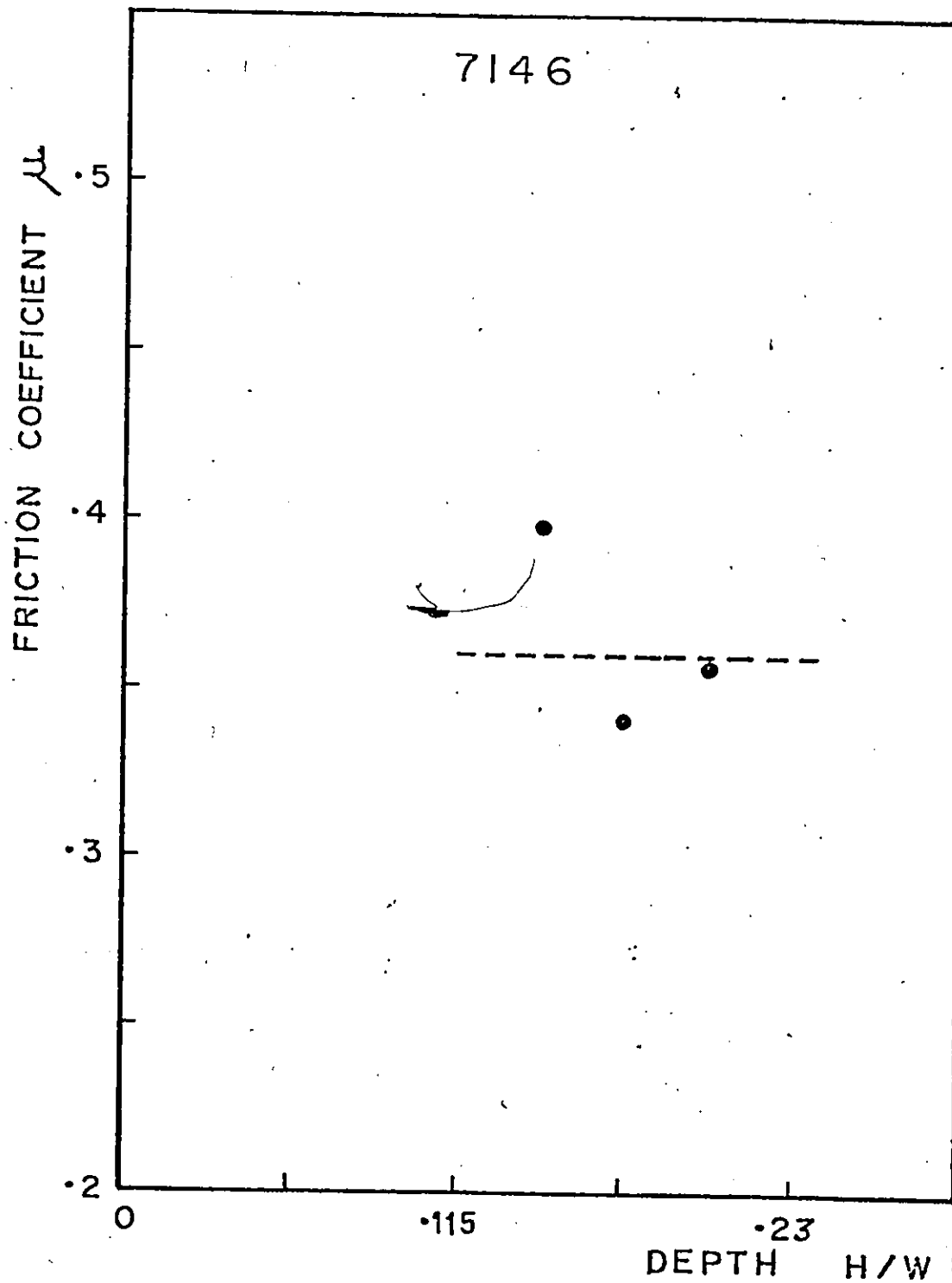


Fig. 50

- Friction coefficient μ calculated from experimental strains for 7146 material

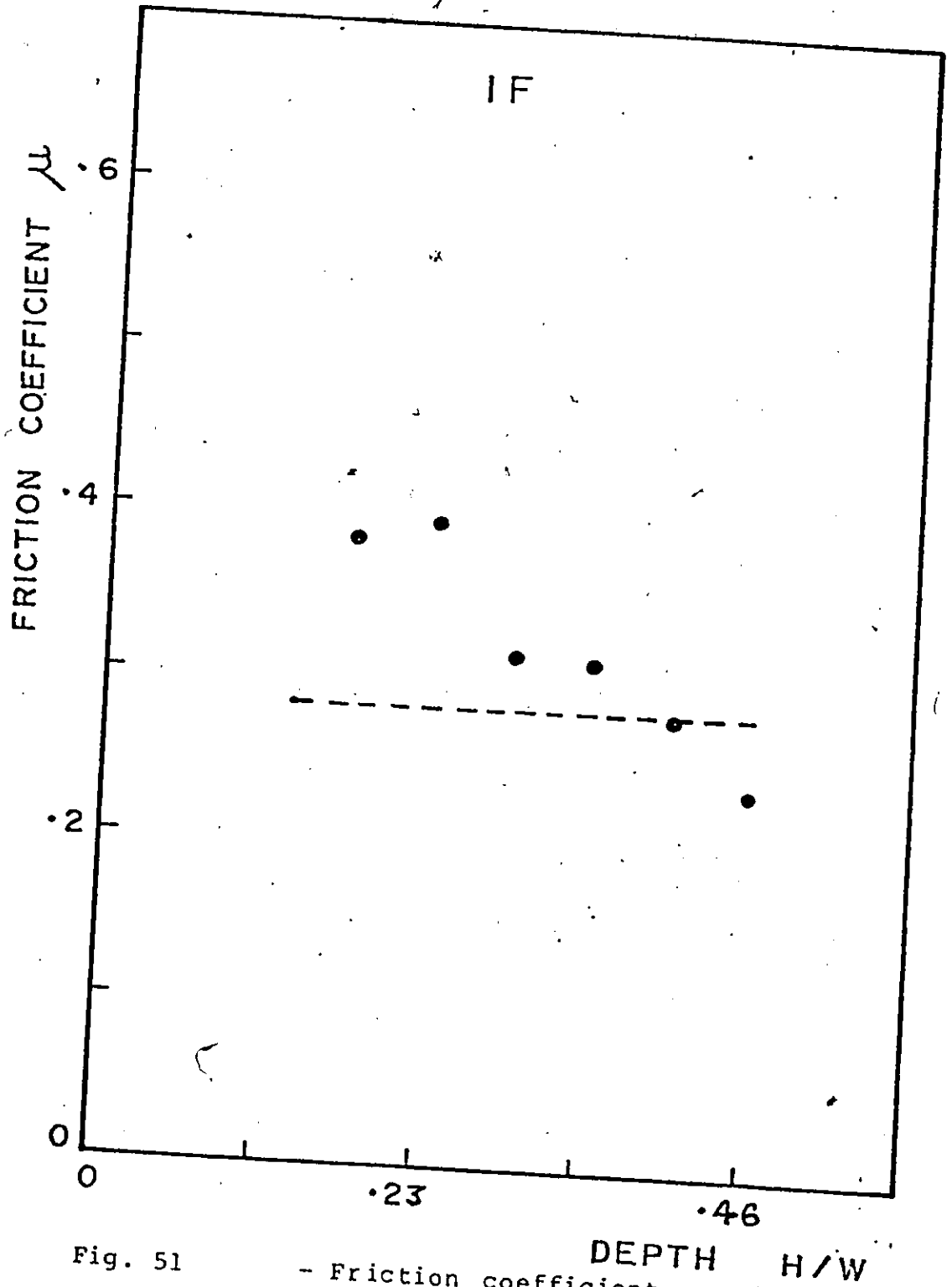


Fig. 51

- Friction coefficient μ calculated from experimental strains for IF material

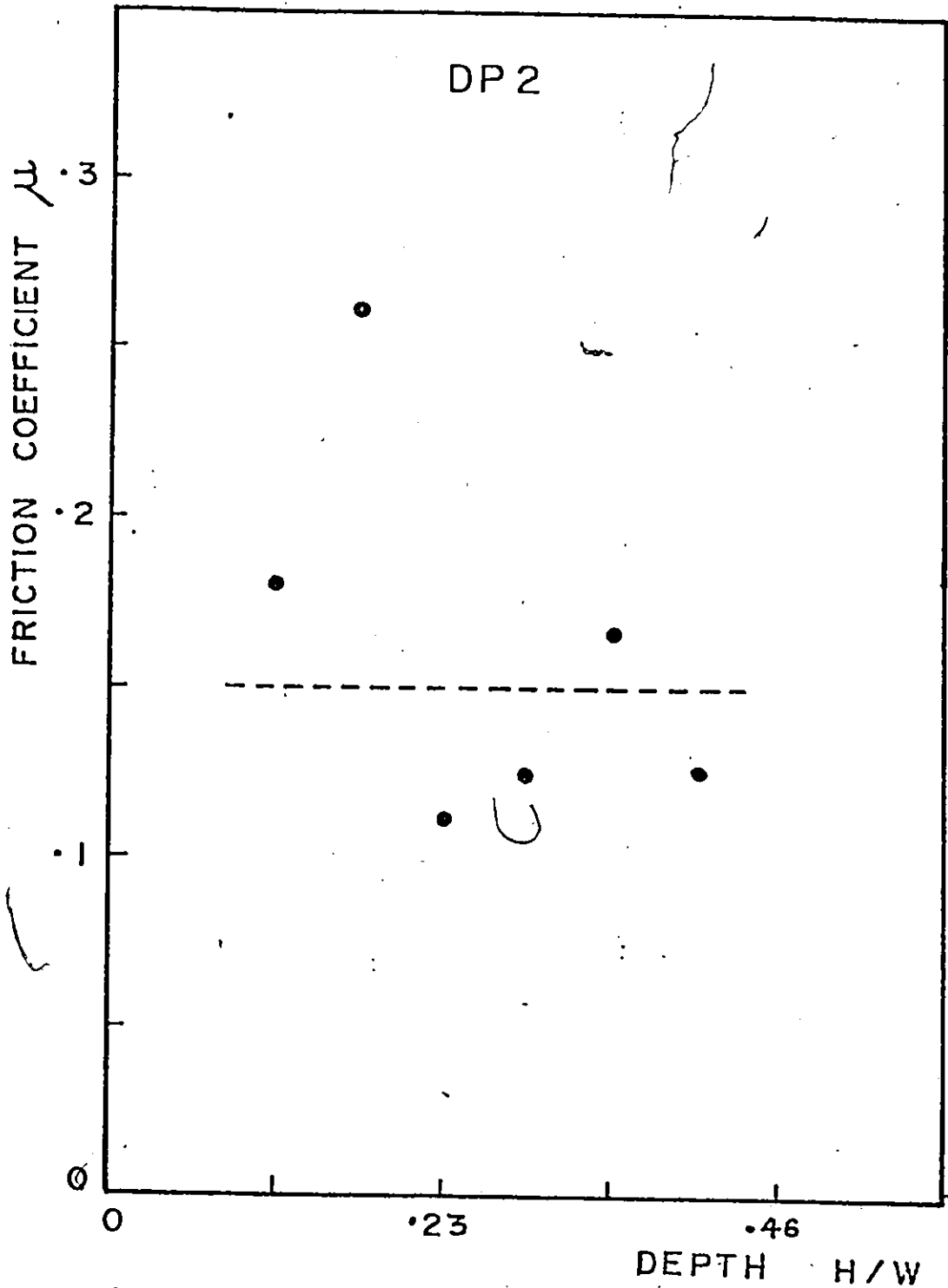


Fig. 52 - Friction coefficient μ calculated from experimental strains for DP2 material

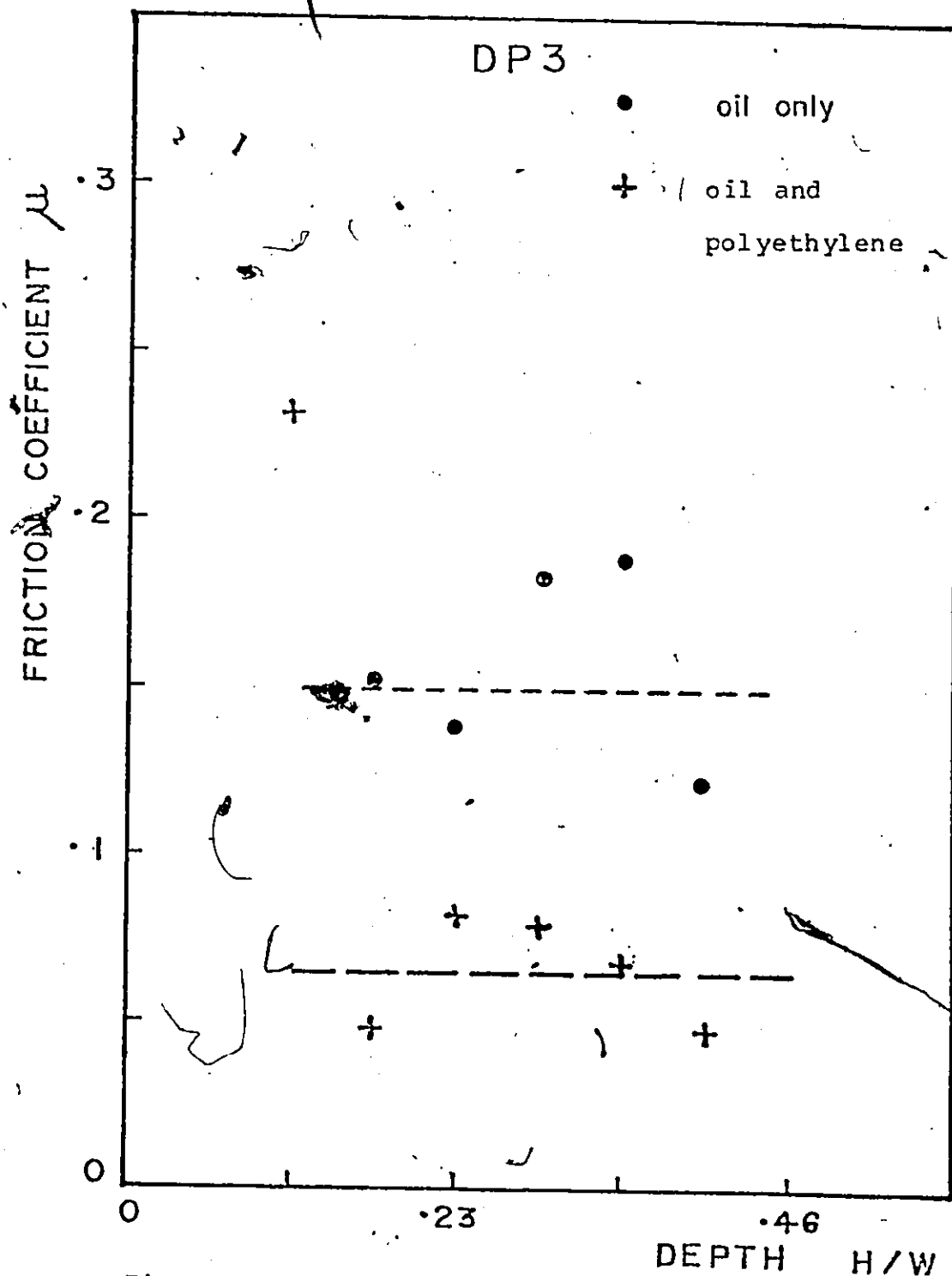


Fig. 53

- Friction coefficient μ calculated from experimental strains for DP3 material, both types of lubrication

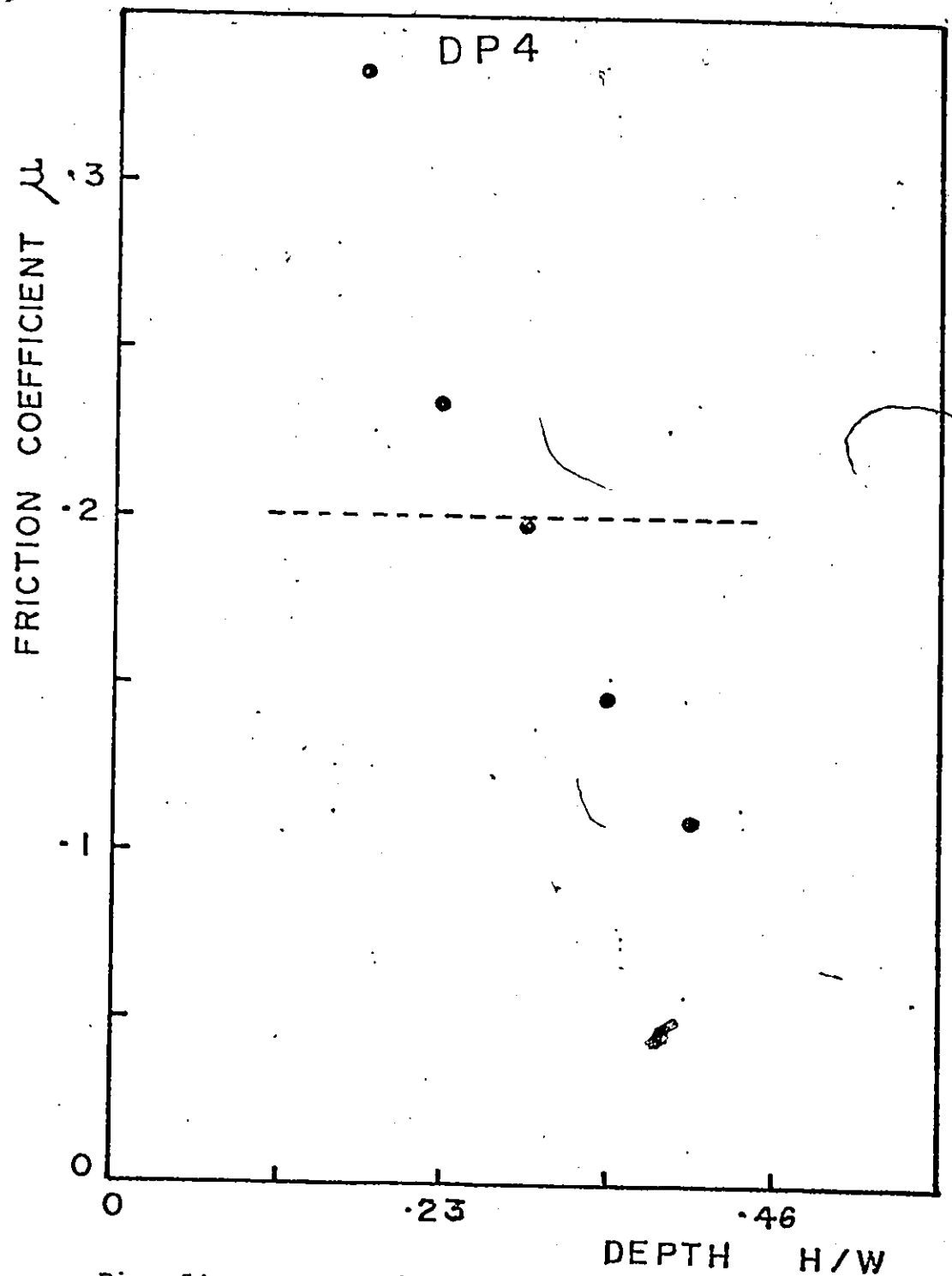


Fig. 54 - Friction coefficient μ calculated from experimental strains for DP4 material

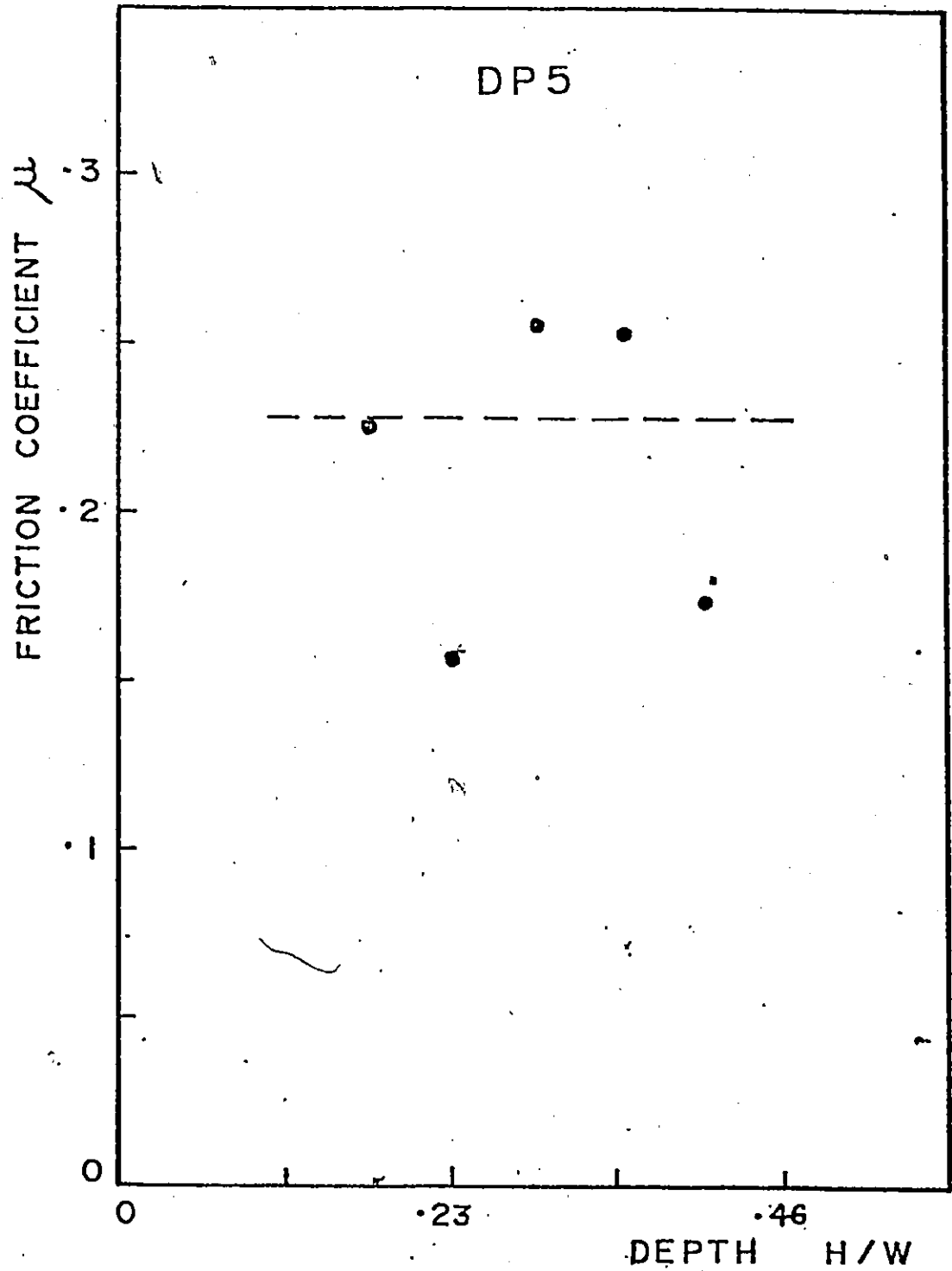


Fig. 55

- Friction coefficient μ calculated from experimental strains for DP5 material

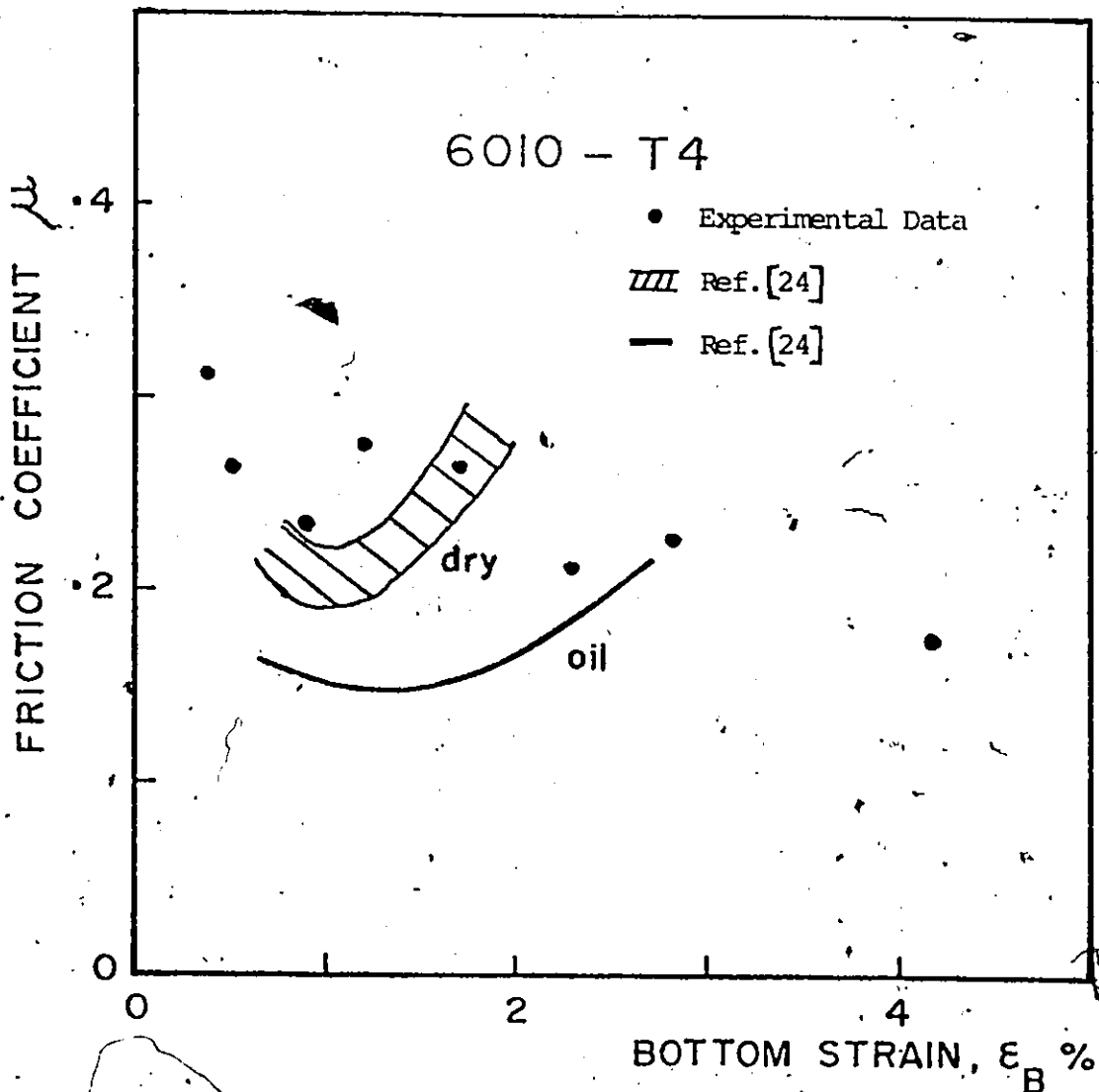


Fig. 96

- Comparison 6010-T4 friction coefficient μ with work of Ref. [24]

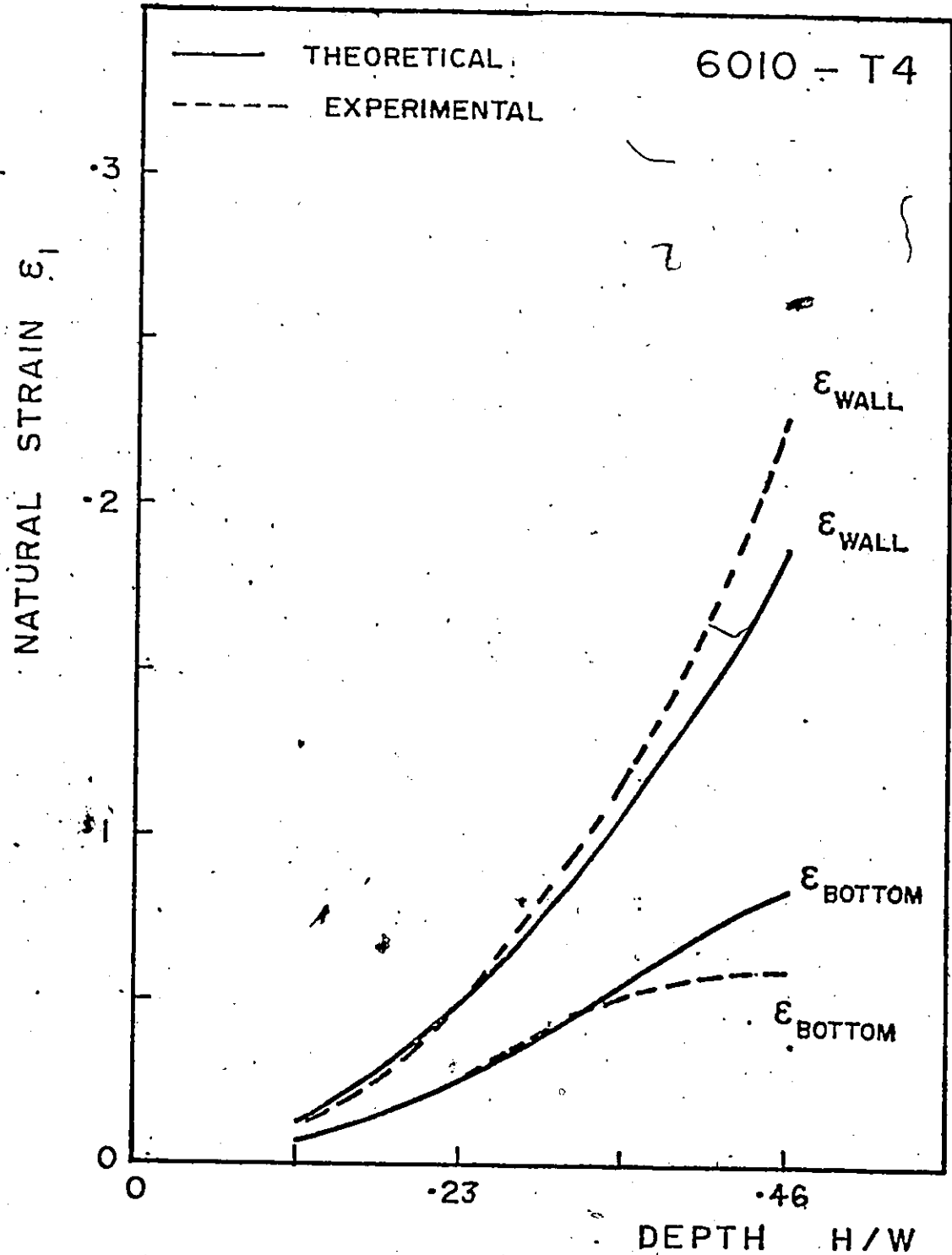


Fig. 57

- Comparison of experimental strains with those computed from the refined model for the 6010-T4 material

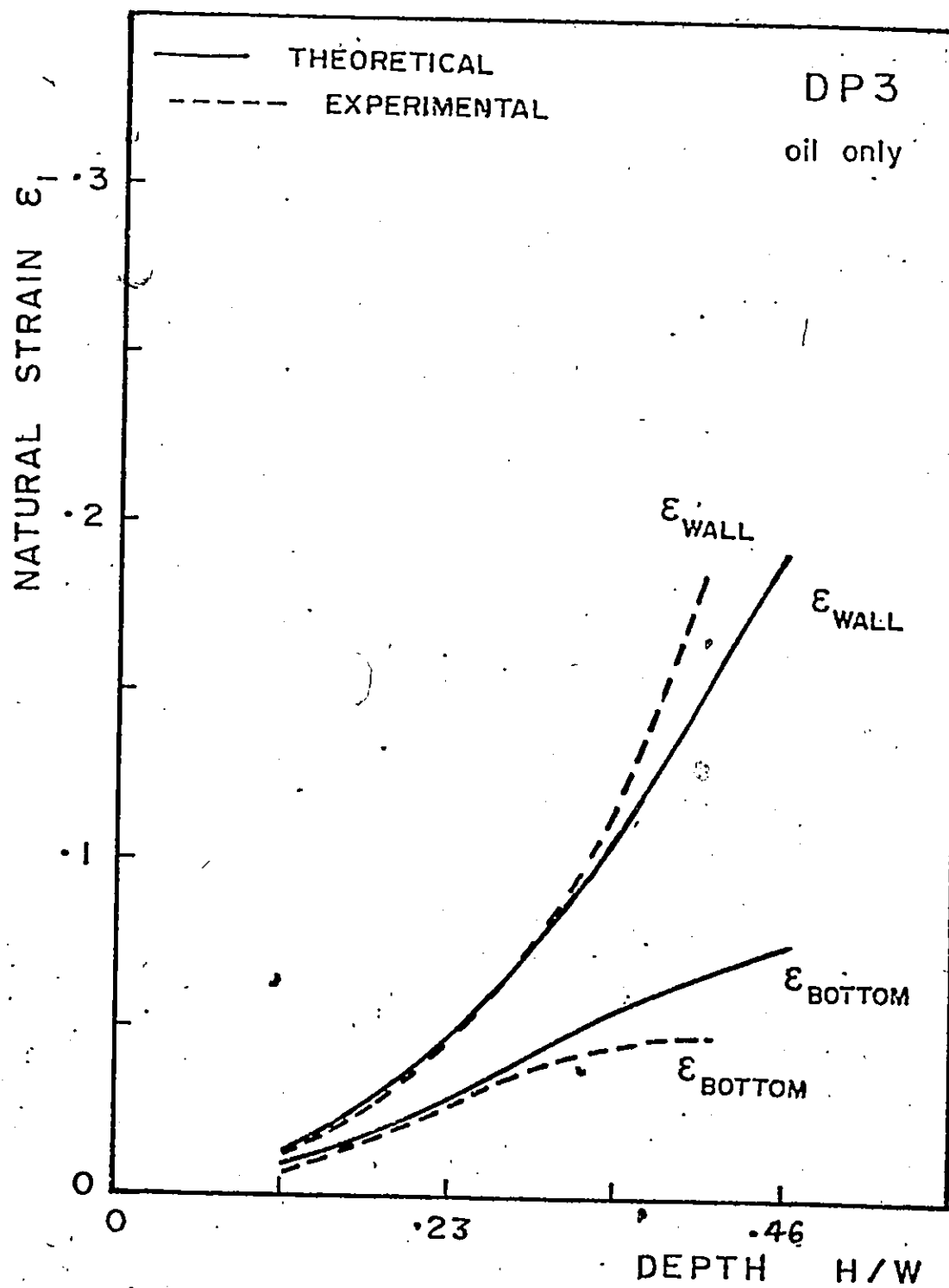


Fig. 58

- Comparison of experimental strains with those computed from the refined model for the DP3 material, oil only lubrication

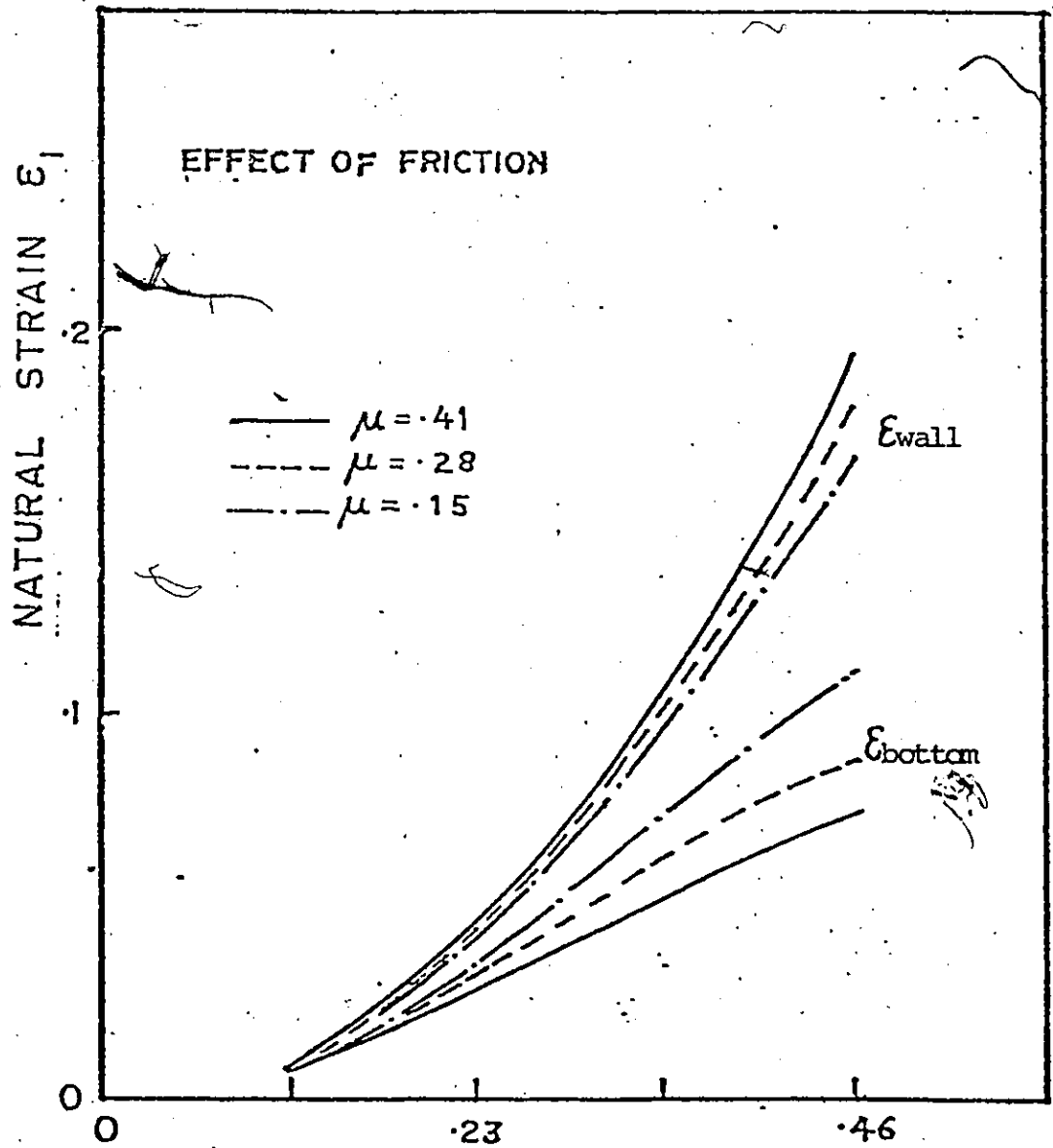


Fig. 59 - Effect of changing the friction coefficient μ on the theoretical strains

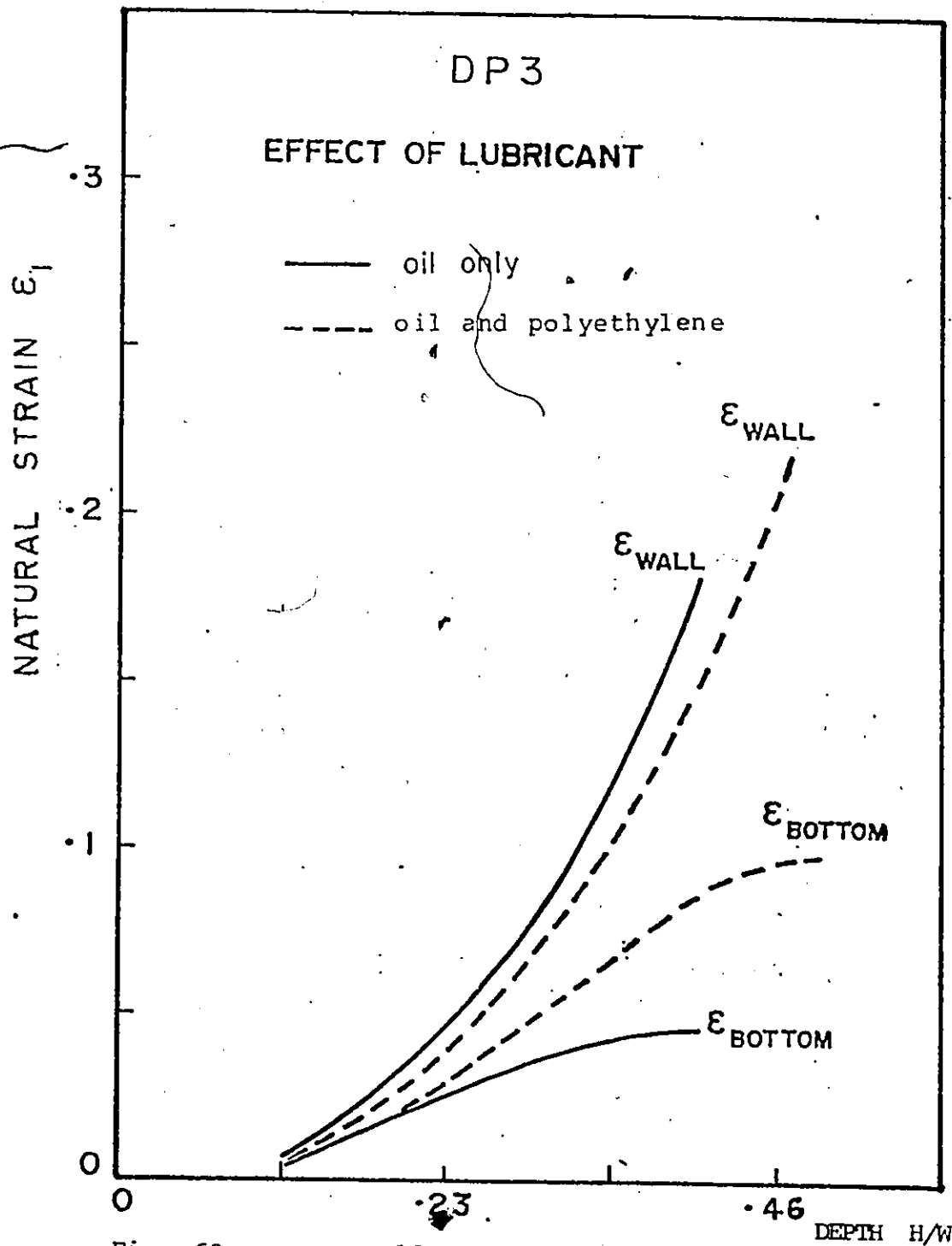


Fig. 60

- Effect of changing the friction coefficient μ on the experimental strains

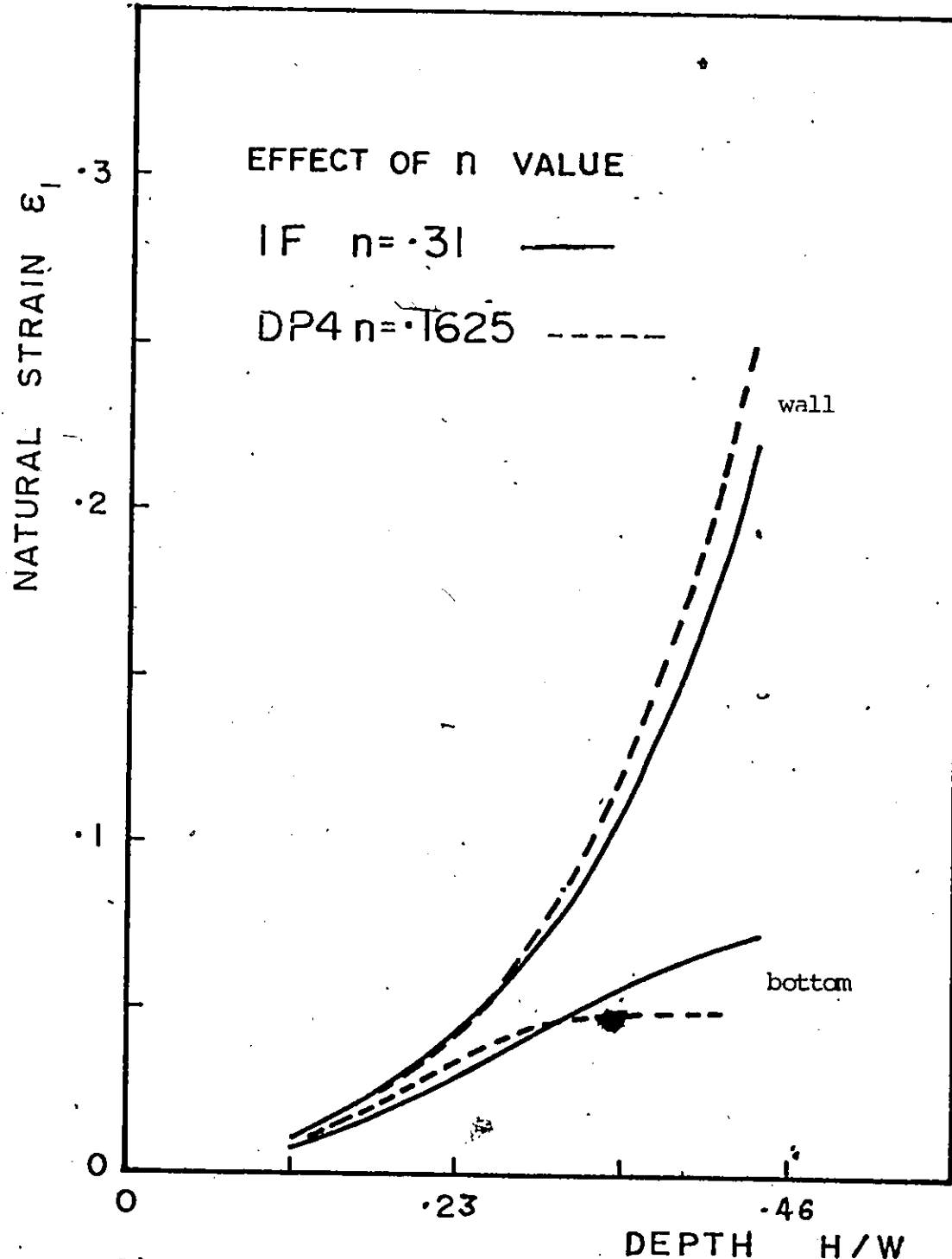


Fig. 61 - Effect of changing the n value on the experimental strains

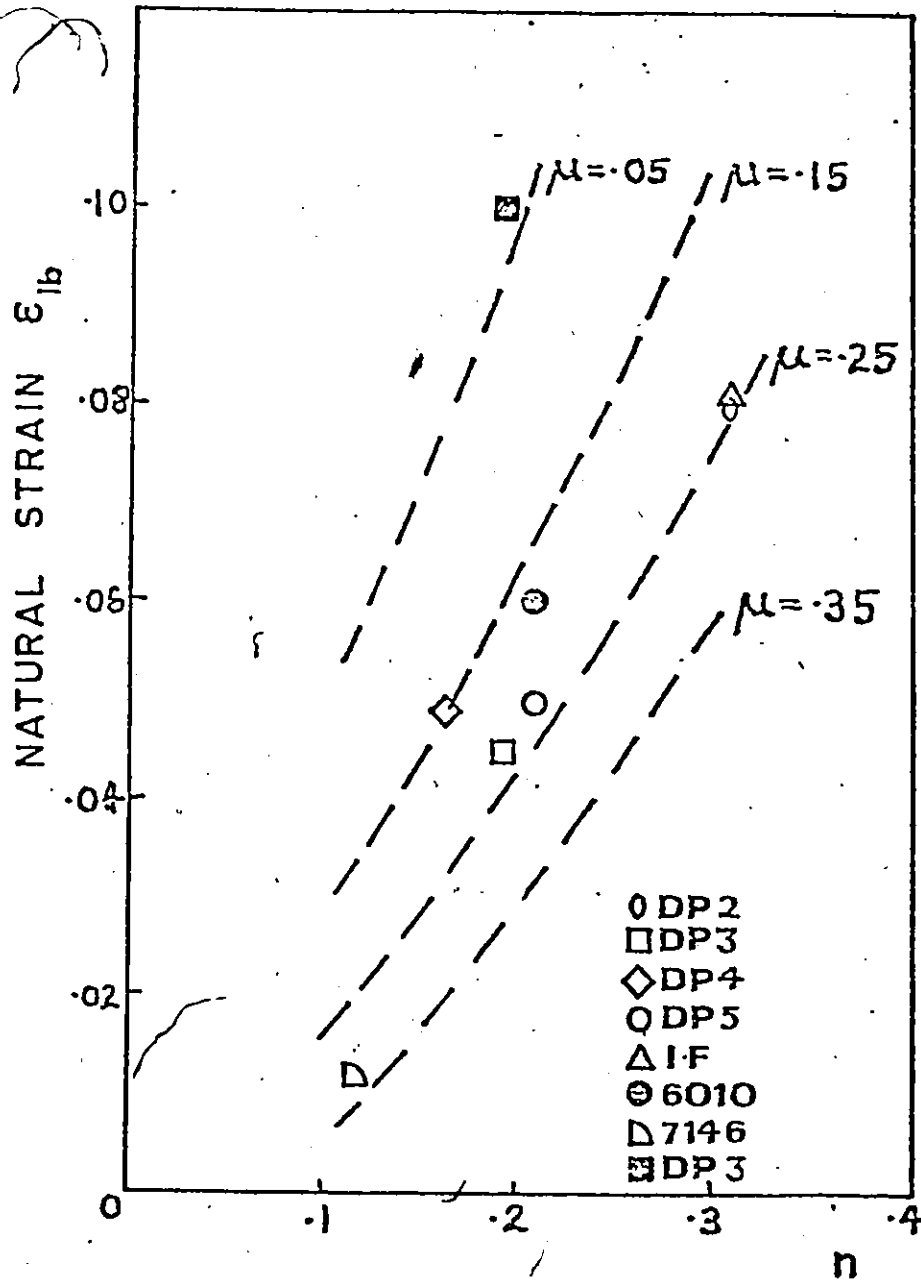


Fig. 62 - Experimental bottom strain ϵ_{1b} versus friction for several n values

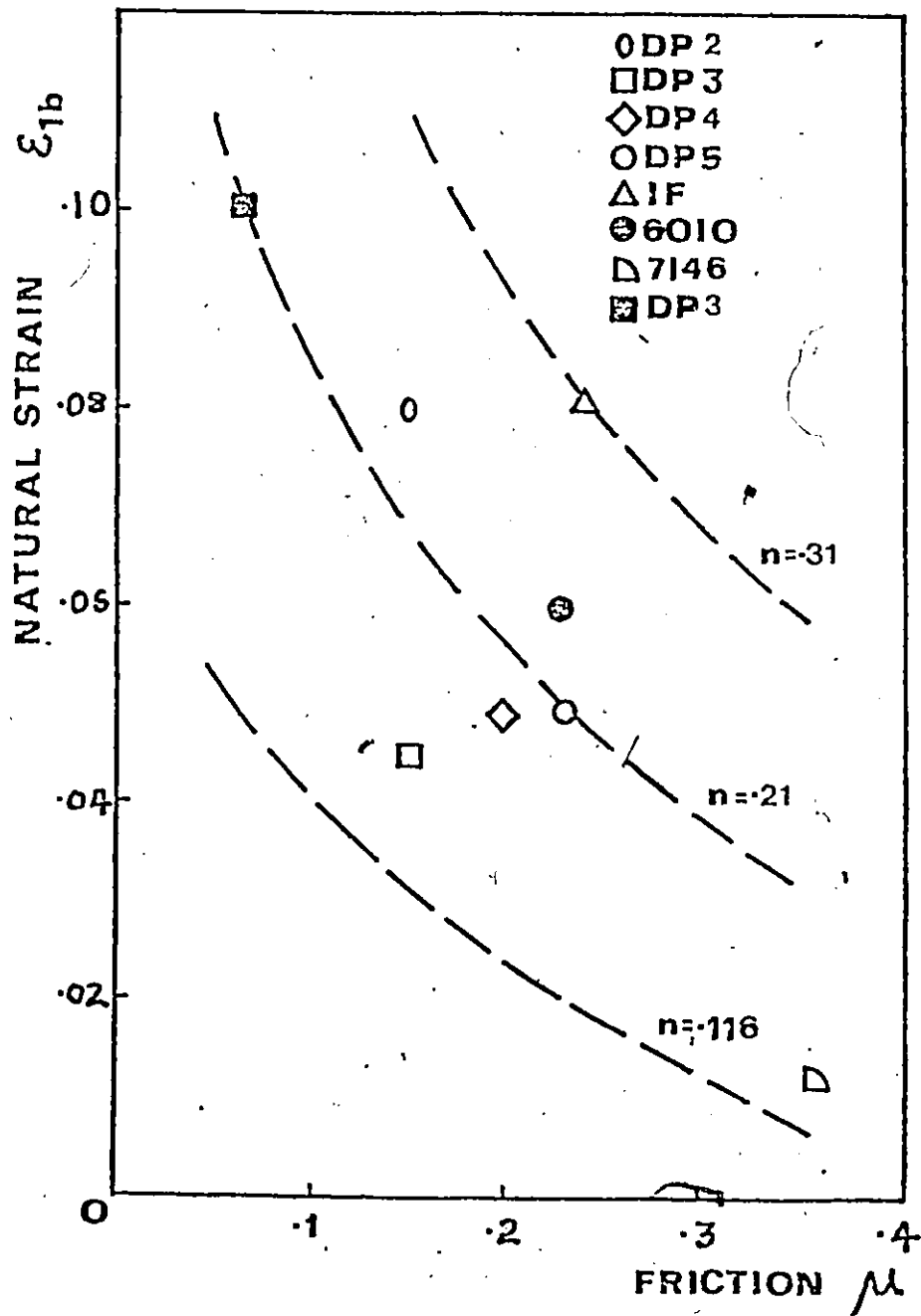


Fig. 63

- Experimental bottom strain ϵ_{1b}
versus n value for several values
of friction

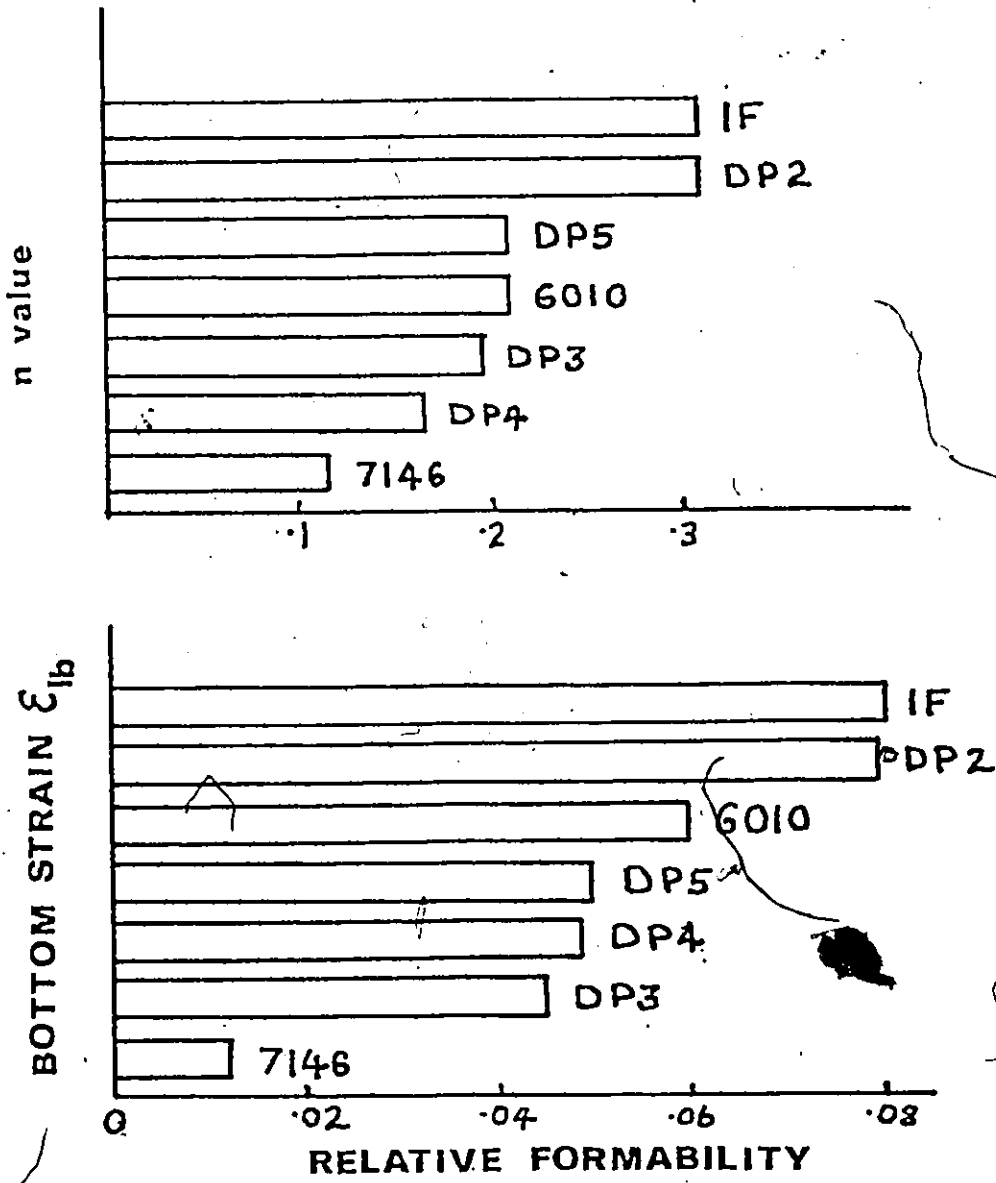


Fig. 64

- Bar chart of material ranking from n value and the maximum experimental bottom strain

CHAPTER VII
GENERAL DISCUSSION

The ranking of materials from the experimental bottom strain does not agree perfectly with any of the four ranking criteria suggested in chapter four. The n value ranking is the closest and does give a good ranking for materials with widely differing n values, but not for materials with very similar n values. The major disadvantage of all the rankings suggested in chapter four is that the friction effects are not accounted for.

With the experimental bottom strain ranking, friction is accounted for. Rough estimates of the friction coefficients can be determined from the experimental strains. It is observed from the friction values that the friction in pressing operations is higher than is generally thought and the friction does vary with the straining.

All tests with oil only lubrication were lubricated in such a manner as to keep the lubrication condition the same for all tests but the results obviously show that different materials have different friction coefficients. Preliminary tests on the rig showed a small variation in the

bottom strain, about 0.01 natural strain between two tests on the same material indicating that the friction varies slightly even if the material is the same. Obviously more accurate results would be obtained if the average value of several tests were used.

From the slope of the constant n value lines in figure (62) and the experimental results of the DP3 steel for the two lubrication conditions there is clearly significant amounts of bottom strain produced when the friction coefficient is lowered. This justifies the attempts to reduce friction in real press operations. It should be noted that the average value of the friction coefficients is around 0.2. The increase in bottom strain when the friction is reduced from 0.2 to 0.15 is not as great as when the friction is reduced from 0.1 to 0.05, see figure (62), which means that as the friction is decreased larger and larger gains can be made from further decreases in friction.

The values of friction determined from the experimental strains show that the friction is different for different materials. It is obvious that friction is a parameter which is dependent on many variables. From the results produced in this work all that can be determined is that the amount of bottom strain and the amount of sliding around the punch nose could be possible variables. The

punch loads versus depth curves are similar for all materials when normalized.

In all tests it was impossible to obtain a plane strain condition; the simple tension condition being closer to the experimental conditions. The three inch width of the test sample is obviously insufficient to produce plane strain. A much wider specimen would give results closer to plane strain. Using a wide specimen for plane strain and a thinner one for simple tension would give a chance at seeing how the strain condition would affect the strain distribution.

The modelling of chapter five, whether using the Ludwig equation (3.2) or the digitized stress-strain curve, could be used in conjunction with the experimental results so that it should be possible to use the model to extend the experimental results to other geometries and friction conditions. This would make the shallow pan experiments more useful than as a single simulative test since a wide range of geometries and frictions could then be covered.

It can be seen from equation (5.11) that the strength index, K in the Ludwik equation (3.2) is cancelled out and does not affect the formability of the material in shallow pans. The poorer formability of high strength materials is not due to the strength but due to poor n values and lower limit strains.

While the modelling in chapter five was only for a pure stretching of a shallow part, this type of modelling could be extended to cover drawing in for deeper parts or parts with re-entrant shapes.

CHAPTER VIII

8.1 CONCLUSIONS

A shallow pan simulative test, as described here could be used to rank materials for their formability in producing strain in the bottom of shallow parts. The bottom strain measured from the simulative test would be the best means of ranking materials.

The various methods of ranking materials from the tensile parameters, n^* , ϵ_u , U.T.S./Y.S. ratio and $\frac{1}{\sigma} \frac{d\sigma}{d\epsilon}$ at 2% strain are not completely appropriate, since all of the methods are not directly related to the bottom strains and do not account for the friction.

Friction is important in determining the ranking of materials for producing bottom strain. The values of friction from the experiments were higher than the values generally expected in press operations. The value of friction is dependent on many properties. There was a variation in the value of friction with material, the average value being approximately $\mu = 0.2$. Values of friction determined here are in agreement with previous work on determining friction in pressing operations.

The modelling is useful in understanding how the

geometry, friction and material parameters affect the bottom strain. All of these parameters affect the bottom strain in a very complex way. The model could be used to extend the usefulness of the shallow pan experimental results.

8.2 SUGGESTIONS FOR FURTHER WORK

A study of the variables which influence friction in a pressing operation and the typical friction values for materials would be of great interest. This is an area of metalforming where a lot more work could be done.

The modelling technique could be extended to other geometries, such as shallow pans with re-entrant shapes, or with draw in allowed.

An analysis of n^* and $\frac{1}{\sigma} \frac{d\sigma}{de}$ curves should be done so that the best way of presenting the materials work hardening characteristics for determining strain distributions can be found.

The shallow pan experiments should be continued and compared to real press applications.



APPENDIX A

REFINEMENTS TO ANALYTICAL MODEL

A.1 MATERIALS

Since it is doubtful whether the Ludwik equation accurately describes a material's stress-strain curve the actual tensile stress-strain curves were used in the refined model described by 20 or more data points. By interpolating or extrapolating from the data points using a polynomial of order three or more the whole range of the tensile curve is approximated.

The strain condition, β was also set up in the refined model such that it could be varied from the plane strain condition. While it is possible to have the strain condition vary between the wall and bottom sections, this was not used in the modelling. An average of the wall and bottom strain condition was used as the strain condition in the theoretical simulations of the experimental tests.

While the limit strain used in the modelling was determined by the local necking criteria, the model was set up so that an arbitrary strain limit, such as from a forming limit curve, could be used instead.

A.2 GEOMETRY

The geometry of the test piece is more accurately described by using an equation which accounts for the changes in the lengths of the sections due to the wrapping around the punch and clamp radii. Equation (5.2) is replaced by the following equation

$$\begin{aligned} C'D + A'B' &= a - R + (R + R_c + t_0) \tan(\theta/2) \\ B'C' &= (1 - C'D - A'B') / \cos\theta \end{aligned} \quad (A.1)$$

This is an approximation where the points B' and C' are determined by the intersection of the tangents for the points where the wall and bottom sections first touch the radii, see Figure (65). Note that the bottom section is now taken as the addition of sections A'B' and C'D.

Using the above formulation the lengths of both sections undergo slight changes in length as the depth increases. The angle θ is also slightly different than the angle θ_0 in the basic model. These refinements give the difference of about 7% between the basic and refined model theoretical strains. Further sophistications to the model are possible but the benefits are not likely to be large. One exception is the use of friction as a function of bottom strain instead of a constant value. This could be very easily incorporated into the model with significant effects.

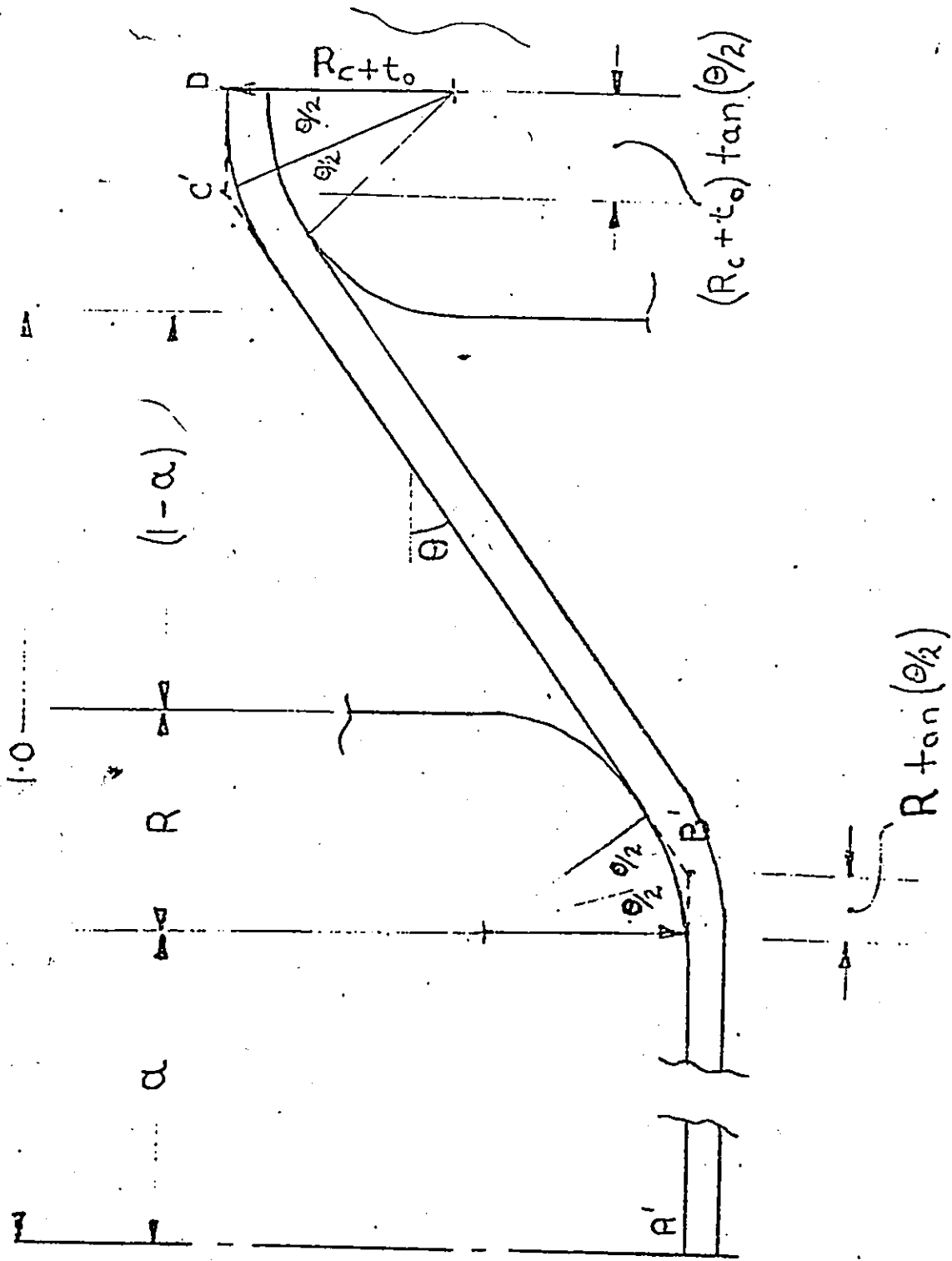


Figure 65 Refined Ir'del Geometry

REFERENCES

- [1] Business Week: "Oil-The Threat of a World Slowdown", No.2590, McGraw Hill, June 18, 1979, pp. 114-5.
- [2] Oil and Gas Journal: vol. 77, no. B, Petroleum Publications Co., Tulsa, March 20th, 1979.
- [3] Energy Policy and Conservation Act: 94th Congress, United States Congressional Code, vol. II, 1st. Session, 1975, p. 1778.
- [4] M. S. Rashid, G.D. Lawrence: "Wheel Weight with GM 980X Steel", SAE Paper No. 780138, Feb. 1978.
- [5] G. Speich, R. L. Miller: "Mechanical Properties of Ferrite/Martensite Steels", Paper, AIME Conference, New Orleans, March 1979.
- [6] R. G. Davies: "The Deformation Behaviour of a Vanadium Strengthened Dual Phase Steel", Met. Trans. A, 9A, Jan. 1978, p. 41.
- [7] M. S. Rashid: "GM 980X-Potential Application and Review", SAE Paper No. 770211, Feb. 1977.
- [8] P. J. Vander Arend, J. M. Rigsbee: "Laboratory Studies of Structure-Property Relationship in Dual Phase HSLA Steels", Paper, AIME Conference, Chicago, Oct. 1977.
- [9] J. Gerbase, J. D. Embury, R. M. Hobbs: "The Mechanical Behaviour of Some Dual Phase Steels and their Relationship to Theoretical Models", Paper, AIME Conference, New Orleans, March 1979.
- [10] R. G. Davies: "The Mechanical Properties of Zero Carbon Ferrite-plus-Martensite Structures", Met. Trans A, 9A, March 1978, p. 51.
- [11] S. T. Mileiko, J. of Mat. Science, vol. 4, 1969, pp.974-77.
- [12] D. J. Bailey and R. Stevenson: "High Strength Low Carbon Sheet Steel by Thermomechanical Processing I-Strengthening Mechanisms", Met. Trans. A, 10A, Jan. 1979, p. 113.

- [13] A. P. Coldren, A. Cornford, J. P. Hiam, G. Tither: "Development and Mill Trial of AS-Rolled Dual-Phase Steel", Symp. "Modern Developments in HSLA Formable Steels", Chicago, Oct. 1977.
- [14] R. G. Davies: "On the Ductility of Dual Phase Sheet Steels", AIME Conference, Chicago, Oct. 1977.
- [15] J. Y. Koo, G. Thomas: "Design of Duplex Fe/x/0.1 C Steels for Improved Mechanical Properties", Met. Trans. A, 8A, 1977, p. 525.
- [16] A. E. Cornford, J. R. Hiam, R.M. Hobbs: "Properties of As-Rolled Dual Phase Steels", SAE Paper No. 790007.
- [17] D. J. Bailey: "A Family of Thermomechanically Treated (TMT) High Strength Steels", SAE Paper No. 760715.
- [18] D. Aichbhaumik, R. R. Goodhart: "Effect of Annealing Cycles on the Properties and Microstructures of Several Dual Phase Steels", SAE Paper No. 790010.
- [19] F. Weinburg: Tools And Techniques in Physical Metallurgy, vol. II, Marcel Dekker, New York, 1970, pp. 265-328.
- [20] J. S. Hoggart, T. R. Thompson: "Assessment of the Formability of Sheet Metals from the Ferrite Test", Aust. Inst. of Metals Publication, Metals Congress 1978, Melbourne, Australia.
- [21] A. S. Kasper: Met. Progress, 96, 1969, p. 159-164.
- [22] S. P. Keeler, W. A. Backofen: Trans. ASM, 56, 1963, p. 25.
- [23] G. H. Goodwin: "Application of Strain Analysis to Sheet Metal Forming Problems in the Press Shop", SAE Paper No. 680093.
- [24] J. L. Duncan, B. S. Shabel, J. Gerbose: "A Tensile Strip Test for Evaluating Friction in Sheet Metal Forming", SAE Paper No. 780391.
- [25] L. F. Ramos, D. K. Matlock, A. Kräuss: "On the Deformation Behaviour of Dual Phase Steels", Met. Trans. A, 10A, Feb. 1979. p. 259.

- [26] D. Aichbhaumik, R. R. Goodhart: "Effect of Annealing Cycles on the Properties and Microstructures of Several Dual Phase Steels", SAE Paper No. 790010.
- [27] J. L. Duncan, J. Kolodziejcki, G. Glover: Proc. 9th Biennial Congress IDDRG, ASM Publication, 1976 p. 131.
- [28] K. Yoshida et al: Sheet Met. Ind., Oct. 1971, p. 772.
- [29] H. Conrad: "Effect of the Strain Rate Sensitivity of the Flow Stress on the Stretch Formability of Sheet Metals", J. Mech. Working Technology, vol. 2, 1978, pp. 67-74.
- [30] A. K. Ghosh: "Necking in Materials with Strain Hardening and Strain Rate Sensitivity", Proc. Symp. "Formability, Analysis, Modelling, and Experimentation", AIME Publication, Chicago, Oct. 1977.